NASA CR-363

THROUGH-FLOW SOLUTION FOR AXIAL-FLOW TURBOMACHINE BLADE ROWS

By Patrick Kavanagh and George K. Serovy

Prepared under Grant No. NSG-62 by
IOWA STATE UNIVERSITY
Ames, Iowa

for

NATIONAL AERONAUTICS AND SPACE ADMINISTRATION

For sale by the Clearinghouse for Federal Scientific and Technical Information
Springfield, Virginia 22151 – Price $3.00

THROUGH-FLOW SOLUTION

FOR AXIAL-FLOW TURBOMACHINE BLADE ROWS

by

Patrick Kavanagh and George K. Serovy

Iowa Engineering Experiment Station
Iowa State University

SUMMARY

A method of analysis for the blade-to-blade flow through a turbomachine blade row made up of a finite number of blades having finite thickness distributions is presented. The fluid is assumed incompressible and nonviscous. The analysis assumes steady flow relative to the blades along a given stream surface of revolution. At stations far upstream and downstream of the blade row the flow is known and axisymmetric.

The blade-to-blade flow equation is formulated in terms of a stream function, resulting in a boundary value problem with associated boundary conditions expressed for the stream function. An iterative numerical solution method based on finite difference approximations and applicable to general blade cascade configurations is developed and programmed for computer solution. Flow patterns and head coefficient distributions for several selected cascade configurations and flow conditions are presented to indicate the validity of the present program and the prospects for further development.

An experimental investigation conducted in water on two-dimensional cascades of NACA 65(A_{10})-810 compressor blades is described. Cascade configurations involving three different blade setting angles in combination with minimum-loss incidence and turning angles for a constant blade solidity were tested over a range of Reynolds numbers from about 89, 000 to 134, 000. Measured profile head distributions are compared with available data from previous cascade investigations conducted in air, and with theoretically computed results.

INTRODUCTION

In design of axial-flow turbomachines it is necessary to analyze the flow of a fluid through a succession of closely-spaced blade rows. At present, a complete solution to this complex, three-dimensional flow problem is not available. However, solutions have been obtained for simplified approximations to the complete problem.

Methods of flow analysis involving only two coordinates play an impor-

tant part in determination of flow patterns in turbomachines. Since these methods are two-dimensional in mathematical sense one may say that the flow is analyzed in a surface. From the standpoint of simplicity, the best choice of surface is a stream surface. As an example, the meridional plane in flow without whirl past a body of revolution is a stream surface, and choice of a reference surface other than the meridional plane would only detract from the simplicity. In the more complicated case of the axisymmetric approximation of flow through a blade row of a turbomachine in which the blade mean surfaces serve as stream surfaces in the relative flow the principle still stands. Even so, the meridional plane is commonly used (6) rather than the blade mean surface. Hence, two flow problems may be considered in a turbomachine, one comprising axisymmetric flow on stream surfaces of revolution (the hub-to-tip flow problem) and the other the flow between blades of the rotor or stator on these surfaces (the blade-to-blade flow problem, ignoring secondary flow). The solution of the blade-to-blade flow problem is found using stream surfaces determined in the hub-to-tip flow problem, and the two problems in combination preserve the essential features of the original problem.

The first attempt at theoretical determination of flow through a blade row was made by Lorenz (16) who introduced the concept of an infinite number of blades to treat the resultant axisymmetric flow. Bauersfeld (1) later developed a method of designing blades under the restriction that the blade forces should not influence the meridional flow and that the blade force field must be normal to the stream surfaces defining the blade surface. The later work of Stodola (32), Spannhake (30), and Keller (13) further clarified and strengthened the theory. Ruden (24) proved that the through-flow solution under the assumption of an infinite number of blades gives a circumferentially averaged value of the fluid properties. The through-flow theory was further generalized by Wislicenus (37) who determined the influence of blade forces on meridional flow through inclination of the vortex filaments against the meridional plane.

Extension of through-flow methods from an infinite number to a finite number of blades was made by Reissner and Meyerhoff (20) who used a power-series expansion, the terms of which were determined by comparison of the equations for an infinite number of blades and for a finite number of blades. Marble and Michelson (17) obtained a solution for an infinite number of blades for a prescribed loading and cylindrical bounding walls, and investigated the problem of mutual interference of adjacent blade rows and off-design operation. Wu and Wolfenstein (39) analyzed compressible flow in axial turbomachines having infinite number of blades, applying radial equilibrium to both the design and off-design problem. Wu (38) also presented a general through-flow theory for the case of finite number of blades of finite thickness with arbitrary hub and casing shapes and stream surfaces of general shape. Stanitz and Ellis (31) and Kramer (14) have obtained solutions to the blade-to-blade flow problem in centrifugal impellers by using numerical methods.

The theoretical and numerical difficulties in three-dimensional through-flow solutions are great. Even greater are the difficulties involved in adapting such solutions to practical design application. The design equations must

be simple but accurate enough so that the relative significance of design variables can be studied. Also it must be possible to compute many designs quickly from which the most suitable one can be selected.

In practice, the design of axial-flow compressors has most frequently been based on blade-element flow and analysis of axisymmetric flow at stations between the blade rows (12).

In blade-element flow it is assumed that stream surfaces through a blade row are largely undistorted and that the flow remains on nearly conical stream surfaces independent of radial gradients. Simple radial equilibrium is assumed, and appropriate loss distributions may be applied at the calculation stations (8). The flow past any blade element or section is assumed to be the same regardless of whether the element is in a two-dimensional cascade or in an actual blade row. Hence the designer can use empirical design information obtained chiefly from experimental two-dimensional cascade data to correct for discrepancies between the real and design flows. Similar practical design procedures for axial-flow machines based on axisymmetric flow at stations between the blade rows have been used by Bowen et al. (2) and by Smith et al. (28); the method used by Bowen et al. was later extended by Holmquist and Rannie (11). Also radial equilibrium and blade-element theory has been applied in axial-flow compressors and pumps by Serovy and Anderson (27), Swan (34), and by Robbins and Dugan (21) to estimate off-design performance.

Present-day requirements in the design of compact, high-performance pumps demand corresponding adjustments in conventional and conservative design techniques (7). The assumption of axisymmetric flow and blade-element theory cannot give satisfactory, physically valid solutions when large deviations from the assumption of blade-element flow occur. The need for improved design methods incorporating more complete flow solutions is thus indicated.

In this report a numerical method of general applicability for estimating the blade-to-blade flow of a frictionless and non-cavitating fluid is presented. Finite difference approximation to the flow field and governing flow equations in given blade cascades and on axisymmetric stream surfaces is used. Iterative solutions of the system of linear equations resulting from the finite difference approximations are obtained on a digital computer. Sample solutions so obtained for a number of cascade configurations are presented to test the method. The results of these solutions are presented in the form of flow or streamline patterns and as blade profile head distributions.

In addition, an experimental investigation was conducted on two-dimensional cascades of NACA 65(A_{10})-810 compressor blades in water. Configurations involving three different blade setting angles in combination with design incidence and turning angles for a constant blade solidity were tested over a low range of Reynolds number under non-cavitating flow conditions. Results obtained for profile head distributions are compared with available data from previous cascade investigations conducted in air.

ANALYSIS OF FLOW IN ROTATING BLADE ROWS

In analysis of flow past solid boundaries (such as those typical of the bladed passages of turbomachinery) two extreme cases as represented by the potential and laminar solutions for the flow pattern can be cited (see Figure 1). These solutions are the limiting cases for flow at very high and very low Reynolds numbers, respectively. Potential solutions for the velocity and pressure fields indicate that drag forces are non-existent, regardless of the fluid deformation involved. However, in laminar flow solutions, the dominant viscous effects lead to pressures and velocities radically different than those in potential flow, with the resulting flow characterized by so-called deformation drag (22). In real flow situations values of Reynolds number are intermediate to those for purely laminar flow or potential flow. Analysis of the flow in such cases which takes into account real fluid effects is complex, involving an essential interdependence of the main flow, the boundary layer and any separated regions. Complete solution of the flow of a real fluid through a turbomachine blade row is beyond reach as is evidenced by the fact that only a few solutions to viscous flow problems involving much simpler boundary conditions are presently known (26).

In many cases, however, theoretical determination of flow in turbomachinery based on ideal (potential flow) analysis can serve to approximate the distribution of velocities and pressures and indicate effects of changes in design parameters. Such theoretical solutions constructed according to the boundary geometry require boundary layers of negligible thickness at all points. Conclusions drawn from these solutions are warranted if it is appreciated that as long as the boundary layer remains thin the pressure must be essentially the same at the boundary as at the edge of the boundary layer.

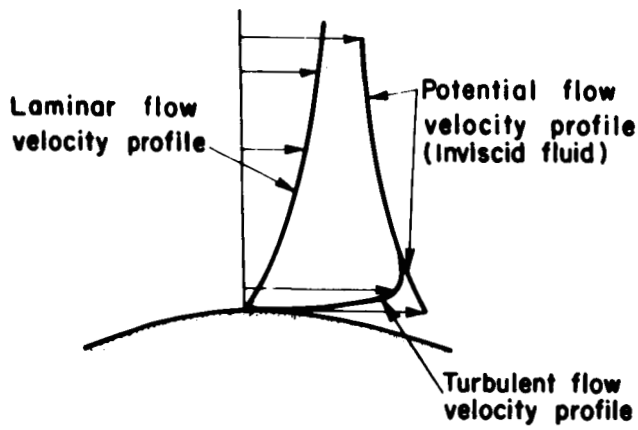

Figure 1, above. Flow velocity profiles showing influence of the boundary over a range of Reynolds number from laminar to potential flow.

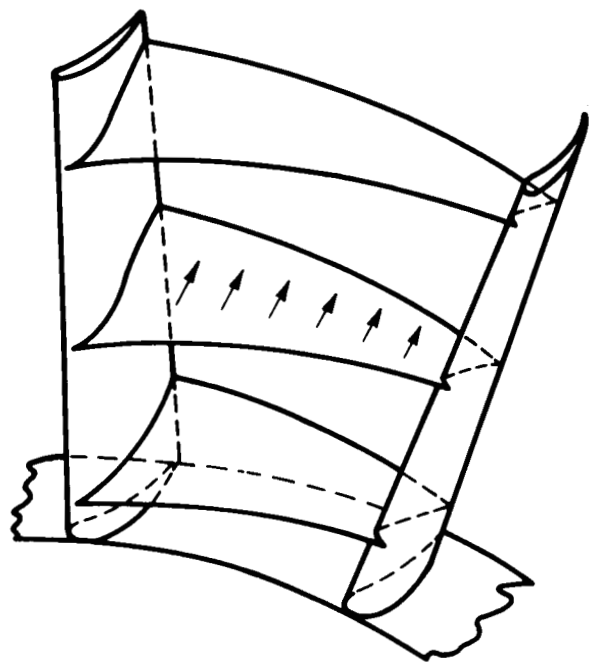

Figure 2, at right. Stream surfaces of the first kind in flow through a blade row.

MATHEMATICAL MODEL

The mathematical model proposed here is intended to approximate the real flow in a rotating blade row in the blade-to-blade flow problem and to permit computation of velocity and pressure distributions over the blade profile for given operating conditions. Stream surfaces in the real blade-to-blade flow, shown in Figure 2, are so-called stream surfaces of the first kind (38) traced by fluid particles located initially on circular arcs of constant radius about the machine axis. In this analysis secondary flows, or cross-currents to the primary flow (4), which appear in stators and rotors (even in the ideal fluid analysis) and which deform the stream surfaces are ignored. Also, hub-to-tip solutions or approximations to the flow in a meridional plane are not attempted here. Consequently, the blade-to-blade stream surface is taken to be of an assumed constant form and axisymmetric.

It is assumed that the fluid is inviscid and of constant density. Also, cavitation is not allowed. The blade row is assumed to rotate at constant angular velocity. In the case of a stationary blade row the angular velocity is simply set equal to zero. The blade row is made up of a finite number of like blades having prescribed camber and finite thickness distribution. As a result, at stations inside the blade row the characteristics of the flow change in the circumferential direction across each flow passage formed by adjacent blades (but ideally in identical fashion for each passage).

If the flow inside a rotor were observed at a particular point in an absolute reference frame, it is clear that as different points of the blade row and the flow pass successively through the observation point, a steady flow relative to the rotor would appear unsteady, and even discontinuous because of the finite thickness of the blades. By referring, then, to a reference frame attached to the rotor, the formulation of the equations of motion is greatly simplified; the usual laws of steady fluid motion and a relatively simple set of boundary conditions can be used. It is noted that steady flow cannot occur simultaneously with respect to the stator and rotor blade rows in a turbomachine. Following the preceding discussion, a steady relative flow at the exit of a rotor produces unsteady absolute flow in the following stator row, and vice versa. Therefore, the assumption often made that steady flows exist in the stators and rotors of turbomachines is incorrect. In this analysis, however, the relative flow at stations sufficiently far upstream and downstream of the rotating blade row is assumed to be steady.

Because the boundary walls (the hub and the casing) and the stream surfaces are surfaces of revolution it will be convenient to employ a relative cylindrical coordinate system in which the meridional angle is measured from a rotating blade.

FUNDAMENTAL EQUATIONS

Euler's equation for incompressible flow is (22)

$$\frac{d\vec{V}}{dt} = -g\nabla h$$

where $\vec{V}$ is the absolute velocity of the flow and h is the piezometric head expressing the sum of pressure head and elevation above some geodetic datum. The derivative with respect to time on the left hand side of the equation is the absolute substantial derivative. In terms of observations made from a reference frame attached to a blade row rotating with constant angular velocity $\vec{\omega}$, the Euler equation becomes (35)

$$\frac{d\vec{W}}{dt} - \omega^2\vec{r} + 2\vec{\omega} \times \vec{W} = -g\nabla h \tag{1}$$

In this equation $\frac{d\vec{W}}{dt}$ is the substantial derivative of the velocity of the fluid particle under consideration measured relative to the rotating reference frame. The second term is the acceleration of the point fixed in the rotating blade row and coincident with the fluid particle under consideration ($\vec{r}$ is the radius vector measured from the machine axis to the particle of fluid). The vector $2\vec{\omega} \times \vec{W}$ is the Coriolis component of acceleration.

With the assumption of steady flow relative to the rotating blades, the only contribution to the substantial derivative in Equation 1 is due to the non-uniformity of the relative velocity field. Hence, Equation 1 can be written as

$$\vec{W} \cdot \nabla\vec{W} - \omega^2\vec{r} + 2\vec{\omega} \times \vec{W} = -g\nabla h \tag{2}$$

Further simplification of this equation can be made using the identity

$$\vec{W} \cdot \nabla\vec{W} = \frac{1}{2}\nabla W^2 - \vec{W} \times (\nabla \times \vec{W})$$

in which the space derivatives may be computed at a given instant in either the relative or absolute reference frame. Substitution of the identity into Equation 2 yields

$$-\vec{W} \times (\nabla \times \vec{W}) - \omega^2\vec{r} + 2\vec{\omega} \times \vec{W} = -g\nabla \left(h + \frac{W^2}{2g}\right) \tag{3}$$

Next, with substitution for the vorticity of the relative flow in terms of the vorticity of the absolute flow from the relation (35)

$$\nabla \times \vec{W} = \nabla \times \vec{V} - 2\vec{\omega}$$

Equation 3 becomes

$$-\vec{W} \times (\nabla \times \vec{V}) - \omega^2\vec{r} = -g\nabla \left(h + \frac{W^2}{2g}\right) \tag{4}$$

Finally, since the "wheel speed", U, is ωr, then

$$\frac{1}{2}\nabla U^2 = \omega^2 \vec{r}$$

Using this last result in Equation 4, then

$$\vec{W} \times (\nabla \times \vec{V}) = g\nabla H' \tag{5}$$

in which a relative total head, H', has been introduced. The relative total head (which is not the total head of the relative flow) is defined by the relation

$$H' = h + \frac{W^2 - U^2}{2g} \tag{6}$$

Evidently, according to Equation 5, the vorticity and relative flow velocity vectors are tangent to level surfaces of H'. In the case of a stationary blade row, ω vanishes, W becomes V and H' becomes the total head, H.

Another relation between H' and H can be obtained. When a velocity triangle for flow in a rotor is drawn (see Figure 3) it is easily seen that the relative total head, and the total head obey the relation

$$H' = H - \frac{V^2}{2g} + \frac{W^2 - U^2}{2g}$$

$$= H + \frac{1}{2g}\left[-V^2 + (U - V_u)^2 + V^2 - V_u^2 - U^2\right]$$

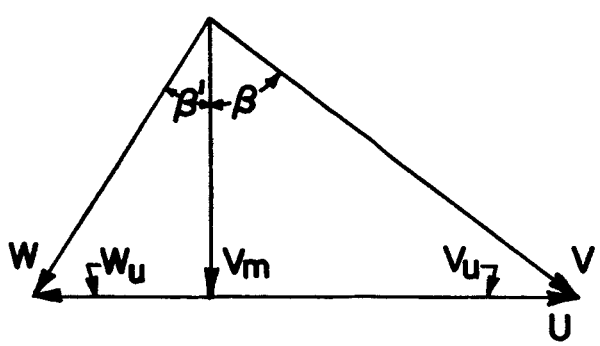

Figure 3. Velocity triangle.

This in turn can be reduced to

$$H' = H - \frac{\omega r V_u}{g} \tag{7}$$

in which the factor rV_u is the angular momentum per unit mass of fluid with respect to the machine axis.

The scalar product taken between the relative flow velocity, $\vec{W}$, and Equation 5 yields the result

$$\vec{W} \cdot \nabla H' = 0$$

which indicates that the substantial derivative of H' in the steady relative flow vanishes, i.e.,

$$\frac{dH'}{dt} = \vec{W} \cdot \nabla H' = 0$$

Thus a fluid particle in traversing the blade row experiences a change

$$\Delta H' = \Delta \left(H - \frac{UV_u}{g}\right) = 0 \tag{7a}$$

which is an expression of Euler's turbine equation.

If for the axisymmetric flow at the inlet station to a rotating blade row it is assumed that the whirl velocity distribution is that of a potential vortex $[V_u = \frac{c}{r}]$ and that total head is constant with radius (note that this results in uniform H' at the inlet), then, according to Equation 7a the relative total head is uniform everywhere in the flow through the blade row. The equation of motion from Equation 5 is in this case

$$\vec{W} \times (\nabla \times \vec{V}) = 0 \tag{8}$$

and the vorticity and relative velocity vectors are seen to be parallel. Also, for the absolute flow to be irrotational it is obvious that gradients in relative total head would be zero and constant energy change per unit weight of fluid flowing is implied.

At this point it is instructive to critically review the assumption of steady and axisymmetric flow into a rotor of a machine, and to examine the rotational tendencies of the flow. Consider, as an example, a machine stage consisting of a stator row followed by a rotor. According to Kelvin's theorem (19), an irrotational flow which enters the stator blade row leaves the blades as an

irrotational flow. If the stator and rotor blade rows can be considered as not close to each other, and if trailing vortices are not shed from the stator blades (i.e., the whirl discharge from the stator row is free-vortex so that spanwise distribution of circulation is constant) then the characteristics of the flow at a fixed point relative to the rotor can be taken as constant. However, if the rotor is close to the stator blade row, vortices are shed from the stator blades because of periodic variation in circulation caused by the flow unsteadiness. The flow through the rotor, then, would properly be treated on the basis of unsteady and rotational flow (38).

FLOW ON AXISYMMETRIC STREAM SURFACES

Equation of Motion in Curvilinear Coordinates

In view of the difficulties involved in determination of the flow pattern in a turbomachine for even the simple case involving an inviscid, constant-density fluid, it is necessary to approximate the form of the stream surfaces. The relative blade-to-blade flow through an actual rotor made up of a finite number of blades is approximated as a flow on axisymmetric stream surfaces which are surfaces of revolution generated by rotating given streamlines in a meridional plane of the rotor about the axis of the machine. The details involved in the assumption of axisymmetric stream surfaces will be discussed in the following section, Axisymmetric Stream Surface Assumption.

It is assumed that the relative total head, H', is uniform throughout the flow at the inlet station to the blade row. For purposes of discussion and solution of the blade-to-blade flow problem the equation of motion (Equation 8) is best expressed in terms of a general curvilinear coordinate system having symmetry with respect to the axis of the machine. In this way, a particular family of coordinate surfaces comprise the axisymmetric stream surfaces.

Consider a curvilinear coordinate system given in functional relation to conventional cylindrical coordinates θ, r and z by the equations

$$\theta = \theta$$

$$m = m(r,z)$$

$$n = n(r,z)$$

In either coordinate system, θ represents the meridional angle as measured in the relative reference frame rotating with the rotor. The cylindrical coordinates r and z are the radius as measured from the machine axis and the distance as measured along that axis, respectively. It is apparent from the stated relations that m- and n- coordinate surfaces possess axial symmetry. Also, the (θ, m, n) coordinate system is taken to be orthogonal. Consequently, when blade-to-blade axisymmetric stream surfaces are assumed, they correspond to the n-coordinate surfaces, while m-coordinate surfaces are normal surfaces to the stream surfaces. A cylindrical

coordinate system would be a special case of the more general system with r corresponding to n, and z corresponding to m.

An elementary curvilinear rectangle with sides parallel to m- and n-coordinate surface traces in a meridional plane is shown in Figure 4. Also shown are angle increments $d\phi$ and $d\psi$, along with the radii of curvature r_m and r_n for the n- and m-coordinate traces, respectively. The two radii r_m and r_n serve as linearizing factors enabling the relations $dm = r_m d\phi$, and $dn = r_n d\psi$ to be written. Hence, the differential arc length ds measured from point (θ, m, n) to a point $(\theta + d\theta, m + dm, n + dn)$ is $(r^2 d\theta^2 + r_m{}^2 d\phi^2 + r_n{}^2 d\psi^2)^{1/2}$.

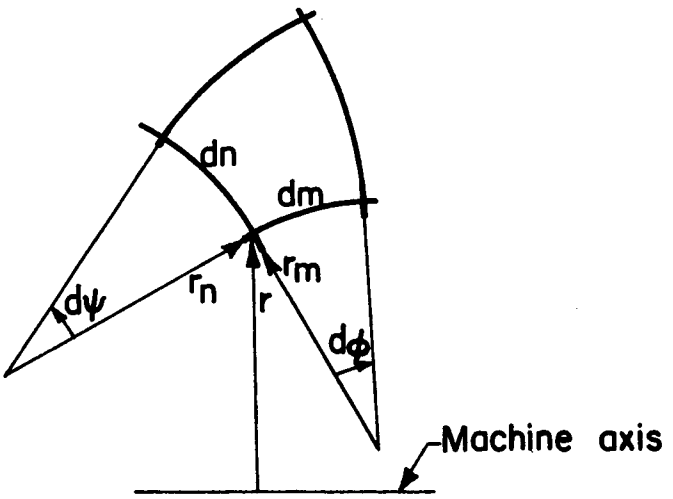

Figure 4. Elementary curvilinear rectangle.

Next, the relative flow velocity vector is written

$$\vec{W} = [W_u, W_m, W_n]$$

The vorticity of the relative flow can be expressed by making reference to standard formulas for curl expressed in curvilinear coordinates (3) or simply by computing components as the circulation per unit area around appropriate elementary curvilinear rectangles oriented with sides parallel to the curvilinear axes.

Hence,

$$\nabla \times \vec{W} = \left[\frac{1}{r_m r_n}\left(\frac{\partial r_n W_n}{\partial \phi} - \frac{\partial r_m W_m}{\partial \psi}\right),\right.$$

$$\left.\frac{1}{r_n r}\left(\frac{\partial r W_u}{\partial \psi} - \frac{\partial r_n W_n}{\partial \theta}\right), \frac{1}{r r_m}\left(\frac{\partial r_m W_m}{\partial \theta} - \frac{\partial r W_u}{\partial \phi}\right)\right]$$

In the above vector relations the θ, m, and n components of the vorticity of the relative flow are the ordered components, respectively, within the brackets. If the indicated differentiations are performed, then,

$$\nabla \times \vec{W} = \left[\frac{W_n}{r_m r_n}\frac{\partial r_n}{\partial \phi} + \frac{1}{r_m}\frac{\partial W_n}{\partial \phi} - \frac{W_m}{r_m r_n}\frac{\partial r_m}{\partial \psi} - \frac{1}{r_n}\frac{\partial W_m}{\partial \psi},\right.$$

$$\frac{W_u}{r_n r}\frac{\partial r}{\partial \psi} + \frac{1}{r_n}\frac{\partial W_u}{\partial \psi} - \frac{W_n}{r_n r}\frac{\partial r_n}{\partial \theta} - \frac{1}{r}\frac{\partial W_n}{\partial \theta},$$

$$\left.\frac{W_m}{r r_m}\frac{\partial r_m}{\partial \theta} + \frac{1}{r}\frac{\partial W_m}{\partial \theta} - \frac{W_u}{r r_m}\frac{\partial r}{\partial \phi} - \frac{1}{r_m}\frac{\partial W_u}{\partial \phi}\right]$$

It appears in viewing Figure 4 that

$$dr_m = dn, \quad dr_n = dm$$

and it follows that

$$\frac{\partial r_n}{r_m \partial \phi} = \frac{\partial r_m}{r_n \partial \psi} = 1$$

Also, due to the axial symmetry of the coordinate surfaces, each meridional picture is identical, implying that

$$\frac{\partial r_m}{\partial \theta} = \frac{\partial r_n}{\partial \theta} = 0$$

Substitution of these four derivative values into the preceding equation for the vorticity of the relative flow yields

$$\nabla \times \vec{W} = \left[\frac{W_n}{r_n} + \frac{\partial W_n}{\partial m} - \frac{W_m}{r_m} - \frac{\partial W_m}{\partial n},\right.$$

$$\left.\frac{W_u}{r}\frac{\partial r}{\partial n} + \frac{\partial W_u}{\partial n} - \frac{1}{r}\frac{\partial W_n}{\partial \theta}, \frac{1}{r}\frac{\partial W_m}{\partial \theta} - \frac{W_u}{r}\frac{\partial r}{\partial m} - \frac{\partial W_u}{\partial m}\right]$$

A final expression obtained after some rearrangement in the second and third components is

$$\nabla \times \vec{W} = \left[\frac{W_n}{r_n} + \frac{\partial W_n}{\partial m} - \frac{W_m}{r_m} - \frac{\partial W_m}{\partial n},\right. \tag{9}$$

$$\left.\frac{1}{r}\left(\frac{\partial r W_u}{\partial n} - \frac{\partial W_n}{\partial \theta}\right), \frac{1}{r}\left(\frac{\partial W_m}{\partial \theta} - \frac{\partial r W_u}{\partial m}\right)\right]$$

The angular velocity of the rotor is a constant vector lying on the machine axis. In terms of the curvilinear coordinate system the angular velocity is

$$\vec{\omega} = [0, \omega \frac{\partial r}{\partial n}, -\omega \frac{\partial r}{\partial m}]$$

Addition of $2\vec{\omega}$ to the vorticity of the relative flow gives the vorticity of the absolute flow. Hence,

$$\nabla \times \vec{V} = [\frac{W_n}{r_n} + \frac{\partial W_n}{\partial m} - \frac{W_m}{r_m} - \frac{\partial W_m}{\partial n},$$

$$\frac{1}{r}\left(\frac{\partial(rW_u + \omega r^2)}{\partial n} - \frac{\partial W_n}{\partial \theta}\right), \frac{1}{r}\left(\frac{\partial W_m}{\partial \theta} - \frac{\partial(rW_u + \omega r^2)}{\partial m}\right)] \tag{10}$$

The final desired expression for the equation of motion (Equation 8) is obtained after the indicated vector product of the relative velocity and the vorticity of the absolute flow is made and the resultant components are equated to zero. Thus,

$$[\frac{W_m}{r}\left(\frac{\partial W_m}{\partial \theta} - \frac{\partial(rW_u + \omega r^2)}{\partial m}\right) - \frac{W_n}{r}\left(\frac{\partial(rW_u + \omega r^2)}{\partial n} - \frac{\partial W_n}{\partial \theta}\right),$$

$$\frac{W_n^2}{r_n} + \frac{1}{2}\frac{\partial W_n^2}{\partial m} - \frac{W_n W_m}{r_m} - W_n \frac{\partial W_m}{\partial n} + \frac{W_u}{r}\left(\frac{\partial(rW_u + \omega r^2)}{\partial m} - \frac{\partial W_m}{\partial \theta}\right), \tag{11}$$

$$\frac{W_u}{r}\left(\frac{\partial(rW_u + \omega r^2)}{\partial n} - \frac{\partial W_n}{\partial \theta}\right) - \frac{W_m W_n}{r_n} - W_m \frac{\partial W_n}{\partial m} + \frac{W_m^2}{r_m} + \frac{1}{2}\frac{\partial W_m^2}{\partial n}] = 0$$

As indicated earlier, the case for flow with uniform total head through a stationary row of blades can be handled simply as a special case in any of the preceding relations by setting the angular speed, ω, to zero, and by replacing W by V wherever it appears. Also, any of the relations, whether for stationary or rotating blade rows, can be expressed in cylindrical coordinates by replacing m and n wherever they appear in order by z and r, noting that in such a case r_m and r_n are infinite.

Axisymmetric Stream Surface Assumption

Consider a steady relative flow on axisymmetric stream surfaces

through a rotating blade row. The stream surfaces are n-coordinate surfaces. At a point on a given stream surface the relative flow velocity vector lies in the tangent plane to the surface; therefore

$$\vec{W} = [W_u, W_m, 0]$$

The component equations of motion for the assumed axisymmetric stream surfaces and for uniform H' (Equation 11) become

$$\left[\frac{W_m}{r}\left(\frac{\partial W_m}{\partial \theta} - \frac{\partial(rW_u + \omega r^2)}{\partial m}\right), \frac{1}{2}\frac{\partial W_n^2}{\partial m} + \frac{W_u}{r}\left(\frac{\partial(rW_u + \omega r^2)}{\partial m} - \frac{\partial W_m}{\partial \theta}\right),\right. \tag{12}$$

$$\left.\frac{W_u}{r}\left(\frac{\partial(rW_u + \omega r^2)}{\partial n} - \frac{\partial W_n}{\partial \theta}\right) - W_m\frac{\partial W_n}{\partial m} + \frac{W_m}{r_m} + \frac{1}{2}\frac{\partial W_m^2}{\partial n}\right] = 0$$

Axisymmetric stream surfaces exist if Equation 12 and the conditions

$$\frac{\partial W_n}{\partial m} = \frac{\partial W_n}{\partial \theta} = 0$$

are satisfied. (Note that if natural coordinates involving rectangular axes θ, m, n at a given point along a streamline are used, then the two derivatives just cited are in general not zero, and as such imply the curvature of the streamline.)

To amplify what is involved in the assumption of axisymmetric stream surfaces and to discuss some of the more important points in approaching the flow solution the following discussion is appropriate.

Consider, first of all, the simple case of axisymmetric flow with uniform head, H, and zero whirl into an annular passage free of blades. It is seen from Equation 12 under the stated conditions that the derivatives

$$\frac{\partial W_m}{\partial \theta}, \frac{\partial W_n}{\partial m}, \text{ and } \frac{\partial W_n}{\partial \theta}$$

vanish. Thus the flow has axisymmetric stream surfaces. In fact, the flow itself is axisymmetric and the flow problem is reduced to one in a meridional plane concerning the hub-to-casing flow pattern, the equation of motion obtained from the third component equation being simply

$$\frac{dV_m}{dn} + \frac{V_m}{r_m} = 0$$

Next, extension to axisymmetric flow through a blade row is possible with the assumption of an infinite number of infinitely thin blades. The through-flow in this approximation is obviously axisymmetric. Therefore, the flow

analysis can be dealt with in either a relative or absolute frame of reference since both the relative and absolute flows are steady and axisymmetric. However, to account for the blades in the flow passage and their attendant influence on the flow, the small changes in pressure in the peripheral direction between adjacent blades can be represented in the equations of motion in terms of a distributed body force acting normal to a given but arbitrary blade surface (24). Briefly, the solution for the flow pattern in the meridional plane entails a first approximation of the form of the streamlines followed by iterations on the form until the solution obtains (6).

In practical design (i.e., blade-element method (12)) the through-flow determination is often abandoned in favor of finding the axisymmetric flow only at stations located between blade rows where the blade forces do not exist. An important feature of the blade-element method is that total head gradient terms at the flow stations can be incorporated, accounting for radial distributions of energy resulting from upstream flow characteristics. The energy gradients referred to are the result of energy addition in the upstream rotor blade rows and frictional losses in the upstream flow.

Blade-to-Blade Flow on Axisymmetric Stream Surfaces

The θ- component equation of motion obtained from Equation 12 for relative flow on an axisymmetric stream surface is

$$\frac{\partial W_m}{\partial \theta} - W_u \frac{dr}{dm} - r \frac{\partial W_u}{\partial m} - 2\omega r \frac{dr}{dm} = 0 \tag{13}$$

Interestingly enough, this same equation can be obtained as follows from the θ- component equation of motion for uniform relative total head expressed in cylindrical coordinates. The component equation

$$[\vec{W} \times (\nabla \times \vec{V})]_{\theta\text{-component}} = 0$$

(see Equation 11) becomes, when converted from the general curvilinear coordinates (θ, m, n) to cylindrical coordinates (θ, z, r)

$$W_z \left(\frac{\partial W_z}{\partial \theta} - \frac{\partial (rW_u + \omega r^2)}{\partial z}\right) - W_r \left(\frac{\partial (rW_u + \omega r^2)}{\partial r} - \frac{\partial W_r}{\partial \theta}\right) = 0$$

With rearrangement,

$$\frac{1}{2} \frac{\partial (W_z^2 + W_r^2)}{\partial \theta} - \left(W_z \frac{\partial}{\partial z} + W_r \frac{\partial}{\partial r}\right)(rW_u + \omega r^2) = 0$$

However, the magnitude of the meridional velocity component is

$$W_m = (W_z^2 + W_r^2)^{\frac{1}{2}}$$

Also,

$$\vec{W}_m \cdot \nabla = [0, W_z, W_r] \cdot \left[\frac{\partial}{r\partial\theta}, \frac{\partial}{\partial z}, \frac{\partial}{\partial r}\right]$$

Therefore, the component equation of motion in terms of coordinates m and θ is

$$\frac{1}{2}\frac{\partial W_m^2}{\partial \theta} - \vec{W}_m \cdot \nabla (rW_u + \omega r^2) = 0$$

or equivalently,

$$\frac{\partial W_m}{\partial \theta} - W_u \frac{dr}{dm} - r\frac{\partial W_u}{\partial m} - 2\omega r \frac{dr}{dm} = 0$$

The last equation is the same as Equation 13.

Stream function and the blade-to-blade flow equation. The blade-to-blade flow equation for a given axisymmetric stream surface involves two unknown velocity components, W_u and W_m. A second relation which is available is the continuity equation. For the two-dimensional stream surface, a stream function, ψ, can be defined satisfying continuity. Consider, as shown in Figure 5, two stream sheets taken from axisymmetric stream surfaces and S' infinitesimally close to each other. The normal distance between the surfaces at a given axial station is dn. The stream sheets S and S' in Figure 5 are bounded by lines of intersection with m-surfaces in the axial direction, and by meridional planes in the circumferential direction.

A dimensionless thickness function, $\tau(m)$, for an annular stream tube with a mean stream surface S is defined by $\tau = dn/dn_i$, where i is the inlet station in the flow. Next, the volume rate of flow through the area element of dimensions τdn_i by $rd\theta$ taken from a cut in the stream tube made by an m-surface is

$$\frac{\partial \psi}{\partial \theta} d\theta = (\tau r d\theta dn_i) W_m$$

Similarly, for an area element of length dm and average depth τdn_i taken from a cut made in the stream tube by a meridional plane, the volume rate of flow is

$$\frac{\partial \psi}{\partial m} dm = -(\tau dm dn_i) W_u$$

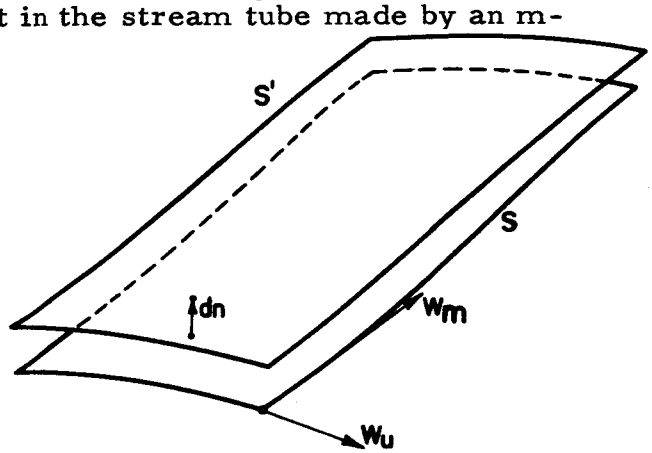

Figure 5. Stream surfaces.

From these two preceding relations the velocity components are expressed in terms of the stream function as

$$W_m = \frac{1}{\tau r dn_i} \frac{\partial \psi}{\partial \theta} \tag{14}$$

$$W_u = -\frac{1}{\tau dn_i} \frac{\partial \psi}{\partial m} \tag{15}$$

Therefore, substitution in Equation 13 for W_m and W_u yields

$$\frac{\partial}{\partial \theta}\left(\frac{1}{\tau r dn_i} \frac{\partial \psi}{\partial \theta}\right) + r \frac{\partial}{\partial m}\left(\frac{1}{\tau dn_i} \frac{\partial \psi}{\partial m}\right) + \frac{1}{\tau dn_i} \frac{\partial \psi}{\partial m} \frac{dr}{dm} - 2\omega r \frac{dr}{dm} = 0$$

which simplifies to

$$\frac{1}{r^2} \frac{\partial^2 \psi}{\partial \theta^2} - \left(\frac{1}{\tau} \frac{d\tau}{dm} - \frac{1}{r} \frac{dr}{dm}\right) \frac{\partial \psi}{\partial m} + \frac{\partial^2 \psi}{\partial m^2} - 2\omega \tau dn_i \frac{dr}{dm} = 0 \tag{16}$$

Equation 16 is the final form of the blade-to-blade flow equation desired. What is involved, then, in solving for the flow pattern through a blade row is integration of Equation 16 with ψ satisfying appropriate boundary conditions. Note that rotational speed has no bearing on the solution for ψ if the stream surfaces are coaxial cylinders $\left[\frac{dr}{dm} = 0\right]$. Also, if τ is constant (equal to unity) and the stream surfaces are coaxial cylinders then the equation is the well-known Laplace equation for plane flow. In the next section, Flow Equation in Dimensionless Form, the flow equation is expressed in dimensionless terms, and the boundary conditions which are imposed on the stream function by the blade-to-blade flow are discussed.

Flow equation in dimensionless form. There are two reasons for making the blade-to-blade flow equation and boundary conditions dimensionless. First, by eliminating the "size and speed" of the machine from the equations, these two items do not have to be specified in a problem. Second, the results obtained from the solution are also dimensionless and can be applied to any one of a set of geometrically similar machines.

Equation 16 may be temporarily rewritten with the dimensional terms as "starred" quantities:

$$\frac{1}{r^{*2}} \frac{\partial^2 \psi^*}{\partial \theta^2} - \left(\frac{1}{\tau} \frac{d\tau}{dm^*} - \frac{1}{r^*} \frac{dr^*}{dm^*}\right) \frac{\partial \psi^*}{\partial m^*} + \frac{\partial^2 \psi^*}{\partial m^{*2}} - 2\omega^* \tau dn_i^* \frac{dr^*}{dm^*} = 0$$

The following (un-starred) dimensionless terms are now defined, and are used exclusively in the remaining treatment:

$$\text{stream function, } \psi = \frac{\psi^*}{\omega^* r_t^{*2} dn_i^*}$$

$$\text{radius ratio, } r = \frac{r^*}{r_t^*}$$

$$\text{length parameter, } m = \frac{m^*}{r_t^*}$$

$$\text{flow coefficient, } W_m = \frac{W_m^*}{\omega^* r_t^*}$$

$$\text{whirl coefficient, } W_u = \frac{W_u^*}{\omega^* r_t^*}$$

In these definitions r_t is a reference radius of the machine.

Substitution for the "starred" terms in the preceding differential equation gives the dimensionless form of the equation:

$$\frac{1}{r^2}\frac{\partial^2\psi}{\partial\theta^2} - \left(\frac{1}{\tau}\frac{d\tau}{dm} - \frac{1}{r}\frac{dr}{dm}\right)\frac{\partial\psi}{\partial m} + \frac{\partial^2\psi}{\partial m^2} - 2\tau\frac{dr}{dm} = 0 \qquad (17)$$

Boundary conditions. In Figure 6, a given axisymmetric relative stream surface has been mapped into a plane for purposes of calculations in the blade-to-blade flow solution. The blade profiles shown are those as cut in the stream surface by the blades. The mapping is conformal, the y-axis corresponding to the θ- coordinate, and the x-axis to the m-coordinate for the stream surface.

Conformability of the mapping in the computing plane is necessary for representation of the repeat of the flow pattern and boundary conditions every blade space around the blade row. Hence, a scale factor which varies with m (or x) is required, except in the case of a cylindrical stream surface which can be simply unwrapped to form a plane with a constant scale.

The boundaries of the flow field to be considered are formed by the suction (s) and pressure (p) surfaces of the blades, and by the lines extending upstream and downstream from the blade leading and trailing edges, respectively. The boundaries s_i and s_o are arbitrarily drawn boundaries and are not necessarily lines of constant y as shown in Figure 6. Boundary p_i has been drawn so that at all points it is displaced vertically $\frac{2\pi r}{n}$ units from s_i where n is the number of blades in the blade row. Similarly, boundary p_o is $\frac{2\pi r}{n}$ units from boundary s_o. Except for the two boundaries s and p inside the blade row these boundaries are not streamlines. The lines i and o are traces cut in the stream surface by two radial planes located far enough up-

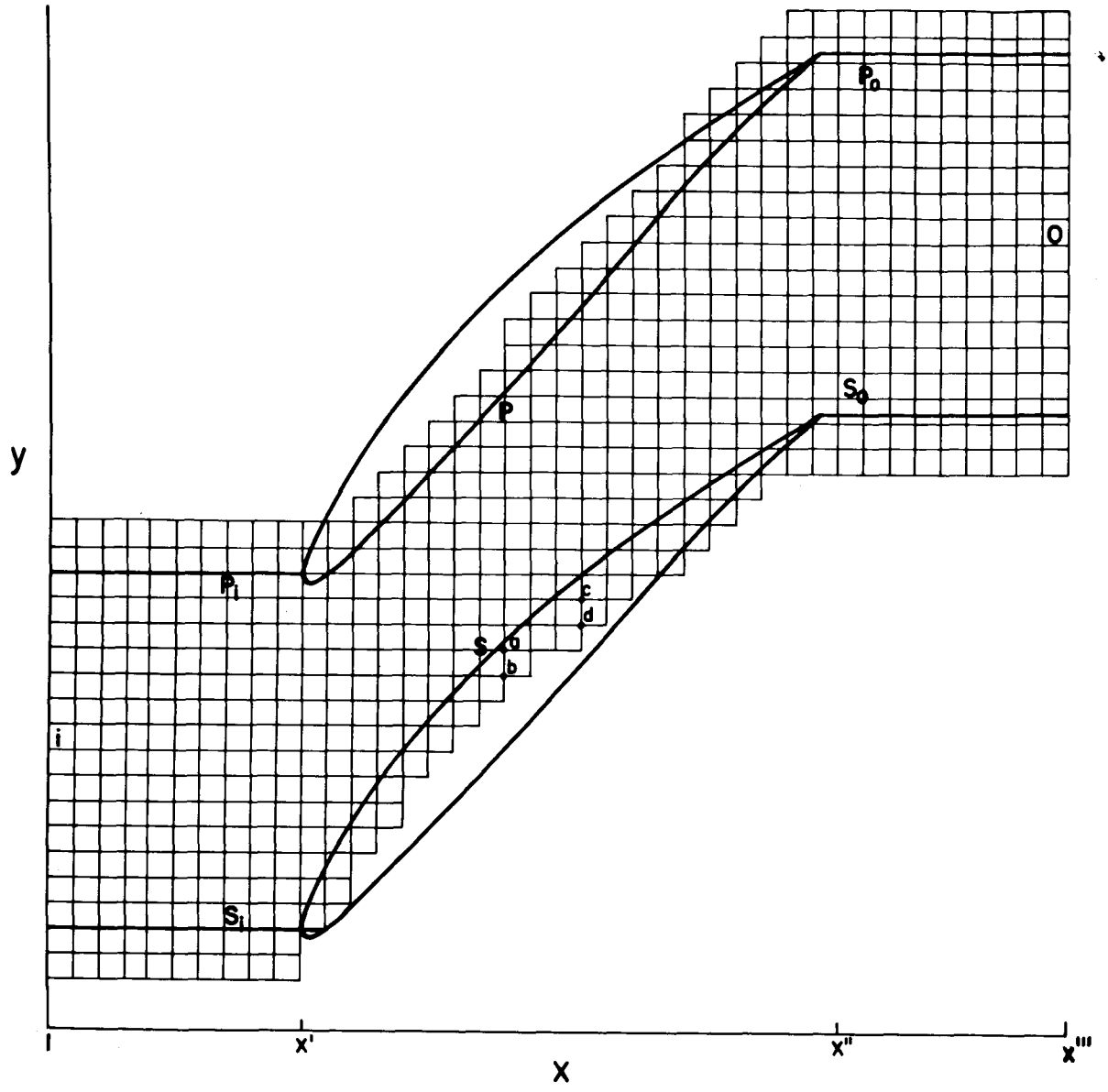

Figure 6. Flow field for an axisymmetric stream surface past adjacent blades in a blade row. A computing mesh for numerical solution is also shown.

stream and downstream so that the flow is essentially uninfluenced by the blades.

By definition, the stream function ψ has constant values on the boundaries p and s. We can arbitrarily assign one of the boundary values and solve for the other based on the operating point of the machine. Therefore, letting ψ on boundary s equal zero ($\psi_s = 0$) and referring back to the previous discussion of the stream function, the flow coefficient at station i can be computed on the basis of Equation 14 in dimensionless form as

$$W_{m,i} = \frac{1}{r_i} \frac{\partial \psi_i}{\partial \theta}$$

If this equation is integrated with respect to θ from the streamline for $\psi = 0$ to the streamline for $\psi = \psi_p$ (the two streamlines are $\frac{2\pi}{n}$ units of θ apart), the value of ψ on the p-boundary is obtained:

$$\psi_p = \frac{2\pi}{n} r_i W_{m,i} \tag{18}$$

At the boundaries i and o the flow is axisymmetric and assumed known based on assigned flow rate, flow inlet angle, and blade loading. Hence, based on the known constant flow and whirl coefficients at these boundaries, the necessary boundary conditions on ψ can be computed from Equations 14 and 15 as

$$\frac{\partial \psi_i}{\partial \theta} = r_i W_{m,i} \tag{19}$$

$$\frac{\partial \psi_o}{\partial \theta} = \tau_o r_o W_{m,o} = \frac{W_{m,i}}{W_{m,o}} r_i W_{m,o} = r_i W_{m,i} \tag{20}$$

$$\frac{\partial \psi_i}{\partial m} = - W_{u,i} \tag{21}$$

$$\frac{\partial \psi_o}{\partial m} = - \tau_o W_{u,o} \tag{22}$$

The remaining boundary conditions are those placed on ψ outside the blade row, but inside the boundaries i and o. In this region the locations of the streamlines are not known until the problem has been solved. It is known, however, that there are two streamlines, one for which $\psi = 0$, and a second one for $\psi = \psi_p$ displaced circumferentially $\frac{2\pi r}{n}$ units away. That is, there is a circumferential periodicity of the flow. Actually the flow is completely periodic outside the blade row since the flow pattern at any point is duplicated at another point $\frac{2\pi r}{n}$ units away. Therefore, as the final boundary conditions the periodicity conditions may be expressed for pairs of points on boundaries

s_i , p_i and on boundaries s_o , p_o by

$$\psi_{(p_i)} = \psi_{(s_i)} + \psi_p \tag{23}$$

$$\psi_{(p_o)} = \psi_{(s_o)} + \psi_p \tag{24}$$

NUMERICAL SOLUTION METHOD

One is often obliged to turn to a numerical method to obtain an approximate solution to a boundary value problem for which the boundary values are not given by simple analytical expressions. Such is the case here in determining the stream function in the blade-to-blade flow problem. The most universal numerical method is the method of finite differences. In this method the continuous region denoting the flow field is replaced by a set of discrete points and the differential equation is replaced at each point by an approximating difference equation. The problem is thus reduced to the solution of a system of algebraic equations. The procedure covers the flow region by a net of discrete points and marks off a polygonal contour so that it sufficiently approximates the boundary. The region in which the solution of the difference equation is sought is formed by the lattice points of the net with the polygonal boundary. The assigned boundary values on the original boundary are transferred through extrapolations to lattice points on the polygonal boundary.

For approximations using dense nets the number of algebraic equations is so large that direct methods, which would yield the exact solution after a finite number of steps if no round-offs were effected, are impractical. Therefore methods which are basically iterative are resorted to. The main disadvantage of all numerical techniques, whether direct or iterative, is that they give numerical values for unknown functions at a set of discrete points instead of analytical expressions defined over the region.

Following in this section are the details of the numerical solution for the blade-to-blade flow problem. The layout of the computing mesh for the flow field and the finite difference expression of the flow equation are presented, followed by discussion of numerical treatment of the boundary conditions and differentiation of the stream function for flow velocities. Organization of the solution method for computer application along with sample solutions are presented in the later section, Application of the Numerical Solution Method.

Finite Difference Mesh

Once the blade channel formed by the intersection of the axisymmetric stream surface and two adjacent blades in the blade row has been laid out to a convenient scale (prefereably a large scale) a square lattice or mesh of computing points is constructed over the flow field (see Figure 6.) The

meridional coordinate of the computing mesh is x and the circumferential coordinate y. Boundary i corresponds to x = 1 and boundary o to x = x'''. The extent of the computing mesh in the y direction is from y = 1 to y = y'''. The mesh is constructed so that the forward-most edge of the blade profile lies on a mesh point. The x-coordinate of this point is designated as x'. The x-coordinate of the rear or trailing edge of the blade profile is, in general, not a mesh point.

For purposes of locating the boundaries in the solution method and for identification of particular regions in the flow field the following definitions are made (see Figures 6 and 7):

a. one mesh division in x or y directions is a distance of one unit, regardless of the scale used in constructing the blade profiles and flow field;

b. the point (x, y_p) is a mesh point on the p_i, p, p_o boundary, or is the first mesh point inside if there is no mesh point on the boundary for the particular integer x;

c. the point (x, y_s) is a mesh point on the s_i, s, s_o boundary, or is the first mesh point outside if there is no mesh point on the boundary for the particular integer x;

d. $\Delta_p(x)$ and $\Delta_s(x)$ are the positive y-distances from the mesh points (x, y_p) to the p_i, p, p_o boundary and the mesh points (x, y_s) to the s_i, s, s_o boundary, respectively. According to this definition, $0 \leq \Delta_p(x) < 1$ and $0 \leq \Delta_s(x) < 1$;

e. the integer x'' is the x-coordinate of the first "panel" of mesh points downstream of the trailing edge of the blade.

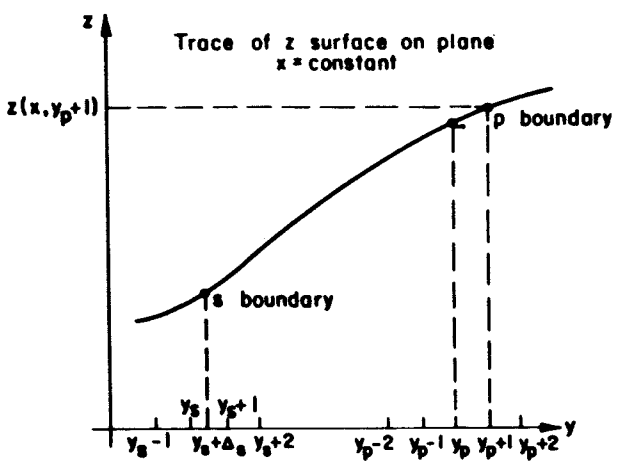

Figure 7. Trace of z (scaled stream function) surface in a constant x-panel illustrating mesh point definitions and extrapolations to exterior points. (An extrapolation to z $(x, y_p + 1)$ is shown.)

Scaling for Computation

The value ψ_s for the stream function on the boundary s has already been assigned as zero. Also the value ψ_p for the stream function on boundary p has been evaluated in Equation 18. As far as the streamline pattern determined in the blade-to-blade flow is concerned, it is immaterial what the actual values of ψ_s and ψ_p are. It is advantageous in the solution method to scale the equations so that calculations involve constant values of ψ_s and ψ_p and a constant mesh division of unity. Accordingly, a mesh scale factor k_2 and a stream function scale k_3 may be defined by the relations,

$$x = k_2 m \quad , \quad y = k_2 r\theta \tag{25a}$$

and

$$z = k_3 \psi \tag{25b}$$

The value of k_2 for any x can be determined from the constructed flow field and computing mesh according to

$$k_2 (x) = \frac{[y_p (1) - y_s (1) + \Delta_p (1) - \Delta_s (1)]n}{2\pi r(x)} \tag{26a}$$

Next, letting z = 100, say, correspond to the value ψ_p, then

$$k_3 = \frac{100}{\psi_p}$$

Substitution for ψ_p from Equation 18 yields

$$k_3 = \frac{15.915n}{r_i \, W_{m,i}} \tag{26b}$$

The flow equation, Equation 17, and the remaining boundary conditions, Equations 19 through 24, when scaled by the factors k_2 and k_3 become

$$\frac{\partial^2 z}{\partial y^2} - N (x) \frac{\partial z}{\partial x} + \frac{\partial^2 z}{\partial x^2} - P (x) = 0 \tag{27}$$

where the parameters N and P are defined as

$$N (x) = \frac{1}{k_2} \left(\frac{1}{\tau(x)} \frac{d\tau}{dm} \bigg|_x - \frac{1}{r(x)} \frac{dr}{dm} \bigg|_x \right)$$

and

$$P (x) = \frac{2k_3}{k_2^2} \tau(x) \frac{dr}{dm} \bigg|_x$$

$$\frac{\partial z}{\partial y} \bigg|_{x=1} = \frac{100}{y_p (1) - y_s (1) + \Delta_p (1) - \Delta_s (1)} \tag{28}$$

$$\frac{\partial z}{\partial y} \bigg|_{x=x'''} = \frac{100}{y_p(x''') - y_s(x''') + \Delta_p(x''') - \Delta_s(x''')} \tag{29}$$

$$\left.\frac{\partial z}{\partial x}\right|_{x=1} = -\frac{k_3}{k_2} W_{u,i} \tag{30}$$

$$\left.\frac{\partial z}{\partial x}\right|_{x=x'''} = -\frac{k_3}{k_2} \tau_o W_{u,o} \tag{31}$$

$$z(x, y_p + \Delta_p) = z(x, y_s + \Delta_s) + 100, \quad (1 < x < x', x'' \leq x < x''') \tag{32}$$

Note that a change in the operating point of the blade row results in no change of the values of z on the blade profile boundaries s and p, but in the boundary conditions, Equations 30 and 31, and in the parameter p of the flow equation itself. This set of equations thus constitutes the boundary value problem in form for numerical solution for the direct blade-to-blade flow problem with a given axisymmetric stream surface and a given set of velocity triangles far upstream and downstream of the blade row. It remains to express Equation 27 in finite difference form.

Flow Equation in Finite Difference Form

To express Equation 27 in finite difference form, consider the lattice point (x, y) and its four equidistant neighbor points (x + 1, y), (x-1, y), (x, y + 1), and (x, y-1). The values of the derivatives in Equation 27 may be approximated by the difference quotients used in the definitions of the derivatives. Hence, using the four neighbor points to the point (x, y), Equation 27 may be approximated by

$$z(x, y+1) + z(x, y-1) - 2z(x, y) + \frac{1}{2} N(x)\, z(x-1, y) - \frac{1}{2} N(x)\, z(x+1, y) + z(x-1, y) + z(x+1, y) - 2z(x,y) - P(x) = 0$$

The approximation is of the order h^3, where h is the distance represented by a unit distance in the x, y coordinates. Rearrangement of the equation gives the approximation to the value of z (x, y) in terms of the z values at the neighbor points:

$$z(x, y) = \frac{2 + N(x)}{8} z(x - 1, y) + \frac{2 - N(x)}{8} z(x + 1, y) + \frac{1}{4} z(x, y - 1) + \frac{1}{4} z(x, y + 1) - \frac{1}{4} P(x) \quad (33)$$

The coefficient matrix for the system of equations generated by Equation 33 in approximating the flow equation at the interior points of the flow field is sparse and diagonally dominant. Such systems of equations are generally well-suited for iterative solution by the method of Gauss-Seidel (10). This was the method used in obtaining the blade-to-blade solutions.

Equation 33 as written, expressing the value of z at an interior point (x, y) is in a form ready for iteration. To perform the iterations, according to Gauss-Seidel an approximate initial set of z (x, y) values is first obtained for the mesh points at which integration is to be made and also at points exterior to the flow boundaries which serve as neighbor points to interior points in the vicinity of the boundaries. Next, a new set of z (x, y) values at interior points is computed from Equation 33 by marching up successive values of y located in panels of constant x values. New values are estimated for z at exterior neighboring points on the basis of the new z values at the interior points, and the cycle is repeated until the absolute value of the difference between the newly integrated and the old value of z at any mesh point is less than some arbitrarily assigned tolerance. Observe in this iterative scheme that not all neighbor points to a given central point at which integration is being performed have old z values, but that the new values of z are incorporated as soon as they become available.

The Gauss-Seidel method is closely related to "relaxation" methods (29) which have found wide application in engineering and physics. The successive corrections to the solution in the two methods are determined in the same way. However, residuals at mesh points, which are "relaxed" in the course of iterations in the relaxation solution are not specifically examined in the Gauss-Seidel method. Whereas the latter method is cyclic in nature and easy to program for a computer, relaxation is not cyclic and thus poorly suited for computer solution.

Range of integration. The range of points in any one constant x-panel over which integration of Equation 33 takes place covers less than a blade space (see Figure 6.) For constant x-panels located outside the blade row ($1 < x < x'$, $x'' \leq x < x'''$) with $\Delta_p(x) \neq 0$, integration is made at mesh points $y(x)$; $y_s(x) \leq y(x) \leq y_p(x)$. If $\Delta_p(x) = 0$ for an x-panel outside the blade row, then integration ranges over the mesh points $y(x)$; $y_s \leq y(x) < y_p(x) - 1$. For constant x-panels located within the blade row ($x' \leq x \leq x'' - 1$) with $\Delta_p(x) \neq 0$, integration is over the mesh points $y(x)$; $y_s(x) + 1 \leq y(x) \leq y_p(x)$. If $\Delta_p(x) = 0$, then integration ranges over the points $y(x)$; $y_s(x) + 1 \leq y(x) \leq y_p(x) - 1$. Additional discussion of the range of integration is presented in the section, Numerical Treatment of the boundary conditions.

Initialization of stream function. The initialization of the scaled stream function, $z(x, y)$, is made by fitting a linear curve through the two points $z(x, y_s + \Delta_s) = 0$, and $z(x, y_p + \Delta_p) = 100$. Hence,

$$z(x,y) = \frac{100\,[y - y_s(x) - \Delta_s(x)]}{y_p(x) - y_s(x) + \Delta_p(x) - \Delta_s(x)} \tag{34}$$

evaluated for $x = 2, 3, \ldots, x''' - 1$, and $y = y_s(x) - 2, y_s(x) - 1, \ldots, y_p(x) + 2$ provides the initial approximation to the set of $z(x, y)$ values with which to begin the iterations. The $z(x, y)$ values along $x = 1$ and $x = x'''$ are, of course, fixed by the boundary conditions implied in the assigned fluid velocities.

Numerical Treatment of the Boundary Conditions

In applying Equation 33 at a mesh point located on or in the neighborhood of the flow boundary, a neighbor point exterior to the boundary is required. Hence, the boundary value of z is the assigned value used in the interpolation procedure between interior and exterior mesh points along a constant x-panel. This is the case whether the boundary point for that value of x is regular (a mesh point) or irregular. In addition, for integration at some mesh points, depending on the combination of blade profile and lattice construction, it may be that a second mesh point along a constant x-panel and located more than one mesh division beyond the boundary is required as a left-hand $(x - 1, y)$ or right-hand $(x + 1, y)$ point neighboring an integration point located near the boundary. In this case the interpolated boundary value should be thought of in terms of an interpolation along the panel of constant y (instead of constant x) involving only one mesh point exterior to the boundary. However, to keep the treatment of the boundary condition as simple as possible, interpolations along panels of constant x are made only, involving the first and second exterior mesh points. This procedure should accommodate most blade profiles and setting angles. The interpolation of the boundary values in effect extrapolates the flow beyond the actual boundaries to pseudo boundaries defined by the exterior mesh points.

An interpolation formula which is a polynomial of degree n or less taking on the same values as the given function for $(n + 1)$ equally-spaced abscissas $y_o, y_o + 1, \ldots, y_o + n$ can be derived as follows: According to the definition of the so-called shift-operator E (10), the function value at the point $(y_o + \delta)$ can be expressed in terms of the value at the point by writing

$$f(y_o + \delta) = E^{\delta} f(y_o) \tag{35a}$$

and, in particular

$$f(y_o + 1) = Ef(y_o), \qquad f(y_o + 2) = E^2 f(y_o)$$

and so on. The first difference expressed for the function at the point x_o is (10)

$$\Delta f\ (y_o) = f\ (y_o + 1) - f\ (y_o)$$

It follows that if Δ is thought of as an operator, then

$$\Delta = E - 1 \tag{35b}$$

Hence, Equation 35a rewritten in terms of Δ becomes

$$f\ (y_o + \delta) = (1 + \Delta)^{\delta} f(y_o) = \left[1 + \delta\Delta + \frac{\delta(\delta-1)}{2}\Delta^2 + \ldots\right] f(y_o) \tag{35c}$$

where Δ raised to the ascending powers represents progressively higher-order difference operators (for example, $\Delta^2 f(y_o) = f(y_o + 2) - 2f(y_o + 1) + f(y_o)$). Finally then, given (n + 1) ordinate values, differences up through the nth order can be taken, Equation 35c becoming a polynomial of degree n. Alternatively, the differences Δ through Δ^n can be replaced according to Equation 35b, the resultant polynomial being one which displays the (n + 1) ordinates explicitly.

The actual extrapolation calculations are arranged for convenience into six different cases which derive from the various combinations for the locations of the mesh points (x , y_p) and (x, y_s). These combinations depend upon location of the constant x-panel inside or outside the blade row, and upon whether or not the points (x, y_p) and (x, y_s) are regular.

Outside the blade row. Consider the periodicity conditions, Equations 23, 24. For the case $\Delta_s(x)$ and $\Delta_p(x)$ non-zero for the particular x-panel, the range of integration has been defined previously as (x, y_s), (x, y_s + 1), . . . , (x, y_p). Hence, extrapolation to the second exterior points beyond the boundaries requires the extrapolated values z (x, y_p + 1), z (x, y_p + 2) and z (x, y_s - 1). To satisfy Equation 32 the extrapolations cited are made by interpolation at interior points one blade space away near the opposite boundary. These interpolated values are, in relation to the required extrapolated values,

$$z\ (x, y_s + \Delta + j) = z\ (x, y_p + j) - 100 \quad j = 1, 2$$

$$z\ (x, y_p - \Delta - 1) = z\ (x, y_s - 1) + 100 \tag{36a}$$

where

$$\Delta = \Delta_s(x) - \Delta_p(x)$$

The interpolations are accomplished using three mesh points in the interpolation formula, Equation 35c. Considering for the moment three unit-spaced generic points (x, y_o), $(x, y_o + 1)$ and $(x, y_o + 2)$ with x constant, Equation 35c gives for the value z at the interpolation point $(x, y_o + \delta)$ among the three given points

$$z(x, y_o + \delta) = \frac{1}{2}(\delta - 1)(\delta - 2)\, z(x, y_o) \tag{37}$$

$$+ (2 - \delta)(\delta)\, z(x, y_o + 1) + \frac{1}{2}(\delta)(\delta - 1) z(x, y_o + 2)$$

Therefore, letting the base generic point (x, y_o) be in turn the points (x, y_s), $(x, y_s + 1)$, $(x, y_p - 2)$ and letting δ take on the values $(1 + \Delta)$, $(1 + \Delta)$, $(1 - \Delta)$ respectively, the solution of Equations 36 and 37 with appropriate substitution of z values as indicated gives

$$z(x,y_p + 1) = K_1 z(x,y_s) + K_2 z(x,y_s + 1) + K_3 z(x,y_s + 2) + 100 \tag{38a}$$

$$z(x,y_p + 2) = K_1 z(x,y_s + 1) + K_2 z(x,y_s + 2) + K_3 z(x,y_s + 3) + 100 \tag{38b}$$

$$z(x,y_s - 1) = K_3 z(x,y_p - 2) + K_2 z(x,y_p - 1) + K_1 z(x,y_p) - 100 \tag{38c}$$

where

$$K_1 = K_1(x) = \frac{1}{2}\Delta\,(\Delta - 1) \tag{39a}$$

$$K_2 = K_2(x) = 1 - \Delta^2 \tag{39b}$$

$$K_3 = K_3(x) = \frac{1}{2}\Delta(1 + \Delta) \tag{39c}$$

To review, these last six equations give the extrapolations required along an

x-panel outside the blade row for which $\Delta_s(x)$, $\Delta_p(x) \neq 0$.

If for the particular x-panel under consideration $\Delta_s(x) \neq 0$, $\Delta_p(x) = 0$, then according to the defined range of integration the extrapolated values required are $z(x, y_p)$, $z(x, y_p + 1)$, $z(x, y_p + 2)$, and $z(x, y_s - 1)$. Hence, in addition to the extrapolations provided by Equations 38 an additional equation giving the value $z(x, y_p)$ is needed. This equation is obtained from Equation 36a with $j = 0$ and Equation 37 with the generic point (x, y_o) corresponding to the point (x, y_s) and with $\delta = \Delta$. The resultant equation after appropriate substitution of z values is

$$z(x,y_p) = K_4 z(x,y_s) + K_5 z(x,y_s + 1) + K_1 z(x,y_s + 2) + 100 \tag{40}$$

where

$$K_4 = K_4(x) = \frac{1}{2}(\Delta - 1)(\Delta - 2) \tag{41a}$$

$$K_5 = K_5(x) = \Delta(2 - \Delta) \tag{41b}$$

Lastly, if $\Delta_s(x) = 0$, then in addition to Equation 38c, extrapolation to the value $z(x, y_s - 2)$ at the second exterior point to the s_i-boundary is required. It can be easily shown that

$$z(x,y_s - 2) = K_3 z(x,y_p - 3) + K_2 z(x,y_p - 2) + K_1 z(x,y_p - 1) - 100 \tag{42}$$

The final boundary conditions to be satisfied outside the blade row are those at the inlet and outlet stations to the blade row, i.e., Equations 28 and 29 associated with the given flow rate through the blade row and Equations 30 and 31 concerning the given whirl coefficients. Equations 28 and 29 are satisfied by a linear distribution of z determined over mesh points in the panels $x = 1$ and $x = x'''$ according to

$$z(1,y) = z(1,y_s + \Delta_s) + \frac{100[y - y_s(1) - \Delta_s(1)]}{y_p(1) - y_s(1) + \Delta_p(1) - \Delta_s(1)} \tag{42a}$$

$$z(x''',y) = z(x''',y_s+\Delta_s) + \frac{100[y-y_s(x''')-\Delta_s(x''')]}{y_p(x''')-y_s(x''')+\Delta_p(x''')-\Delta_s(x''')}$$

in which the range of z over one blade space is 100 as required, and

$z(1, y_s + \Delta_s)$, $z(x''', y_s + \Delta_s)$ are arbitrarily assigned base values. To satisfy Equations 30 and 31, appropriate adjustments in the base values $z(1, y_s + \Delta_s)$ and $z(x''', y_s + \Delta_s)$ are required. However, if such adjustments are made a continual change in the boundary values of z along $x = 1$ and $x = x'''$ results as the iterations proceed; the system of equations is overdetermined if both sets of boundary conditions, Equations 28 and 29, 30 and 31 are applied. Thus Equations 30 and 31 are ignored in the solution method with the result that the inlet and outlet whirl coefficients are calculated only after the solution has been obtained.

Inside the blade row. The values of z required at points exterior to the s-boundary inside the blade row for a particular constant x-panel and for $\Delta_s(x)$ not zero are $z(x, y_s)$ and $z(x, y_s - 1)$. (For example points a, b in Figure 6.) These values are obtained from extrapolations using three points: the first two points interior to the s-boundary and the boundary value, $z(x, y_s + \Delta_s) = 0$. Hence, solution of Equation 37 for $z(x, y_o)$ with base point (x, y_o) corresponding to point (x, y_s) and δ equal to $\Delta_s(x)$ gives

$$z(x,y_s) = \frac{2\Delta_s(x)}{\Delta_s(x) - 1} z(x,y_s + 1) + \frac{\Delta_s(x)}{2 - \Delta_s(x)} z(x,y_s + 2) \qquad (44a)$$

and likewise with base point (x, y_o) corresponding to point $(x, y_s - 1)$ and δ equal to $1 + \Delta_s(x)$,

$$z(x,y_s-1) = \frac{2(1+\Delta_s(x))}{\Delta_s(x)} z(x,y_s) + \frac{1+\Delta_s(x)}{1-\Delta_s(x)} z(x,y_s + 1) \qquad (44b)$$

Note that Equation 44 as written requires that Equation 44a be solved first since the value $z(x, y_s)$ is required in Equation 44b. If $\Delta_s(x) = 0$, then extrapolation to z values at the exterior points $(x, y_s - 1)$ and $(x, y_s - 2)$ are required. (For example, points c, d in Figure 6.) Since the exterior, interior and boundary points are now all equidistant, direct solutions of Equation 37 with point (x, y_o) corresponding to (x, y_s) and $\delta = -1$, and point (x, y_o) corresponding to $(x, y_s - 1)$ and $\delta = -1$ give, respectively,

$$z(x,y_s - 1) = -3z(x,y_s + 1) + z(x,y_s + 2) \qquad (45a)$$

$$z(x,y_s - 2) = 3z(x,y_s - 1) + z(x,y_s + 2) \qquad (45b)$$

As was the case with Equations 44, extrapolation is performed solving Equation 45a first.

If the three generic points (x, y_o), $(x, y_o + 1)$ and $(x, y_o + 2)$ are reordered in the negative y-direction, then the extrapolations to the two exterior points to the p-boundary inside the blade row for a particular constant x-panel can be obtained in a fashion entirely analogous to that just described for the s-boundary. Thus where $\Delta_p(x)$ is not zero, solving once again for $z(x, y_o)$ from Equation 37 and letting that value correspond in turn to $z(x, y_p + 1)$ and $z(x, y_p + 2)$ with δ as $1 - \Delta_p(x)$ and $2 - \Delta_p(x)$ respectively, one obtains

$$z(x,y_p + 1) = \frac{200}{(1+\Delta_p(x))\Delta_p(x)} + \frac{2(\Delta_p(x)-1)}{\Delta_p(x)} z(x,y_p) + \frac{1 - \Delta_p(x)}{1 + \Delta_p(x)} z(x,y_p - 1) \tag{46a}$$

and

$$z(x,y_p + 2) = \frac{200}{(\Delta_p(x)-1)\Delta_p(x)} + \frac{2(2-\Delta_p(x))}{1-\Delta_p(x)} z(x,y_p + 1) + \frac{2 - \Delta_p(x)}{\Delta_p(x)} z(x,y_p) \tag{46b}$$

If $\Delta_p(x) = 0$ (analogous to the s-boundary situation with $\Delta_s(x) = 0$) then

$$z(x,y_p + 1) = 300 - 3z(x,y_p - 1) + z(x,y_p - 2) \tag{47a}$$

$$z(x,y_p + 2) = 3z(x,y_p + 1) - 300 + z(x,y_p - 1) \tag{47b}$$

Examination of Equations 44 through 47 reveals that in each equation at least one coefficient larger than unity in absolute value and, in some instances, coefficients appreciably larger than unity appear if $\Delta_s(x)$ or $\Delta_p(x)$ is close to unity or close to zero. These large coefficients, which cause instability of the iterations through multiplication of current errors in z values, cannot be used except for possibly the final iteration after sufficient convergence of the solution. The instability can be essentially eliminated by replacing the extrapolations in Equations 44 through 47 by linear curve fits, which are lower order, and which use an interior point (not necessarily the first interior point) near the boundary along with the assigned boundary value. The resulting coefficients in the linear curve fit equations are at most 2 in absolute value. These new equations for extrapolations beyond the s-boundary are $(\Delta_s(x) \neq 0)$

$$z\ (x, y_s) = c_1\ z\ (x, y_s + 2) \tag{48a}$$

$$z\,(x,\ y_s - 1) = c_2\ z\,(x,\ y_s + 2) \tag{48b}$$

where

$$c_1 = \frac{\Delta_s(x)}{\Delta_s(x) - 2}\ ,\quad c_2 = \frac{1 + \Delta_s(x)}{\Delta_s(x) - 2} \tag{48c}$$

Also,

$$z\,(x,\ y_s - 1) = -z\,(x,\ y_s + 1) \tag{49a}$$

$$z\,(x,\ y_s - 2) = -2z\,(x,\ y_s + 1) \tag{49b}$$

for $\Delta_s(x) = 0$. The new equations for the extrapolations beyond the p-boundary are

$$z\,(x,\ y_p + 1) = c_3 + c_4\ \ z\,(x,\ y_p - 1) \tag{50a}$$

$$z\,(x,\ y_p + 2) = c_5 + c_6\ \ z\,(x,\ y_p - 1) \tag{50b}$$

where

$$c_3 = \frac{200}{1 + \Delta_p(x)}\ ,\quad c_4 = \frac{\Delta_p(x) - 1}{\Delta_p(x) + 1}\ ,$$

$$c_5 = \frac{300}{1 + \Delta_p(x)}\ ,\quad c_6 = \frac{\Delta_p(x) - 2}{1 + \Delta_p(x)} \tag{50c}$$

Differentiation of Stream Function and Calculation of Head Coefficient

Equation B1 in APPENDIX B evaluated along the blade profile boundaries gives the distribution of head coefficient along those boundaries. The evaluation is made in terms of the change in head coefficient from its value at the inlet station to the blade row. As seen in Equations B1 and B3 the value of inlet flow coefficient and the ratio of local to inlet value of flow coefficient along the blade boundaries are required. The flow coefficient can be computed from Equation 14 in terms of stream function, stream surface thickness ratio and radius ratio (as these terms are defined for Equation 17)

$$W_m = \frac{1}{\tau r} \frac{\partial \psi}{\partial \theta}$$

This equation in terms of the scaled stream function, z, and computing coordinate y becomes (see Equation 25)

$$W_m = \frac{k_2}{k_3 \tau} \frac{\partial z}{\partial y} \tag{51a}$$

The values of the derivative in Equation 51a at stations along the blade profile boundaries can be approximated by numerically differentiating z at mesh points (which are of course equally-spaced) along constant x-panels in the neighborhood of the profile boundaries, followed by interpolation of the resulting derivative function for the required values at the profile boundaries. The derivatives at mesh points are approximated by formally differentiating the interpolation polynomial in Equation 35c with respect to δ followed by substitution of the δ which corresponds to the mesh point. If the points (x, y_o), $(x, y_o + 1)$, . . . , $(x, y_o + 4)$ are used (the approximating polynomial is of fourth degree), then differentiation of Equations 35c and evaluation at the mesh points $(x, y_o + 1)$, $(x, y_o + 2)$, $(x, y_o + 3)$ yields the approximations in terms of the ordinates

$$\left.\frac{\partial z}{\partial y}\right|_{(x,y_o+1)} = \frac{1}{12}[-3z(x,y_o) - 10z(x,y_o+1) + 18z(x,y_o+2) - 6z(x,y_o+3) + z(x,y_o+4)] \tag{51b}$$

$$\left.\frac{\partial z}{\partial y}\right|_{(x,y_o+2)} = \frac{1}{12}[z(x,y_o) - 8z(x,y_o+1) + 8z(x,y_o+3) - z(x,y_o+4)] \tag{51c}$$

$$\left.\frac{\partial z}{\partial y}\right|_{(x,y_o+3)} = \frac{1}{12}[-z(x,y_o) + 6z(x,y_o+1) - 18z(x,y_o+2) + 10z(x,y_o+3) + 3z(x,y_o+4)] \tag{51d}$$

Next, by letting the point (x, y_o) in Equations 51b through 51d correspond to the point $(x, y_s - 1)$ inside the blade row, the derivative function is defined at three mesh points in the neighborhood of the s-boundary with a minimum of two points immediately interior to that boundary.

Hence, substitution of the expressions for the derivatives at the three mesh points into the interpolation polynomial in Equation 37 (in which z (x, y) now plays the role of the derivative function) gives for the interpolated value of the derivative at the s-boundary, after considerable algebraic manipulation,

$$12 \left.\frac{\partial z}{\partial y}\right|_{(x,y_s+\Delta_s)} = [(7-3\Delta_s)\Delta_s-3]z(x,y_s-1) + 2[(3\Delta_s-2)\Delta_s-5]z(x,y_s)$$

$$+ 18(1-\Delta_s)z(x,y_s+1) + [(20-6\Delta_s)\Delta_s-6]z(x,y_s+2)$$

$$+ [(3\Delta_s-5)\Delta_s+1]z(x,y_s+3) \qquad (51e)$$

In a fashion entirely analogous to that used to evaluate the derivative of z with respect to y at the s-boundary, evaluation at the p-boundary is made by letting the point (x, y_o) correspond to the point $(x, y_p - 2)$. This results in definition of the derivative function by Equations 51b through 51d at three mesh points in the neighborhood of the p-boundary with a minimum of two points inside the boundary. The value of

$$12 \left.\frac{\partial z}{\partial y}\right|_{(x,\, y_p + \Delta_p)}$$

is readily obtained from Equation 51e by replacing

$$y_s \text{ by } y_p - 1 \text{ and } \Delta_s \text{ by } \Delta_p + 1.$$

APPLICATION OF THE NUMERICAL SOLUTION METHOD

A computer program was written for the numerical solution of the blade-to-blade flow problem based on the techniques discussed in the section NUMERICAL SOLUTION METHOD. Sample solutions obtained using this program are presented following a discussion of the program. A flow diagram of the program is given in APPENDIX E.

Computer Program

Iterative procedures for solving large systems of linear algebraic equations tend, in general, to converge slowly. A technique of over-relaxation (successive-over-relaxation) may be used to accelerate convergence in the Gauss-Seidel method (40). Over-relaxation of Equation 33 requires multiplication of residuals by a relaxation factor, ω. Hence, Equation 33

becomes

$$z'(x,y) = \omega \left[\frac{2 + N(x)}{8} z(x-1,y) + \frac{2 - N(x)}{8} z(x+1,y) \right. \tag{52}$$

$$\left. + \frac{1}{4} z(x,y-1) + \frac{1}{4} z(x,y+1) - \frac{1}{4}P(x)\right] + (1 - \omega)z(x,y)$$

where z' (x, y) is a new, modified value of z (x, y). When the residual is zero the modified and current values are the same. The main difficulty in the method is that of obtaining a good estimate of the optimum relaxation factor (15).

Because of the time disadvantage of performing all iterations in a dense computing mesh, the computer program was written to perform a number of initial and intermediate iterations in less dense meshes prior to the final iterations. The iterations performed in the less-dense meshes require less computing and converge more rapidly. Iterations in the various meshes are designated as the first, second, and third or final pass. The solution method, which has already been explained, applies to each of the passes with the exception that the stream function is initialized prior to the first pass only. In the second and third passes the solution vector obtained from the preceding pass is "expanded and packed" to provide the initial trial vector for the iterations. In going from the first to the second pass, or from the second to the third, the mesh point spacing is halved. Therefore, the expansion and packing operation is essentially the same in either of the mesh refinements.

If elements of the iterated solution vector from the first or second computing pass are designated $\hat{z}$ (i, j), where i = 1, 2, . . ., $\hat{x}'''$, j = 1, 2, . . ., $\hat{y}'''$ ($\hat{x}'''$, $\hat{y}'''$ are the dimensions of the mesh) then the elements may be mapped into every other element of the expanded z matrix giving the initial vector for the next pass. The dimensions of the expanded z matrix are ($2\hat{x}''' - 1$) by ($2\hat{y}''' - 1$). The expansion operation must procede "outside-in". That is, to avoid covering elements stored in the memory of the computer with others during the mapping process, only the outermost elements of the matrix must be moved. The mapping thus takes place according to

$$z\,(2i-1,\ 2j-1) = \hat{z}\,(i,\ j) \quad , \quad i = \hat{x}''', \hat{x}'''-1, \ldots, 1$$

$$j = \hat{y}''', \hat{y}'''-1, \ldots, 1$$

or alternatively

$$z\,(2\hat{x}'''-2i+1,\ 2\hat{y}'''-2j+1) = \hat{z}\,(\hat{x}'''-i+1,\ \hat{y}'''-j+1) \quad , \tag{53}$$

$$i = 1, 2, \ldots, \hat{x}'''$$

$$j = 1, 2, \ldots, \hat{y}'''$$

In Equation 53 the indexing has been arranged in ascending order for purposes of the computer program.

After the mapping has been completed the missing "even" elements of the z matrix in each row and column are "packed-in" according to the following averaging relations:

$$z\,(i+1,\ j) = \frac{1}{2}\,[z\,(i,\ j) + z\,(i+2,\ j)] \tag{54a}$$

where $i = 1,\ 3,\ \ldots,\ 2\hat{x}''' - 3,\ j = 1,\ 3,\ \ldots,\ 2\hat{y}''' - 1$

and

$$z\,(i,\ j+1) = \frac{1}{2}\,[z\,(i,\ j) + z\,(i,\ j+2)] \tag{54b}$$

where $i = 1,\ 3,\ \ldots,\ 2\hat{x}''' - 1,\ j = 1,\ 3,\ \ldots,\ 2\hat{y}''' - 3.$

The special "hat" notation in Equations 53 and 54 is used here only for convenience in describing the mapping relations and is not required in the actual operations in the computer program.

Modification of the input geometry data is also required (in addition to the expansion and packing of the z matrix) due to the mesh refinements in the second and third computing passes. The data serving as input to the program must be provided in terms of the mesh for the third pass (which is 16 times as dense as the mesh for the first pass). The input data to be modified are designated by an "over-bar" notation. Since these data must be saved for the final pass the special notation is necessary in the actual computing.

To modify for the first computing pass, the input values $\bar{y}_s(x)$, $\bar{y}_p(x)$ are read only at every other odd integer value for x. The values read are modified to identify the mesh points corresponding to $(x,\ y_s)$, $(x,\ y_p)$ in the revised mesh according to

$$y_s = \left[\frac{\bar{y}_s\,(4i-3) + 3}{4}\right],\quad i = 1,\ 2,\ \ldots,\ x''' \tag{55a}$$

$$y_p = \left[\frac{\bar{y}_p\,(4i-3) + 3}{4}\right],\quad i = 1,\ 2,\ \ldots,\ x''' \tag{55b}$$

where the brackets imply the greatest integer not exceeding the number inside

the brackets. The integer x''' in Equation 55 is itself a modified value:

$$x''' = \frac{\bar{x}''' + 3}{4} \tag{56}$$

Note, accordingly, that $\bar{x}'''$ must be a member of the set of every other odd integers.

It should also be noted that the mesh points $y_s(x)$ and $y_p(x)$ change their location relative to the flow boundary in the course of mesh refinement. That is, in terms of the computing mesh for the first pass, the distances from the mesh points $y_s(x)$ and $y_p(x)$ to the respective flow boundaries are

$$\Delta_s(i) = \frac{\bar{y}_s(4i-3) + \Delta_s(4i-3) + 3}{4} - y_s(i) \quad , \quad i = 1, 2, \ldots, x''' \tag{57a}$$

$$\Delta_p(i) = \frac{\bar{y}_p(4i-3) + \Delta_p(4i-3) + 3}{4} - y_p(i) \quad , \quad i = 1, 2, \ldots, x''' \tag{57b}$$

Restrictions similar to those noted for values of $\bar{x}'''$ are also placed on $\bar{x}'$ and $\bar{x}''$. The value $\bar{x}'$, which locates the forward-most edge of the blade profiles in the most dense computing mesh, and $\bar{x}''$, which locates the first x-panel downstream of the trailing edge of the profiles, must be mapped in each mesh refinement (see Figure 6). Therefore, as was the case for $\bar{x}'''$, $\bar{x}'$ and $\bar{x}''$ must be of the set of every other odd integers; the modified values for the first computing mesh are

$$x' = \frac{\bar{x}' + 3}{4} \tag{58a}$$

$$x'' = \frac{\bar{x}'' + 3}{4} \tag{58b}$$

Also, according to the definition of the scale factor k_2 in Equation 26a, the modification for the first pass is

$$k_2(i) = \frac{1}{4}\bar{k}_2(4i - 3) \quad , \quad i = 1, 2, \ldots, x''' \tag{58c}$$

In the solution method the forward-most edge of the pair of blade profiles defining the flow field must lie on mesh points in any computing pass (see Figure 6). Hence, the mesh points $(\bar{x}', \bar{y}_s')$ and $(\bar{x}', \bar{y}_s' + \bar{s})$, where $\bar{s}$ is the

blade spacing, must be every other odd mesh points located along the constant $\bar{x}'$-panel.

The radius ratio and thickness function for the stream surface are given in the form of second-degree polynomials in x. Therefore, only the coefficients in the polynomials are input data. The equations for the stream surface radius ratio and thickness function are

$$\bar{r}(x) = a_0 + a_1 x + a_2 x^2 \tag{59a}$$

$$\bar{\tau}(x) = b_0 + b_1 x + b_2 x^2 \tag{59b}$$

where $x = 1, 2, \ldots, \bar{x}'''$. It follows that the derivatives of these two functions as required in Equation 33 are

$$\frac{d\bar{r}}{dm} = \bar{k}_2 (a_1 + 2a_2 x) \tag{59c}$$

$$\frac{d\bar{\tau}}{dm} = \bar{k}_2 (b_1 + 2b_2 x) \tag{59d}$$

where $x = 1, 2, \ldots, \bar{x}'''$. However, values obtained from Equations 59 are not modified due to mesh refinement since they are independent of the computing mesh. The only effect of mesh refinement is that the values from Equation 59 for every other odd integer x are used in the first computing pass, and those at every odd integer x are used in the second pass. The case is the same for the values of loaded local profile angles $\alpha_s(x)$ and $\alpha_p(x)$ used in computing head coefficient in Equation B1 of APPENDIX B; values at every other odd, and at every odd integer are required in first and second computing passes respectively

Modifications of the input data for computations in the intermediate computing mesh for Pass 2 are similar to those for Pass 1. The equations that apply, analogous to Equations 55 through 58, are

$$y_s(i) = \left[\frac{\bar{y}_s\,(2i - 1) + 1}{2}\right], \quad i = 1, 2, \ldots, x''' \tag{60a}$$

$$y_p(i) = \left[\frac{\bar{y}_p\,(2i - 1) + 1}{2}\right], \quad i = 1, 2, \ldots, x''' \tag{60b}$$

$$x''' = \frac{\bar{x}''' + 1}{2} \tag{61}$$

$$\Delta_s(i) = \frac{\bar{y}_s(2i-1) + \bar{\Delta}_s(2i-1) + 1}{2} - y_s(i) \ , \ i = 1,2, \ldots, x''' \tag{62a}$$

$$\Delta_p(i) = \frac{\bar{y}_p(2i-1) + \bar{\Delta}_p(2i-1) + 1}{2} - y_p(i) \ , \ i = 1,2, \ldots, x''' \tag{62b}$$

$$x' = \frac{\bar{x}' + 1}{2} \tag{63a}$$

$$x'' = \frac{\bar{x}'' + 1}{2} \tag{63b}$$

$$k_2(i) = \frac{1}{2} \bar{k}_2(2i - 1) \quad , \quad i = 1, 2, \ldots, x''' \tag{63c}$$

Restrictions imposed by construction of the intermediate mesh for the second computing pass upon mappings of certain mesh points of the fine mesh are compatible with those already stated in regard to the mapping in the first pass. The refinement of the intermediate mesh to the fine mesh in the third and final computing pass requires no modification of geometry data; the input data is used directly.

The computer program is composed of a main program and two subroutines. The primary function of the main program is to generate values for stream surface geometry, prepare for computing passes and modify geometry data, apply the boundary conditions at the inlet and outlet stations of the blade row, initialize or expand and pack the z (x, y) matrix, and to compute arrays that depend on x. The first subroutine extrapolates z to the exterior points and performs the integration at the interior points. The second subroutine computes values of head coefficient along the blade profile and interpolates the z matrix to obtain streamlines in the flow field (see APPENDIX B).

To determine the progress of the iterations at any stage, the maximum absolute change in z at any integration mesh point is monitored by the pro-

gram; also, the average absolute change at all integration points during an iteration cycle is computed. The ratio of the average absolute change for the elements of z in an iteration cycle to that in the preceding cycle approaches a constant value as the iterations converge (25).

To estimate the error at some stage of the iterations, let

$$z' = z + \delta$$

where z' is the current value, z the true value, and δ the error. If j additional iterations are performed ($j = 1, 2, \ldots$) then

$$z'_j = z + q^j \delta \tag{64}$$

where $q = \dfrac{z'_{j+1} - z'_j}{z_j - z'_{j-1}}$ is constant less than 1 in absolute value. With q and $(z'_j - z'_{j-1})$ determined from the iterations the error may be estimated as

$$q^j \delta = \frac{q}{q - 1} (z'_j - z'_{j-1})$$

It is obvious from the estimate for the error that the smaller q is in absolute value, the more rapid the convergence.

The iterations are terminated if the absolute value of change in elements of z at integration points during an iteration is less than 0.0005, or if the number of the iterations has reached a maximum (which is under control of the input data). Also, if the absolute value of the change of an element of z at an integration point during an iteration exceeds a limiting value, the solution is considered divergent; the iterations are then terminated and the next problem tried. Provision is made in the computer program to run as many successive sets of inlet and outlet velocity triangles as desired for a given stream surface and blade profile geometry.

Comments on Development of the Program

During development of the computer program a number of unanticipated problems were encountered. These problems often required a change in the numerical method used or an alteration of the program itself. Among these problems were:

1. Over-determination of the problem with both the whirl and flow co-

efficients prescribed at the inlet and outlet flow stations. Discard of the whirl coefficient boundary condition to avoid the over-determination condition has been discussed in conjunction with Equations 42.

2. Instability of the iterations due to the extrapolations of $z(x, y)$ in Equations 44 through 47 concerned with the assignment of boundary values along the blade profile. The modified extrapolations have been described in Equations 48 through 50.
3. Inaccuracy in numerical estimation of the derivative of z at points along the blade profile boundaries. A method first tried was one based on formal differentiation of the interpolation formula followed by evaluation of the required derivative at the boundary point. This method was discarded in favor of the one which has been described in Equations 51 when, in certain cases, large errors in the derivatives occurred as the result of "kinks" in the "fitting" curves. These kinks arose when there was not complete agreement between the determined solution and the assigned boundary value at the boundary and when a mesh point was close to the boundary.

It was also found in determining solutions for given cascade geometries that it was desirable to initially solve a series of preliminary problems for the cascade configurations in a coarse mesh with various combinations of assigned values $z(1, y_s + \Delta_s)$ and $z(x''', y_s + \Delta_s)$ in Equations 42. From these preliminary solutions, which required a minimum of computing time, inlet and outlet flow conditions to the blade row were determined, and the required values of $z(1, y_s + \Delta_s)$ and $z(x''', y_s + \Delta_s)$ for given flow conditions in the final solutions in fine mesh could be established. In each case the convergence of the solution in the coarse mesh was good, the value of q in Equation 64 being in the range of 0.82 to 0.88 when a relaxation factor of 1.2 was used. Generally less than 100 iterations were required in the coarse mesh solutions to attain increments in z of less than 0.0005 in absolute value at any mesh point. However, convergence in the intermediate mesh was slower, the values of q found ranged from 0.92 to 0.97. A relaxation factor of 1.3 was generally used in the intermediate mesh calculations.

Convergence of solutions in the fine mesh was even slower, the value of q being close to 0.985 for all the problems run with a relaxation factor of 1.38. To avoid excessive computing time, iterations in the intermediate and fine mesh solutions were not carried to a prescribed accuracy but were terminated after a preassigned number of iterations had been performed; a change in absolute value of z of less than 0.007 in 150 iterations is representative for the calculations in the fine mesh. The number of interior points in the fine mesh ranged from about 1800 to 3500. The limiting number of iterations in the final solutions was generally set at 100, 40, and 200 for the coarse, intermediate and fine mesh calculations, respectively. This required 10 minutes or less total computing time on the IBM 7074 computer for a set of inlet and outlet flow conditions.

SAMPLE SOLUTIONS FOR SELECTED CASCADE CONFIGURATIONS

Results of sample solutions are summarized in Figures 8 through 18. Flow patterns as determined by interpolated streamline traces as well as

variations of local head coefficient over the blade profiles are presented.

A streamline pattern for flow through a cascade of symmetric parabolic profiles at zero setting angle is given in Figure 8. Uniform discharge flow was obtained in this problem with zero leaving fluid angle, the boundaries of the flow channel formed by the adjacent profiles and the leaving streamlines $z = 0$ and $z = 100$ being symmetric about a channel centerline. Curves of head coefficient distribution for three different cases of blade incidence angle (i) of the inlet flow with approximately zero leaving fluid angle are shown in Figure 9. As expected, the first set of curves (which corresponds to the streamline pattern of Figure 8) clearly show negative loading of the profile for negative incidence of inlet flow. In the second set of curves close to zero loading of the profile is indicated for an incidence angle of 0.4 degrees, and in the third set of curves positive loading for a positive incidence angle is indicated. (Layout of the cascade is described in Appendix D.)

A sample problem involving a cascade with non-zero setting angle was next solved. The flow through a cascade of thin flat plates set at 45 degrees was determined using an especially sparse computing mesh in Figure 10 in which all points are regular. The assigned boundary values and the ordering of the mesh points is noted on Figure 10. With so few points involved, the set of equations for the problem were written explicitly (according to Equations 33, 38a, and 38c) and solved by a direct method involving inversion of the coefficient matrix. The solution vector was then compared with the iterated

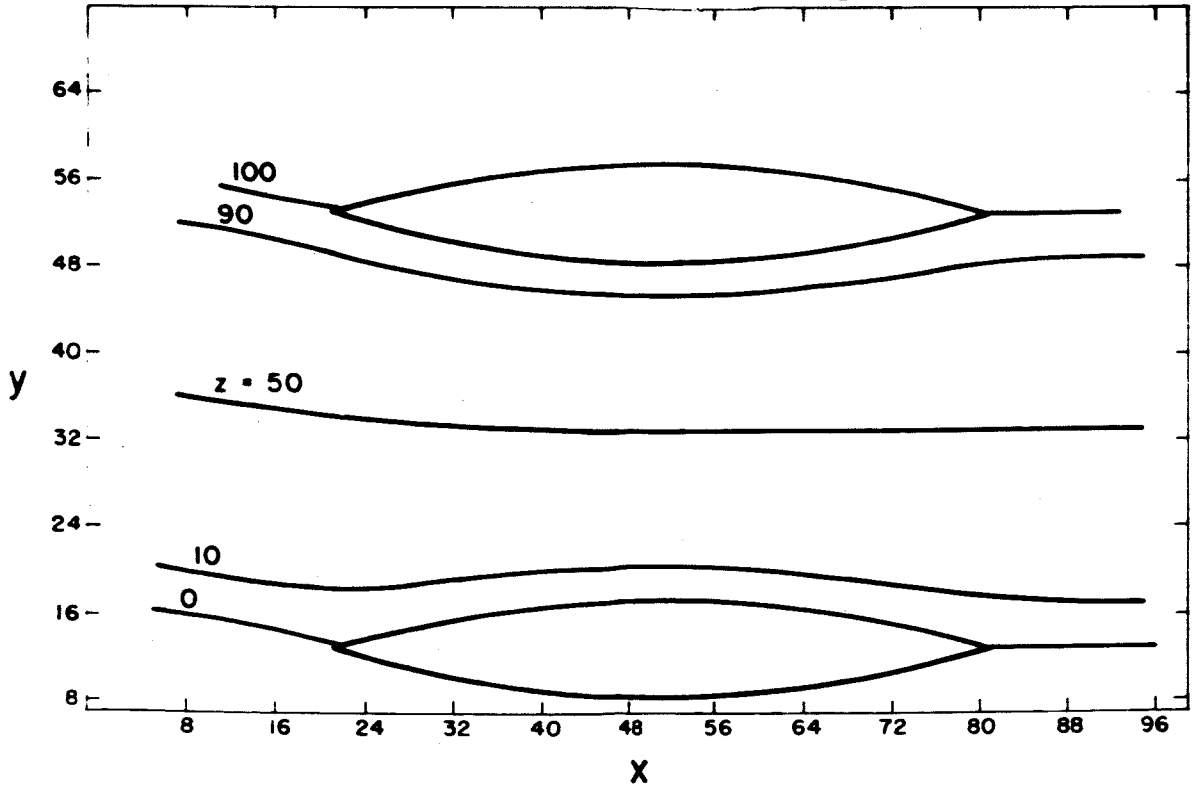

Figure 8. Flow pattern in two-dimensional cascade of symmetric parabolic profiles. $t/c = 0.15$ $\sigma = 1.49$ $\gamma = 0.0$ deg. $\beta_i' = -8.2$ deg.

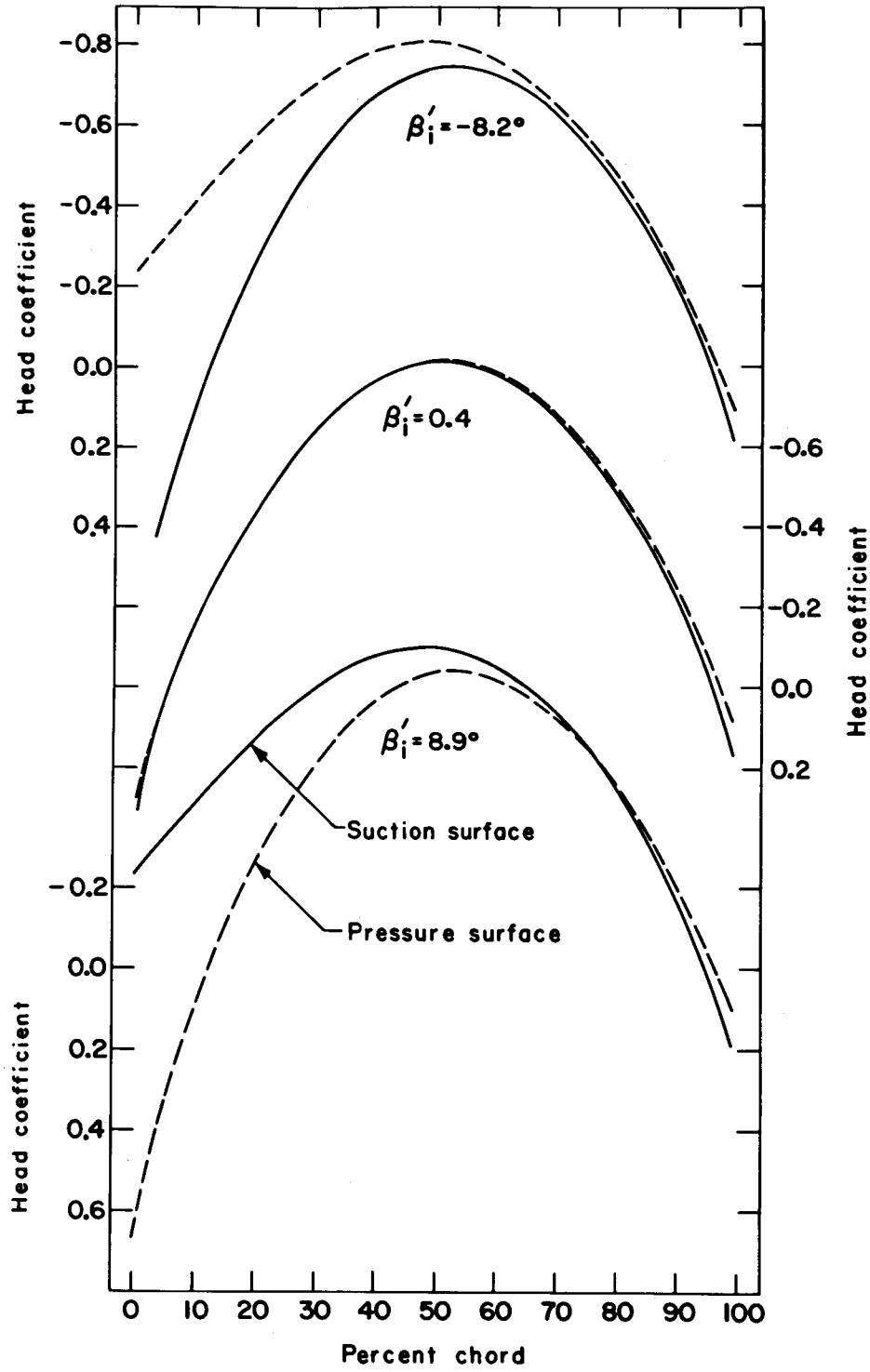

Figure 9. Variation of head coefficient at blade surface with chord in two-dimensional cascade of symmetric parabolic profiles for different inlet fluid angles (β_i'). (Head coefficient defined by Equation B1) t/c = 0.15 σ = 1.49 γ = 0.0 deg.

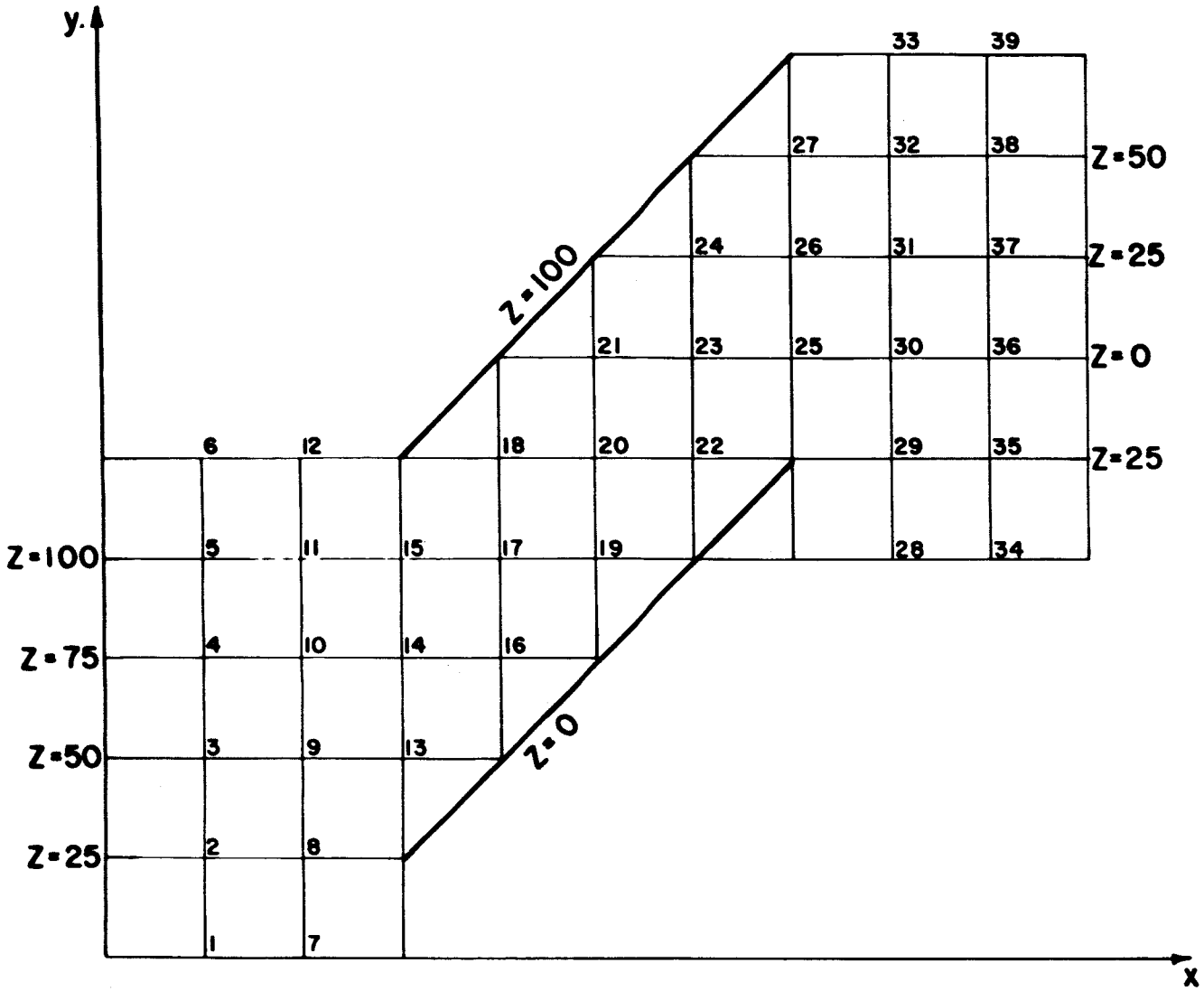

Figure 10. Flow field and computing mesh for direct solution problem.

solution. The augmented coefficient matrix with only non-zero elements written is displayed in Figure 11a. The solution vector is given in Figure 11b with the corresponding elements from the iterated solution enclosed in parentheses. As can be seen the comparison of the two solutions is good.

To investigate the flow through a practical cascade geometry the streamline pattern was determined for flow through a two-dimensional cascade of NACA 65(A_{10})-810 blades with a solidity of 1.5 as shown in Figure 12. (Layout of the cascade is described in APPENDIX C.) Blade setting angle, γ, (see Figure 33) is 18.4 degrees, corresponding to an inlet fluid angle of 30 degrees at design conditions as determined in experimental tests (9). At this low setting angle, uniform flow at the outlet station is evident, and the streamlines $z = 0$ and $z = 100$ are seen to trail in the discharge flow from points on the blades close to the trailing edge. Hence, a Kutta condition appears satisfied, implying a stagnation point at the trailing edge (36). However, the accompany-

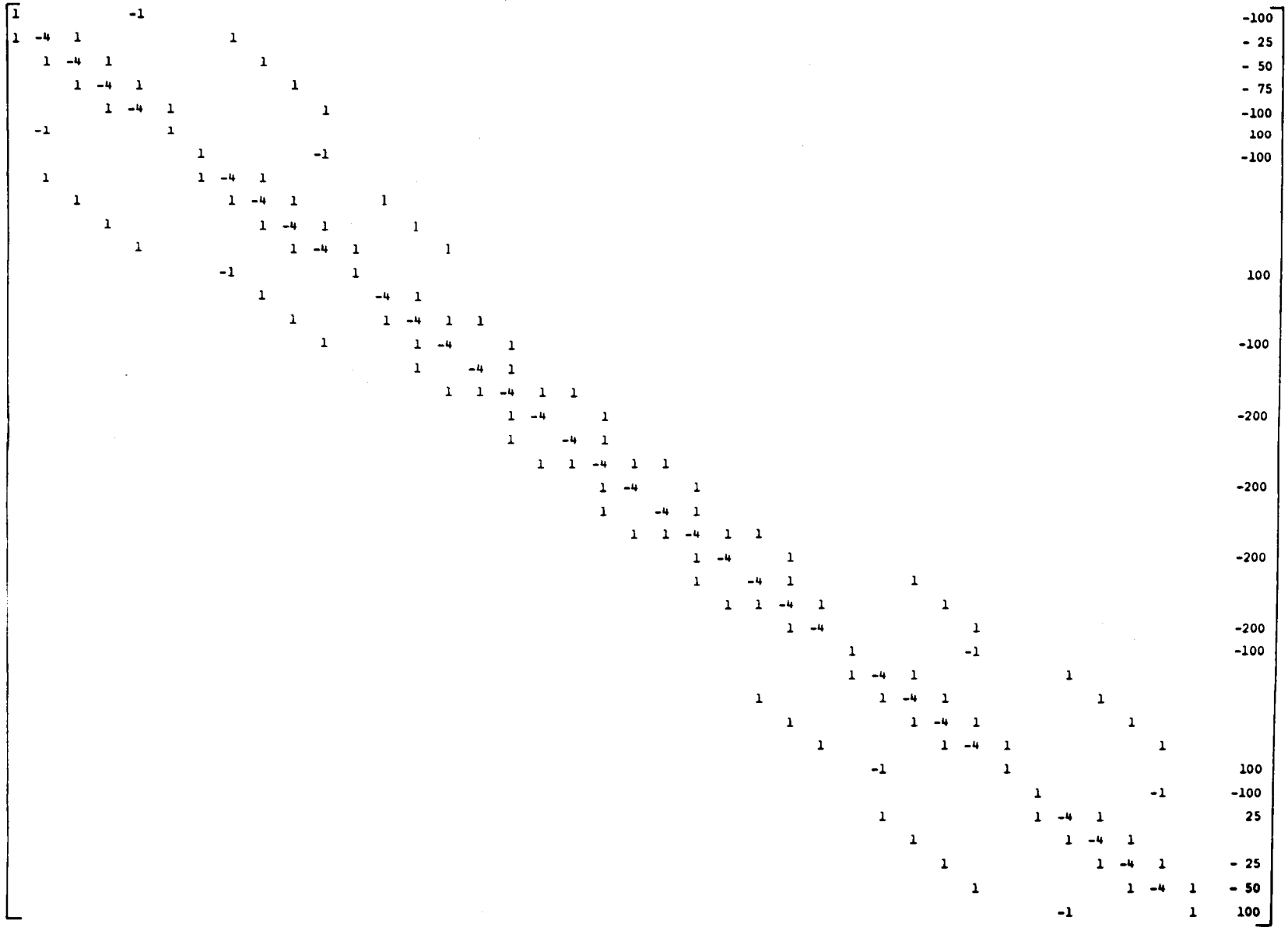

Figure 11a. Augmented coefficient matrix for direct solution of problem in Figure 10.

-10.73429	(-10.73426)
14.74769	(14.74771)
39.33017	(39.33018)
64.02811	(64.02813)
89.26570	(89.26574)
114.74769	(114.74771)
-21.71292	(-21.71287)
5.39491	(5.39493)
28.54485	(28.54487)
52.51658	(52.51660)
78.28708	(78.28713)
105.39491	(105.39491)
16.93778	(16.93779)
39.20626	(39.20628)
65.97123	(65.97126)
21.39947	(21.39948)
46.39162	(46.39164)
74.09790	(74.09791)
24.09790	(24.09791)
49.99999	(50.00000)
75.90208	(75.90209)
25.90208	(25.90209)
53.60835	(53.60835)
78.60051	(78.60052)
34.02873	(34.02873)
60.79369	(60.79371)
83.06219	(83.06220)
-28.54490	(-28.54489)
-5.39494	(-5.39494)
21.71285	(21.71285)
47.48338	(47.48338)
71.45509	(71.45511)
94.60503	(94.60506)
-39.33019	(-39.33019)
-14.74772	(-14.74772)
10.73425	(10.73425)
35.97185	(35.97186)
60.66980	(60.66981)
85.25228	(85.25228)

Figure 11b. Direct and iterated solution vectors for problem in Figure 10.

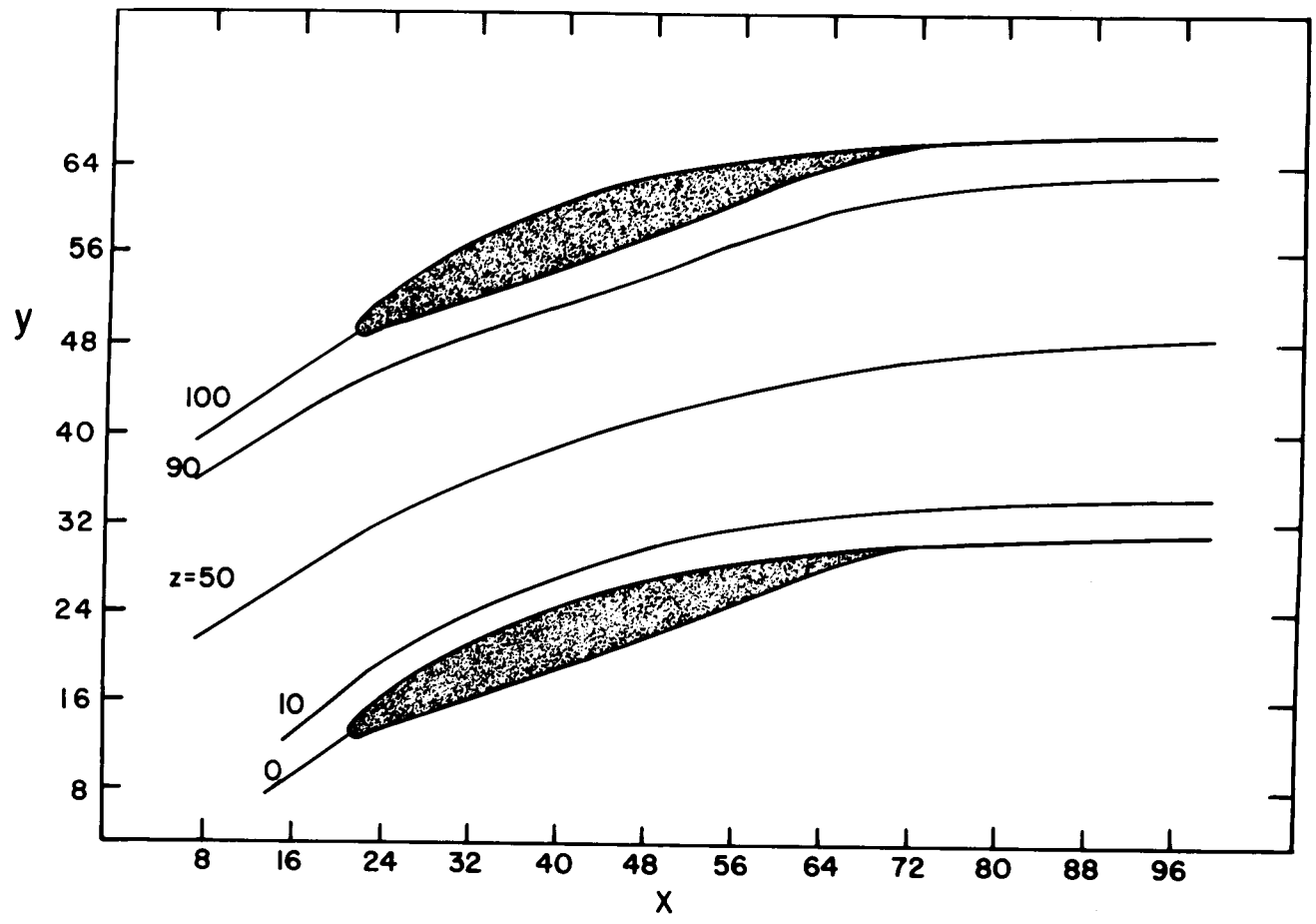

Figure 12. Flow pattern in two-dimensional cascade of NACA $65(A_{10})$-810 blade profiles. $\sigma = 1.5$ $\gamma = 18.4$ deg. $\beta_i' = 33.6$ deg.

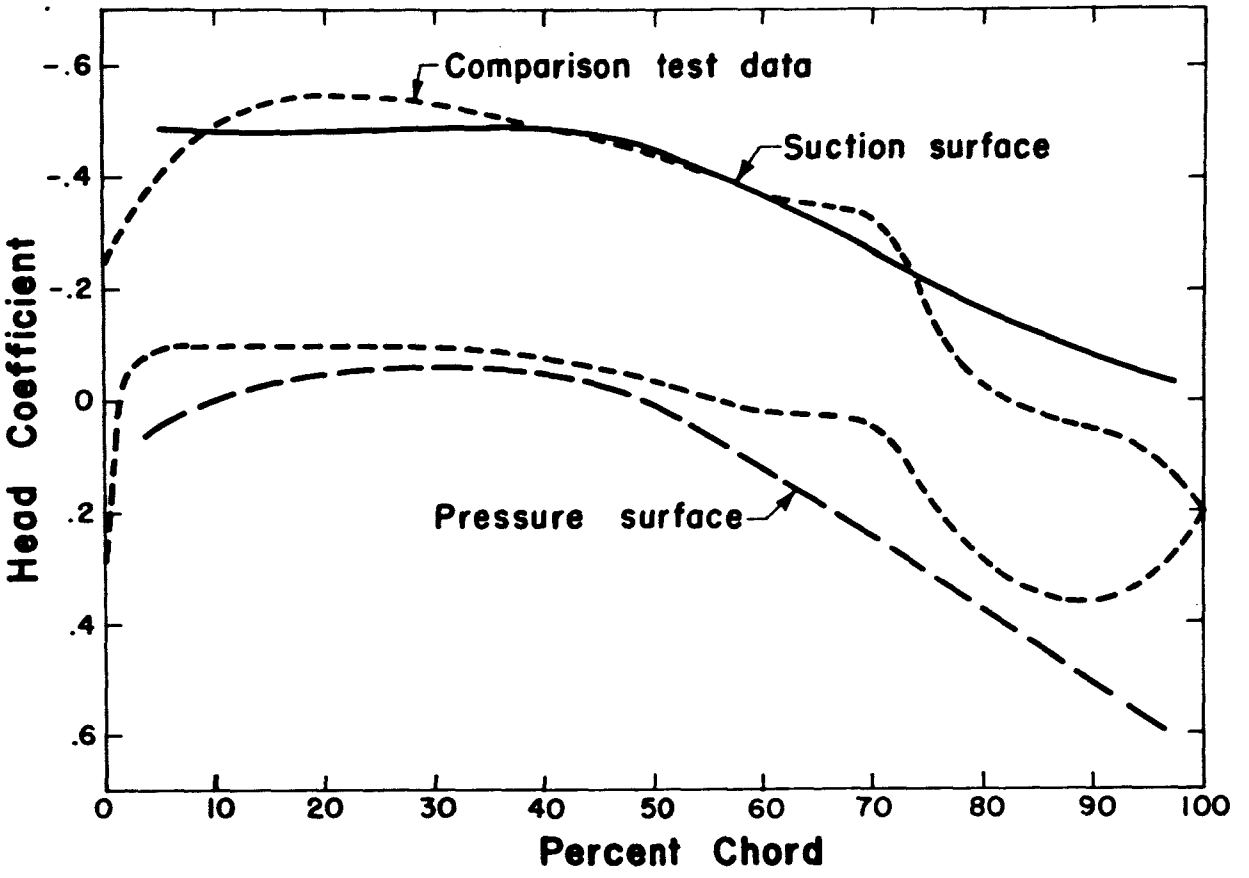

Figure 13. Variation of theoretical and experimental head coefficients with chord in two-dimensional cascade of NACA $65(A_{10})$-810 blade profiles at design inlet fluid angle, β_i' = 30 deg. (Head coefficient defined by Equation B1. Comparison experimental data for air from Ref. 9) σ = 1.5 γ = 18.4 deg.

ing head coefficient distribution for the flow in Figures 13 and 14 give no indication of stagnation at the trailing edge. In fact, there exists a large difference near the trailing edge between velocities on the pressure and suction surfaces of the profile. The difference in velocity is not totally unexpected in view of the formulation of the blade-to-blade flow as flow through a channel formed by adjacent suction and pressure surfaces and by the repeating streamlines $z = 0$ and $z = 100$ outside the blade row. That is, a fluid particle traversing the suction surface would be expected, in general, to outrun a particle traversing the pressure surface, and velocities determined in the neighborhood of the trailing edge of the blades on opposite sides of the channel would not tend to the same value at the trailing edge of the blade. The velocity difference is, of course, a result of the non-symmetric character of the channel boundaries as determined by the particular blade profile, setting angle of the cascade, and by the fluid leaving angle. In addition, differences in velocities occur at the leading edge as well, and for the same reasons. From the foregoing discussion it appears that the traces $z = 0$ and $z = 100$ cannot be considered as material lines in the entering and leaving flows. It is likely that the profile boundary layer in the real flow

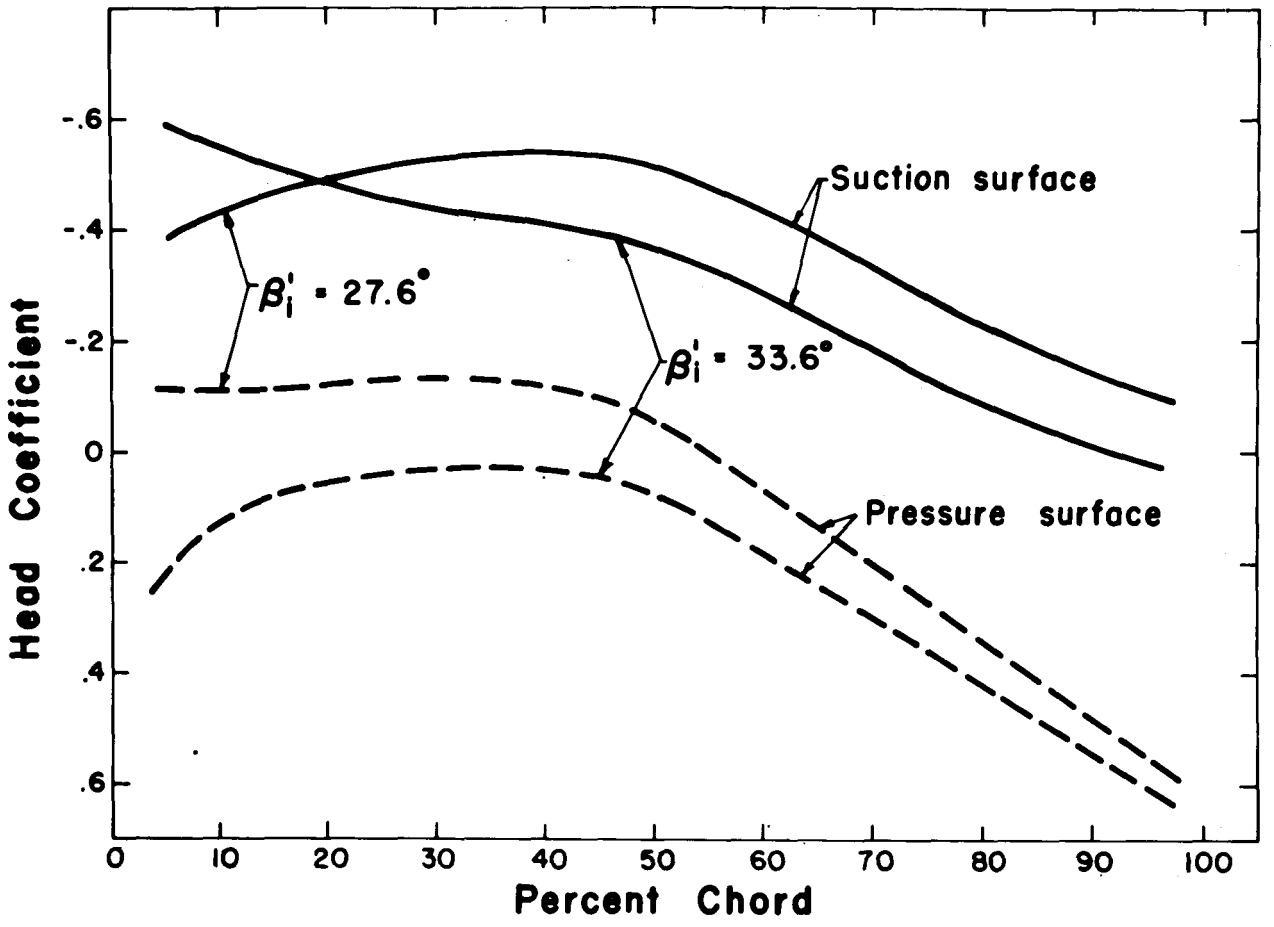

Figure 14. Variation of theoretical head coefficient with chord in two-dimensional cascade of NACA 65(A_{10})-810 blade profiles for two different inlet fluid angles (β_i'). (Head coefficient defined by Equation B1)
$\sigma = 1.5$ $\gamma = 18.4$ deg.

plays an essential role in the adjustment of pressure distribution at the trailing edge as well as in the determination of the circulation on the blade through separation of beginning flow and subsequent roll-up of the starting vortex (22). Also, solutions were attempted in which the leaving flow was to deviate from the suction surface with an apparent stagnation point located forward of the trailing edge on the suction surface. These attempts were not successful; the leaving flow refused to deviate by any appreciable amount inside the blade row and only deflected unrealistically further downstream. The flow pattern in a two-dimensional cascade of 65(A_{10})-810 blades with a higher setting angle of 48.2 degrees and with inlet flow at design incidence is shown in Figure 15.

The flow pattern in a two-dimensional cascade of symmetric parabolic profiles with a profile setting angle of 52 degrees and inlet flow at 0 degrees incidence is shown in Figure 16. The streamline traces in these figures show that the leaving flow is not uniform. The non-uniformity, and location of an

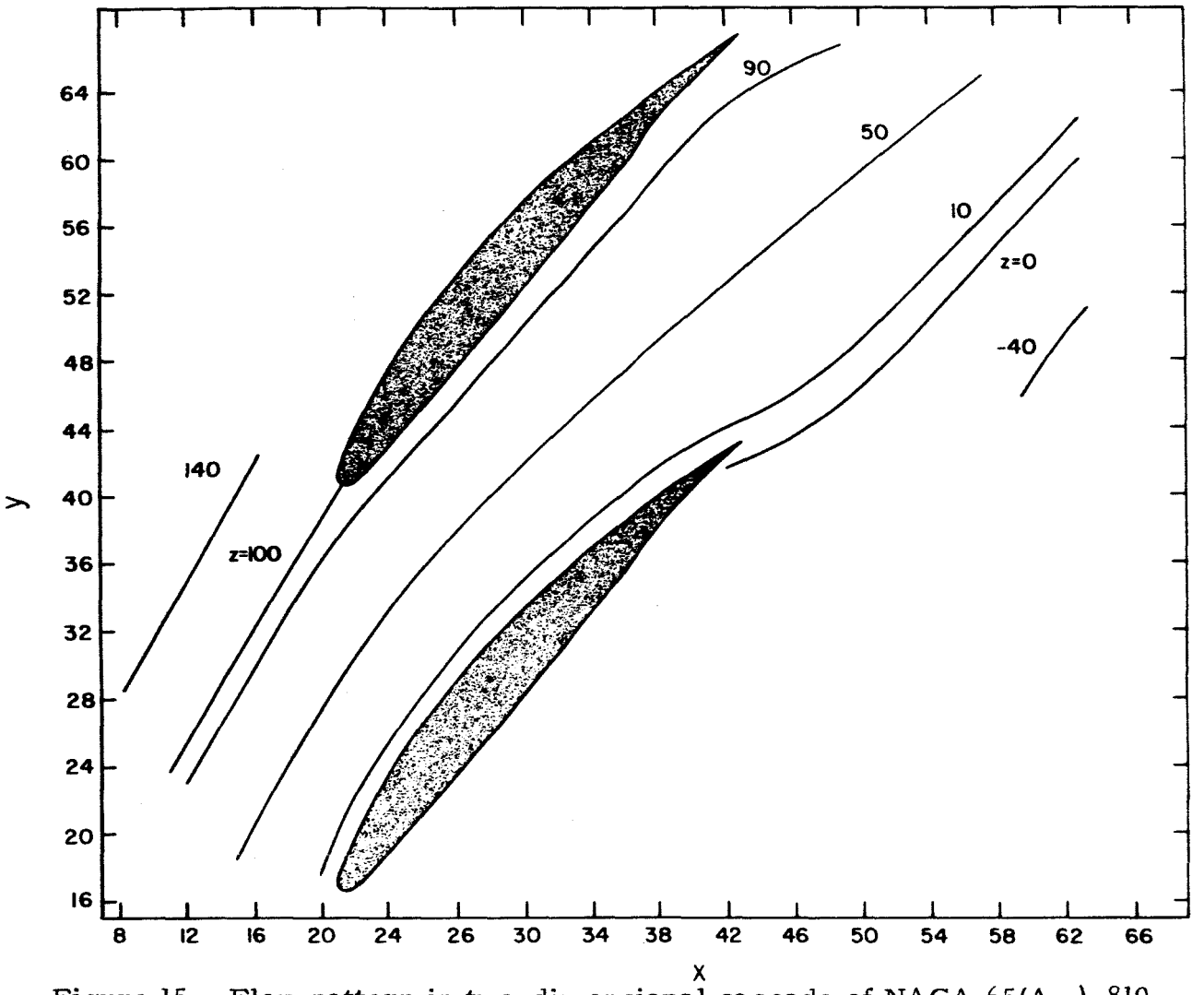

Figure 15. Flow pattern in two-dimensional cascade of NACA $65(A_{10})$-810 blade profiles. $\sigma = 1.5$ $\gamma = 48.2$ deg. $\beta_i' = 60.2$ deg.

apparent stagnation point on the pressure surface ahead of the trailing edge in Figures 15 and 16 are due to the high profile setting angles and profile thickness ahead of the trailing edge. Values of over-all turning of the flow could not be determined for these cascade flows. Readjustment of the stream function value $z\ (x''', y_s + \Delta_s)$ at the outlet station to relocate the stagnation point closer to the trailing edge in Figures 15 and 16 only resulted in further disruption of the leaving flow. Also the readjustment of $z\ (x''', y_s + \Delta_s)$ caused appreciable change in head distribution over the profile as shown in Figure 17 for the parabolic cascade. It should be noted in the head coefficient distributions in Figure 17 that, in spite of an uncambered symmetric parabolic profile and an inlet flow at zero incidence, a negative loading of the profile is evident over 90 percent of chord length for at least two of the three sets of curves.

With location of the trailing edge of the profile not well defined in terms

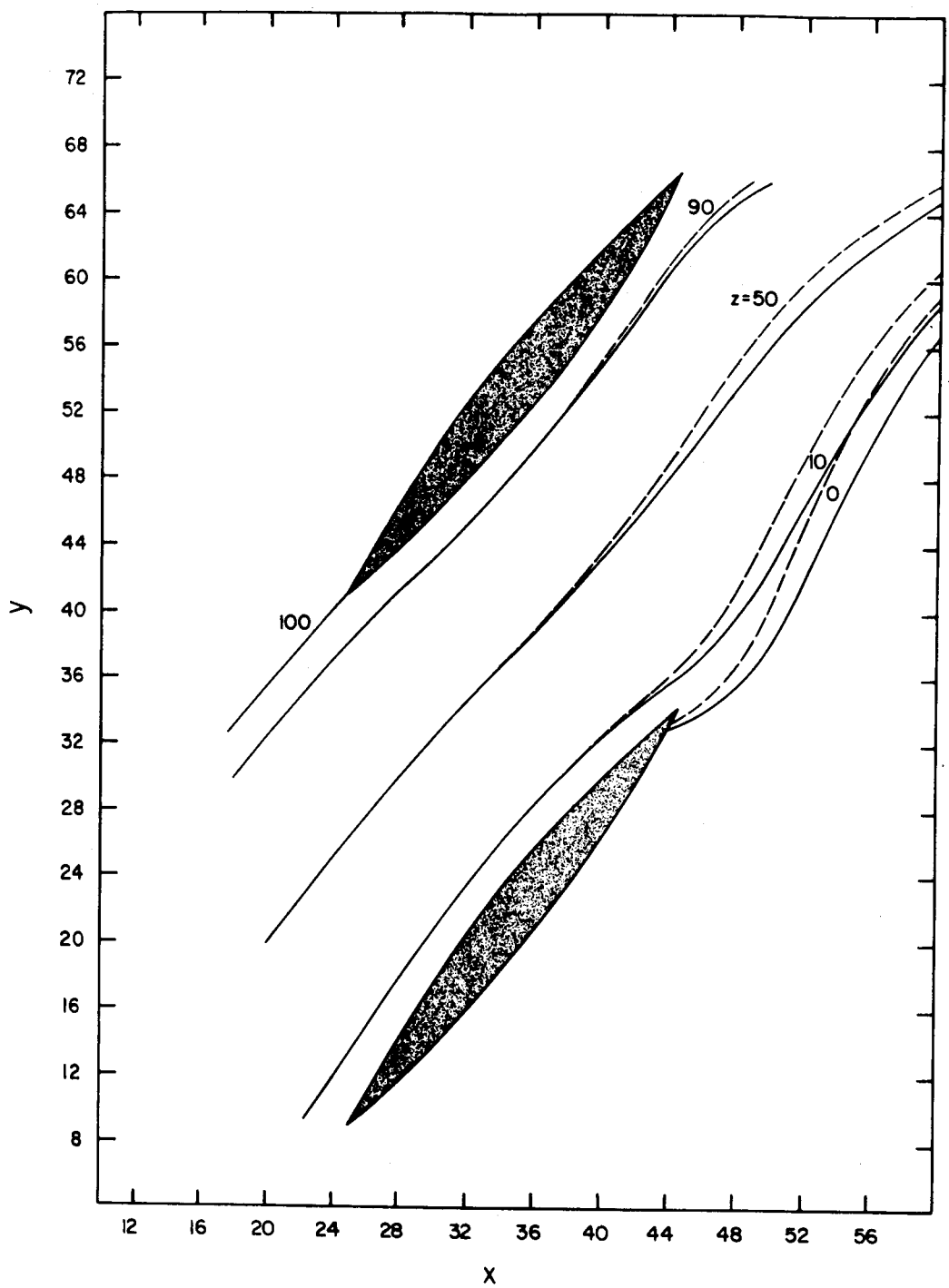

Figure 16. Flow pattern in two-dimensional cascade of symmetric parabolic profiles for two different values of assigned boundary condition at outlet flow station. $t/c = 0.10$ $\sigma = 1.00$ $\gamma = 52.0$ deg. $\beta_i' = 52.0$ deg.

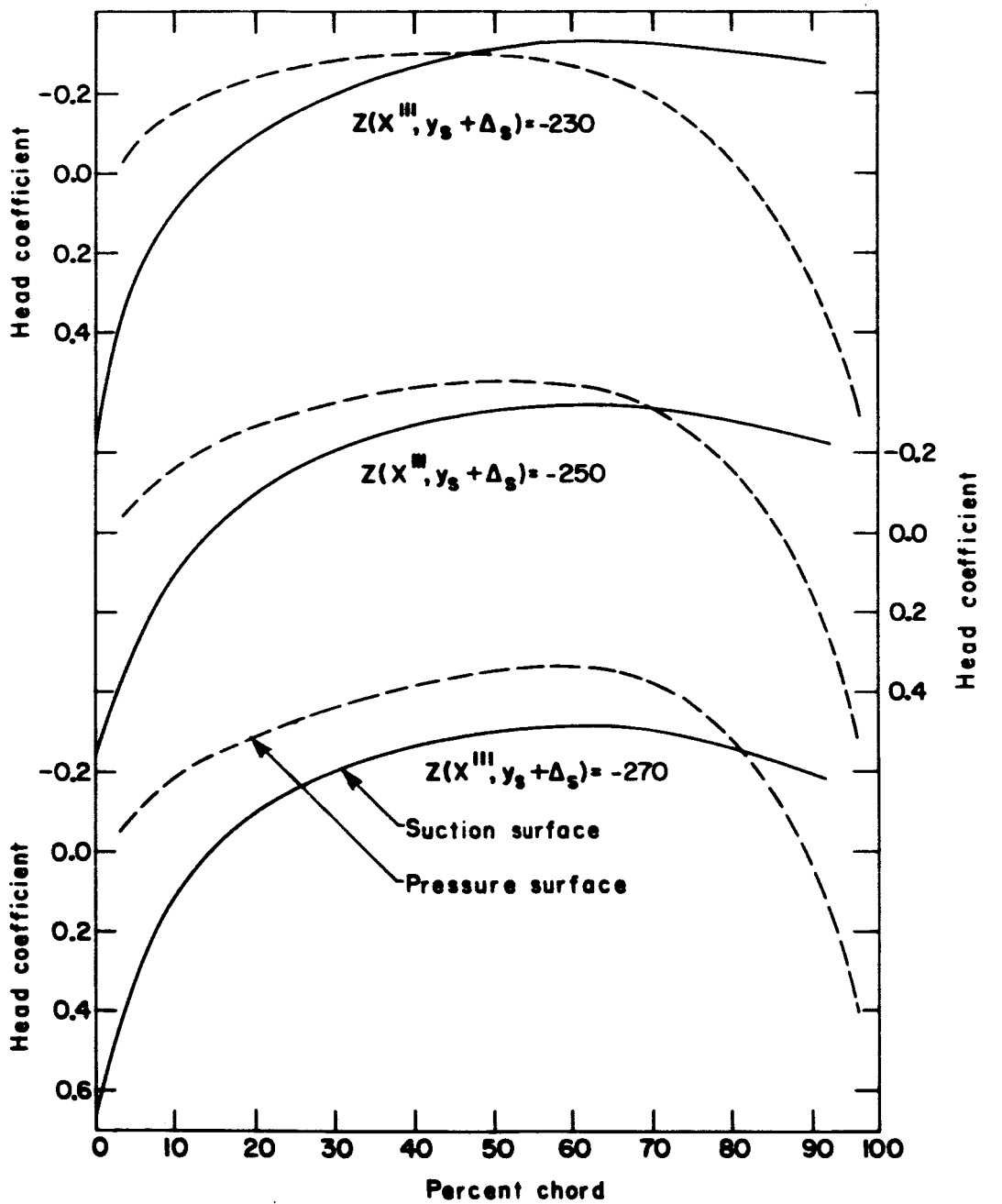

Figure 17. Variation of head coefficient with chord in two-dimensional cascade of symmetric parabolic profiles for three different values of assigned boundary condition at outlet flow station. $t/c = 0.10$ $\sigma = 1.00$ $\gamma = 52.0$ deg. $\beta_i' = 52.0$ deg.

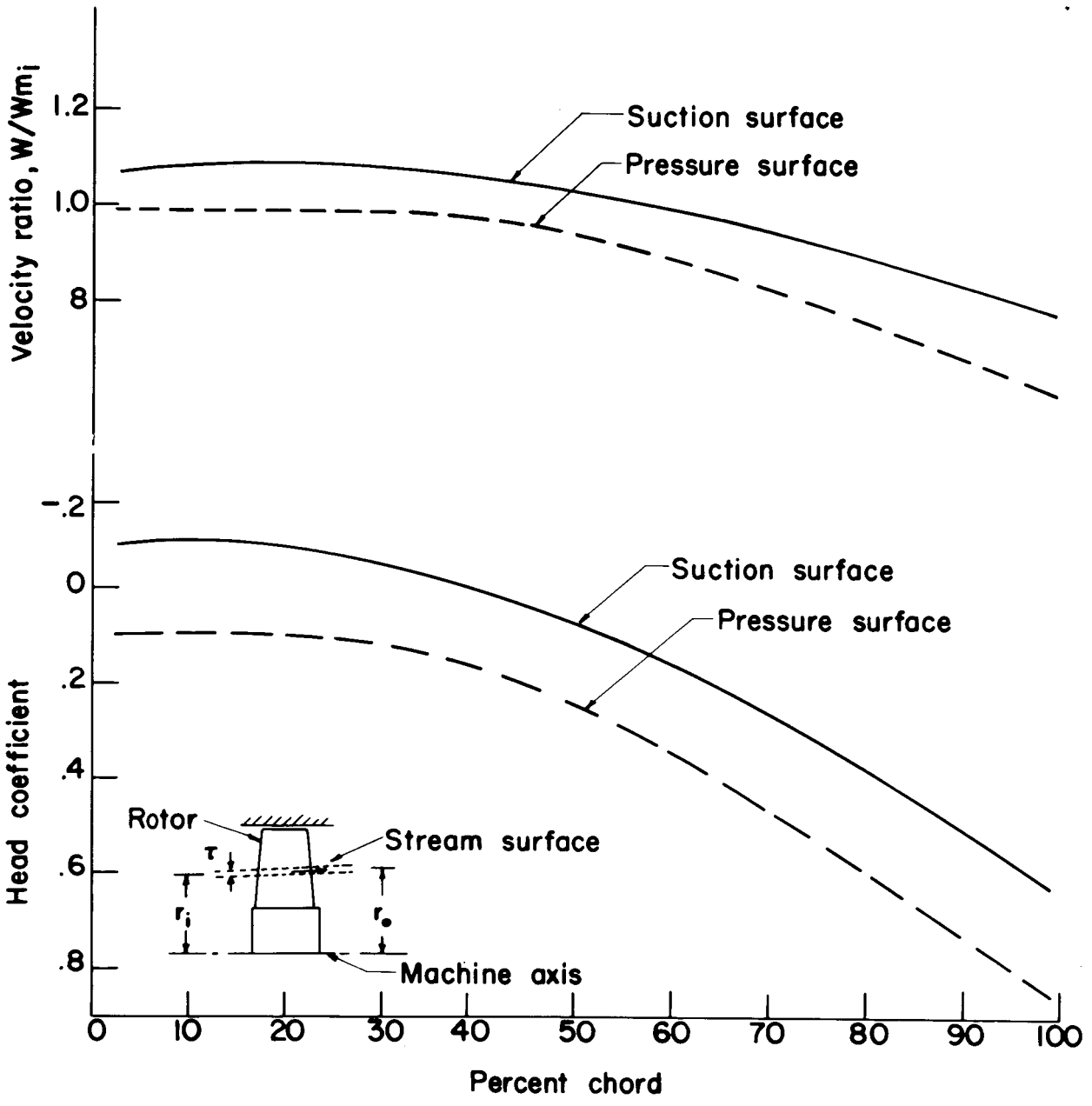

Figure 18a. Velocity and head coefficient variations with chord in a rotating blade row. Linear variation in stream surface radius and in thickness function. (Head coefficient defined by Equation B1) Inlet flow coefficient, $W_{m,i} = 0.5$. $\beta_i' = 32.3$ deg.

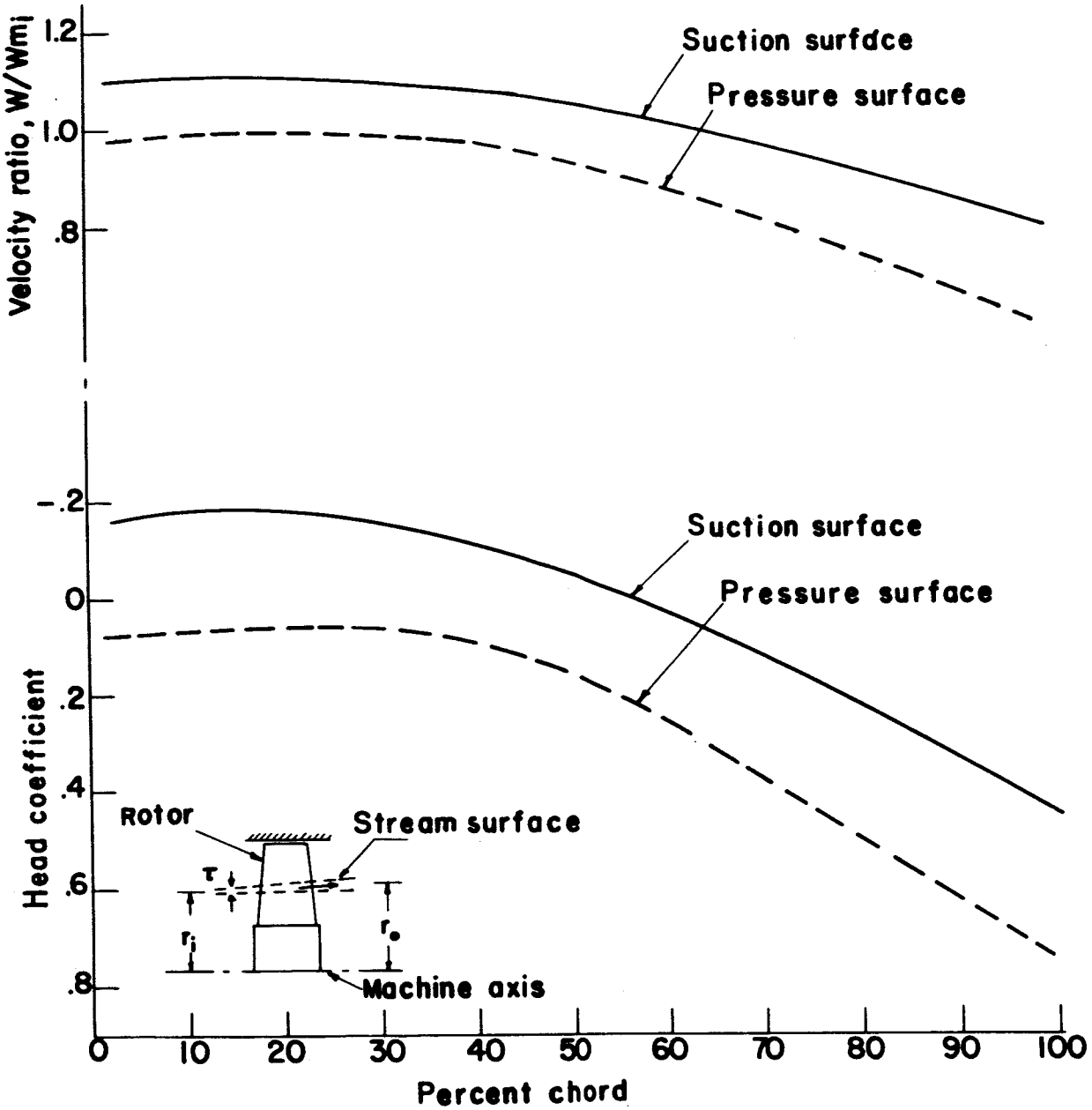

Figure 18b. Inlet flow coefficient, $W_{m,i} = 0.8$. $\beta_i' = 31.8$ deg.

of the computing mesh and with insufficient mesh refinement near the trailing edge, reliable values of head coefficient near the trailing edge could not be determined. Even those data available from the solution for the suction surface beyond the 90 percent chord station were questionable and were not plotted.

Results are shown in Figure 18 for a rotor configuration for which the developed cascade is that in Figure 12. The stream surface used had an assigned linear variation in radius ratio from 0.60 at the inlet station to 0.65 at the outlet, and a linear variation in thickness function from 1.0 at the inlet to 1.1 at the outlet. These specifications were satisfied using a_0, a_1 and a_2 as 0.5995, 0.005 and 0.0 and b_0, b_1 and b_2 as 0.998, 0.002 and 0.0, respectively, in Equations 59. The effect of the change in inlet flow coefficient on profile velocity and head distributions is seen in Figure 18 for the two sets of curves for $W_{m,i} = 0.5$ and $W_{m,i} = 0.8$.

EXPERIMENTAL WATER CASCADE INVESTIGATION

In both analysis and design of axial-flow pumps and compressors in the United States, great emphasis has been placed on estimation of blade performance using correlations based on systematic measurements of performance of two-dimensional blade lattices or cascades. Numerous investigators have reported cascade performance using air as the working fluid. Some unpublished pump performance data have indicated the possibility of discrepancies between air and water cascade performance. To investigate in a preliminary fashion the flow of water through a cascade, a series of experiments using NACA 65(A_{10})-810 blade profiles was conducted in an open-loop water facility. The centrally-located blade in each cascade was instrumented to determine blade-surface distributions of head coefficient. Also, probe surveys were made to determine cascade total-head loss and flow-turning characteristics. The experimental results obtained are compared later in this section with results taken from a comprehensive summary of two-dimensional low-speed air cascade tests of NACA 65(A_{10})-series blades (9) and with results from one of the sample solutions discussed in the previous section.

Test Apparatus

A schematic diagram of the open-loop water tunnel used is shown in Figure 19. The flow proceeded from the constant-head tank through a flow straightener and transition section into the test section and into a discharge barrel. At this point the flow passed through a control valve to a sump. A centrifugal pump returned the water to the head tank. It may be noted that no deaeration system was provided, and no boundary layer control was used in the test section. An external system used for softening the system water has not been shown.

Three cascade test sections corresponding to three different blade-setting

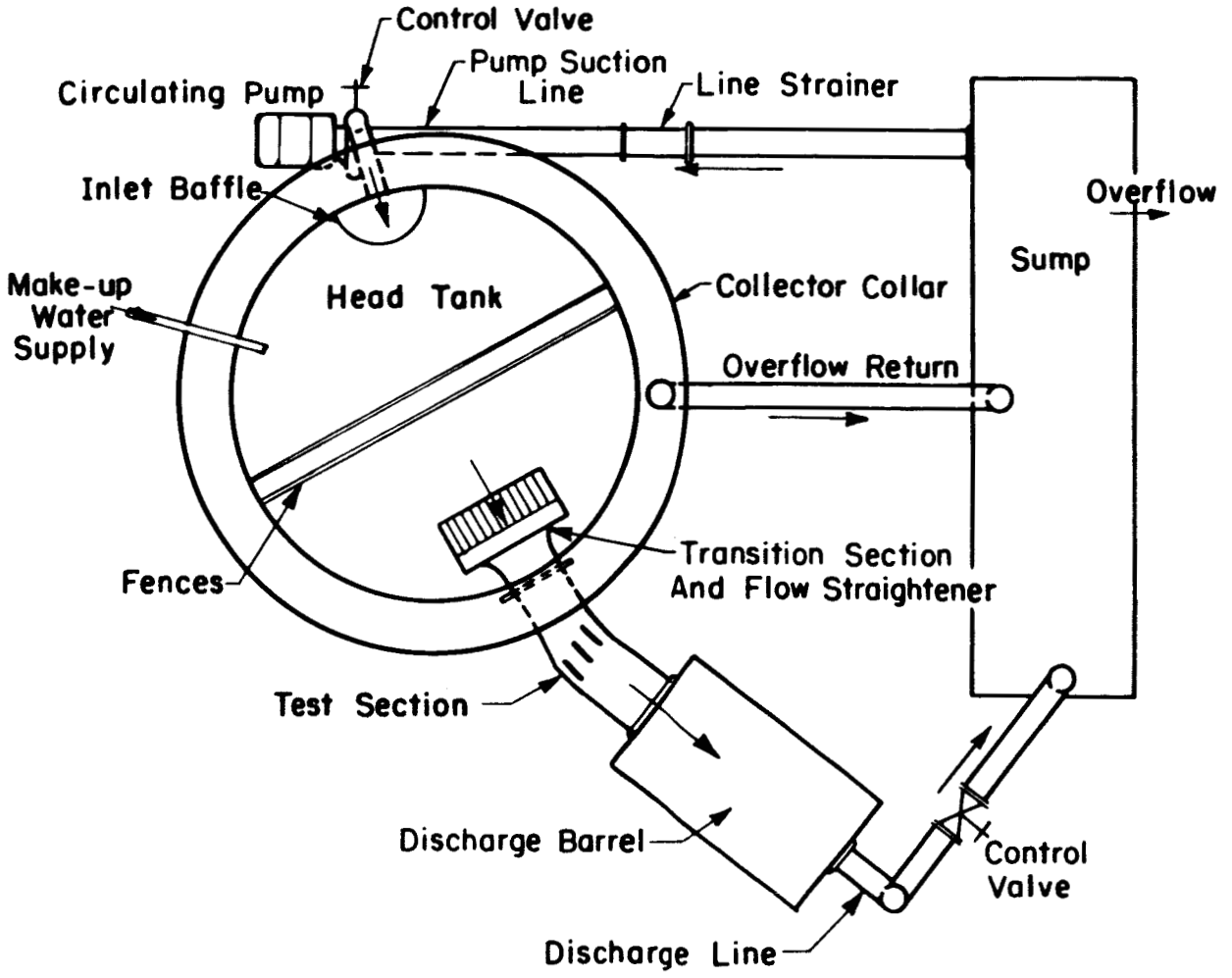

Figure 19. Schematic diagram of the flow circuit.

angles were used in the test program. The test sections without the blades installed are shown in Figure 20. The test sections were fabricated from 1/4-inch and 1/8-inch cold-rolled steel plate. The 1/4-inch plates served as the flat side walls of the cascades and attaching flanges, and the 1/8-inch plates formed the curved end walls. Each test section diffused and turned the flow through a prescribed angle. Test sections were assembled by welding the plates in short widely-spaced beads (to avoid warping the test sections), followed by cementing with epoxy to further strengthen and seal the assembled sections. A test section, when ready for testing with the blades installed, was mounted horizontally in the flow circuit between the upstream transition section and a discharge barrel. An installed test section can be seen in Figure 21. The three test sections were constructed with identical inlet flow channel dimensions so that the same transition section (Figure 20) could be used for all three test sections.

Careful mating of the test and transition sections was required to insure that the flow passage was properly aligned and smooth. The transition section

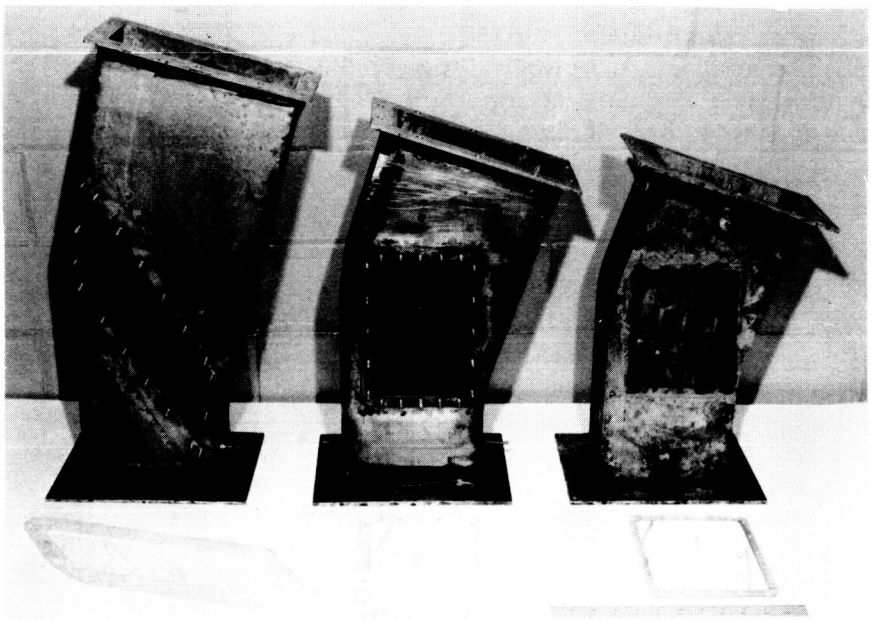

a. The three cascade test sections without blades installed.

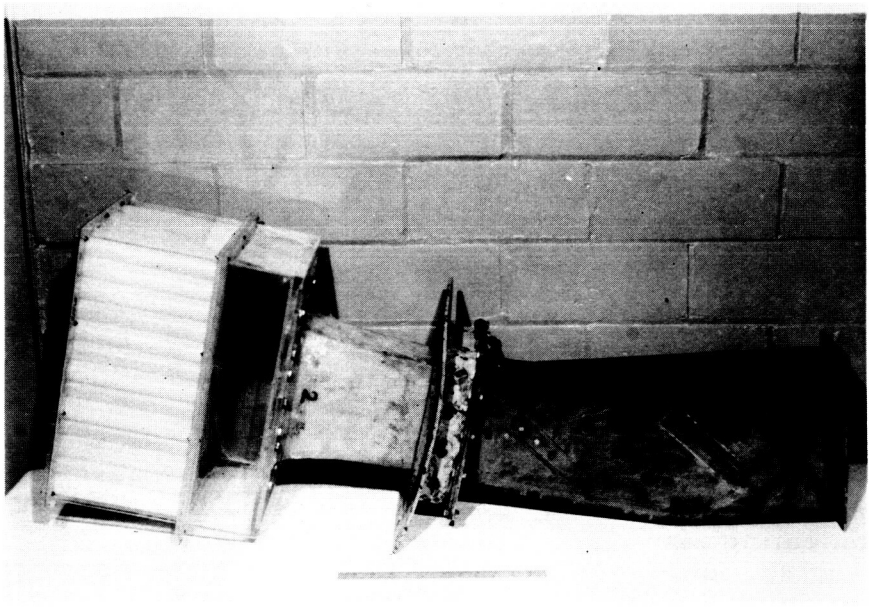

b. A test section with transition and flow straightener sections attached.

Figure 20. Cascade test sections.

used was a convergent nozzle with rectangular flow cross section. The fiberglass nozzle, as can be seen in Figure 20, was integral with a supporting steel box and curved attaching flange (which held the transition section to the side wall of the head tank). The nozzle walls were elliptical in shape and were designed according to relations recommended for cavitation free inlets (23). The nozzle when the transition section was in place protruded inside the head tank.

Difficulty in attaining uniform axial flow in the transition section and in the approach flow to the blade row in the test section was encountered early in the test program. It was apparent from directional probe traverses upstream of the cascade blades that a vortex was being swallowed in the nozzle resulting in an unacceptable whirl of the flow into the cascades. To straighten the flow, two wood fences were built side-by-side with staggered horizontal slats inside the head tank. In addition, a straightener section(fabricated from sheet Plexiglas) with cross-sectional area of approximately seven times the inlet flow area to the test sections and packed with thin-walled plastic tubes 8 inches long and 1-inch in diameter was attached to the upstream side of the transition section (see Figure 20). No measurable whirl of the flow into the test sections was found after these modifications were made.

The elevated head tank had a diameter of 5 feet and capacity of 800 gallons. A constant head was maintained in the tank by supplying a flow rate to the tank exceeding that demanded from the tank through the test section. The opening through which the flow entered the test section was located approximately one foot above the bottom of the tank. This placed the head of water in the tank at about 4 feet above the discharge flow. The excess inflow overflowed the tank into a collecting collar (which can be seen in Figure 21) around the outside of the tank near the top. The spilling water was returned from the collar to the sump (see Figure 19). Make-up water was supplied to the head tank at small flow rates to replace water lost from the system via leaks and to maintain steady-state water temperatures. The amount of make-up water not used for supplying leaks simply overflowed the sump and ran off to a floor drain.

The circulating pump operated at constant speed and had a rated capacity of 350 gpm at 45 feet of total head. Flow rates through the pump were controlled by a valve located in the 3-inch discharge line from the pump. Also, a short length of rubber hose formed a part of the discharge line on the low-pressure side of the control valve to isolate pump vibration from the head tank. Flow rates through the test section were regulated by a control valve downstream of the discharge barrel.

Cascade Blades and Blade Installation

For all tests an NACA $65(A_{10})$-810 blade profile was specified. Details of the profile mean line and thickness distribution are given in Reference 9. Blade chord was 3.75 inches and trailing edge thickness was 0.020 inches. The blade span was 3.75 inches giving an aspect ratio of 1.0. Blade contours were smooth to within $\pm$ 0.005 inches of true contour, and with deviations from fairness not exceeding 0.005 inches per 0.025 inches of surface length.

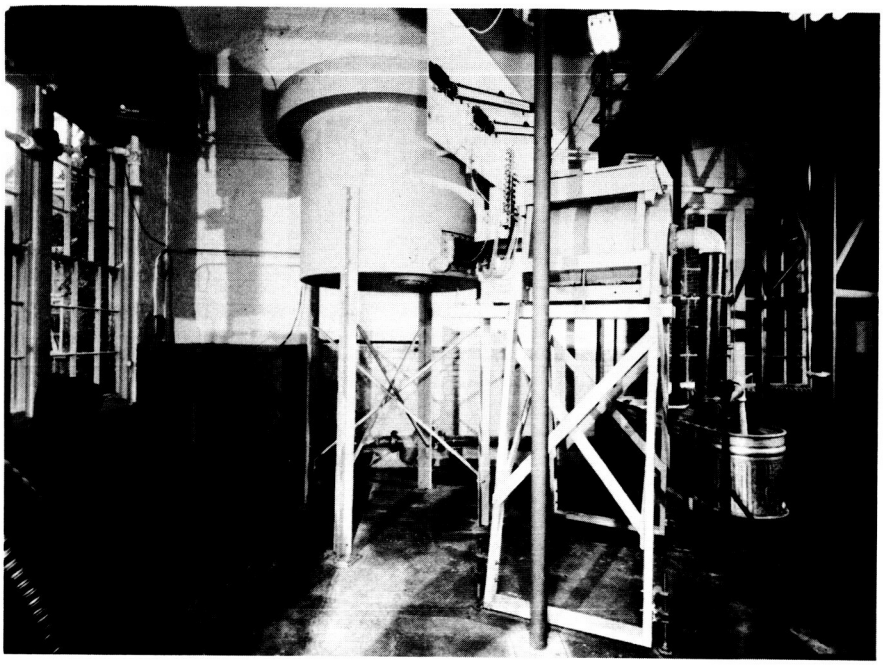

a. General view of test set-up with cascade test section in place.

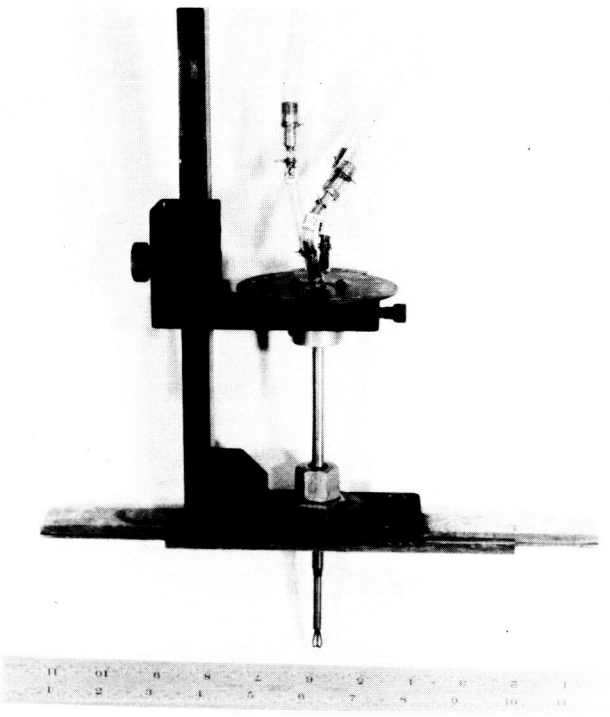

b. Total head-claw probe and positioning device.

Figure 21. Equipment used in experimental cascade measurements.

The blade setting angles used in the three test sections were 18.4, 33.2, and 48.3 degrees, respectively. These values of setting angle corresponded to design incidence of flow into each cascade for inlet flow angles, β_i', of 30, 45 and 60 degrees as determined from low-speed air data (9). Also the assigned flow-turning implied by the fixed end walls of the test section downstream from the cascade was set equal to design turning of 18.2, 17.8 and 15.0 degrees, corresponding to the inlet flow angles of 30, 45, and 60 degrees (9). The curved end walls were purposely designed to produce turning of the flow in a circular arc on approximately the mid-channel streamlines situated between two adjacent blades in an attempt to make the flow appear as reflected in the end walls and in effect to extend the cascade in either direction to one having a greater number of blades. In Figure 20 the increase in diffusion with blade setting angle is evident from the different widths of flow channel at the discharge of the test sections. Because of this changed channel width, a total of 3, 4, and 5 blades were required for the 30, 45, and 60 degree test sections, respectively, to provide a blade row solidity, σ, of 1.50. Figure 22 defines the cascade nomenclature used above.

The cascade aspect ratio was too small to avoid side wall effects on the flow through the blades, but was as large as practical testing considerations and Reynolds number range would allow in view of the maximum available flow rate. In this regard, a plot of flow rate, inlet flow velocity based on inlet cross-sectional area and blade-chord Reynolds number against inlet dynamic head is presented in Figure 23.

The test blades were fabricated from brass by the Jarvis Corporation of Middletown, Connecticut.

In each blade row the central blade was instrumented for static head measurement. The instrumented blade (Figure 24) had a line of pressure taps located around the profile at the mid-span in the flow channel. The tap locations in per cent of chord were, for the suction surface, 1.25, 5, 10, 20, 30, 40, 50, 65, 80 and 90, and for the pressure surface, 2.50, 5, 10, 25, 40, 50, 65, and 85. (Staggering of locations of the first and last taps on the suction and pressure surfaces was necessary because of structural limitations imposed by the blade thinness near the leading and trailing edges.)

The pressure tap holes were 0.015 inches in diameter. These holes were drilled in 21 ga. (0.032-inch O.D., 0.006-inch wall) stainless steel tubes which were then embedded with epoxy cement in 1/32 - inch deep spanwise slots which had been cut in the blade. The embedded ends of the tubes, which extended into the blade past the line of taps, were crimped shut to prevent plugging with epoxy. The taps holes were kept closed during the cementing process by reinserting the drill bits in the holes. The inserted bits also provided a means of maintaining the centerlines of the tap holes normal to the blade surface. The epoxy and any exposed tubing metal was dressed down, to fair with the blade profile. Care was taken to dress the taps holes to a sharp edge around the inserted drill bits. The bits had been coated lightly with oil to prevent adhering of the epoxy and to allow the bits to be withdrawn at the end of the dressing operation.

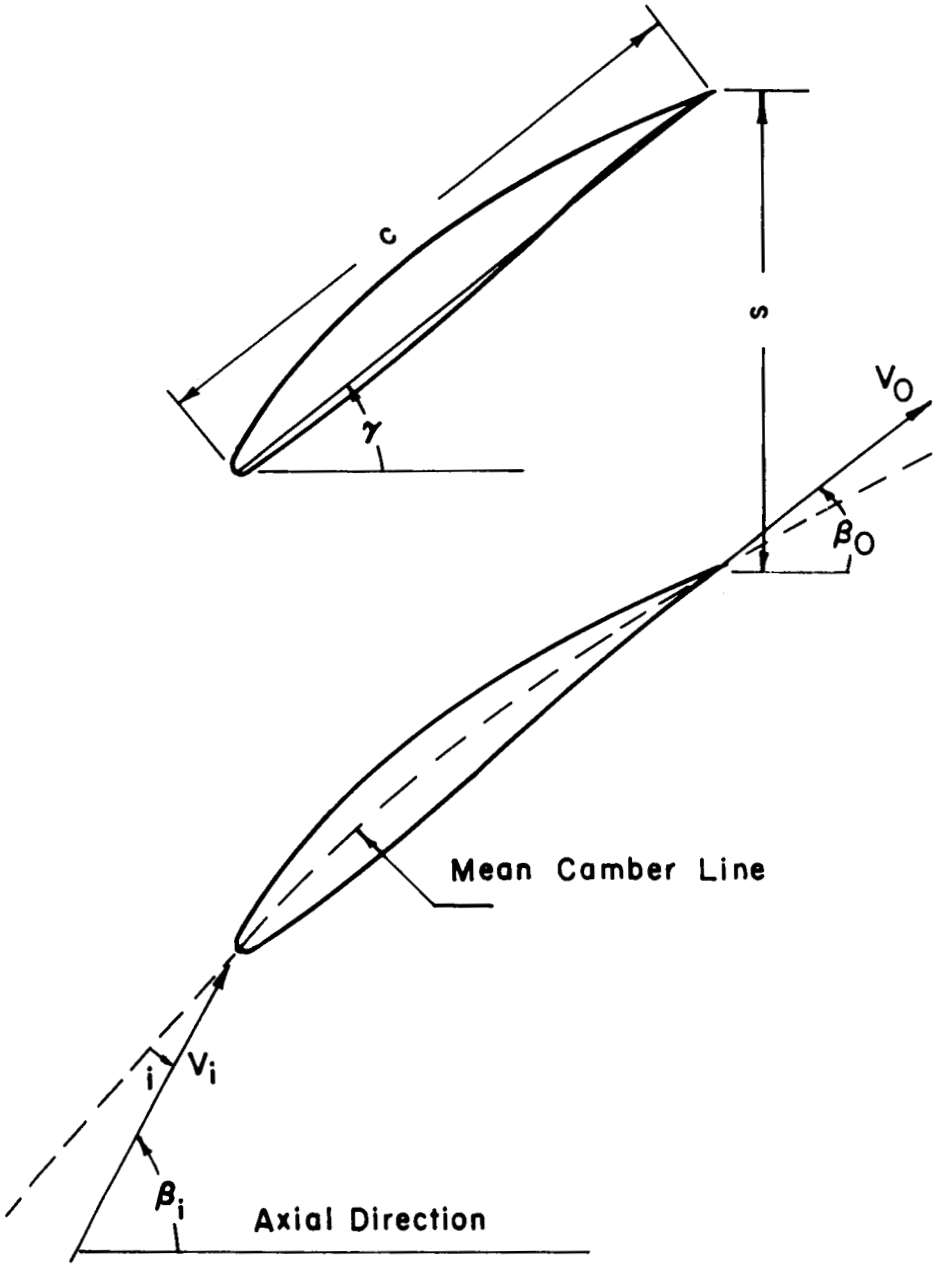

Figure 22. Nomenclature for cascade blade.

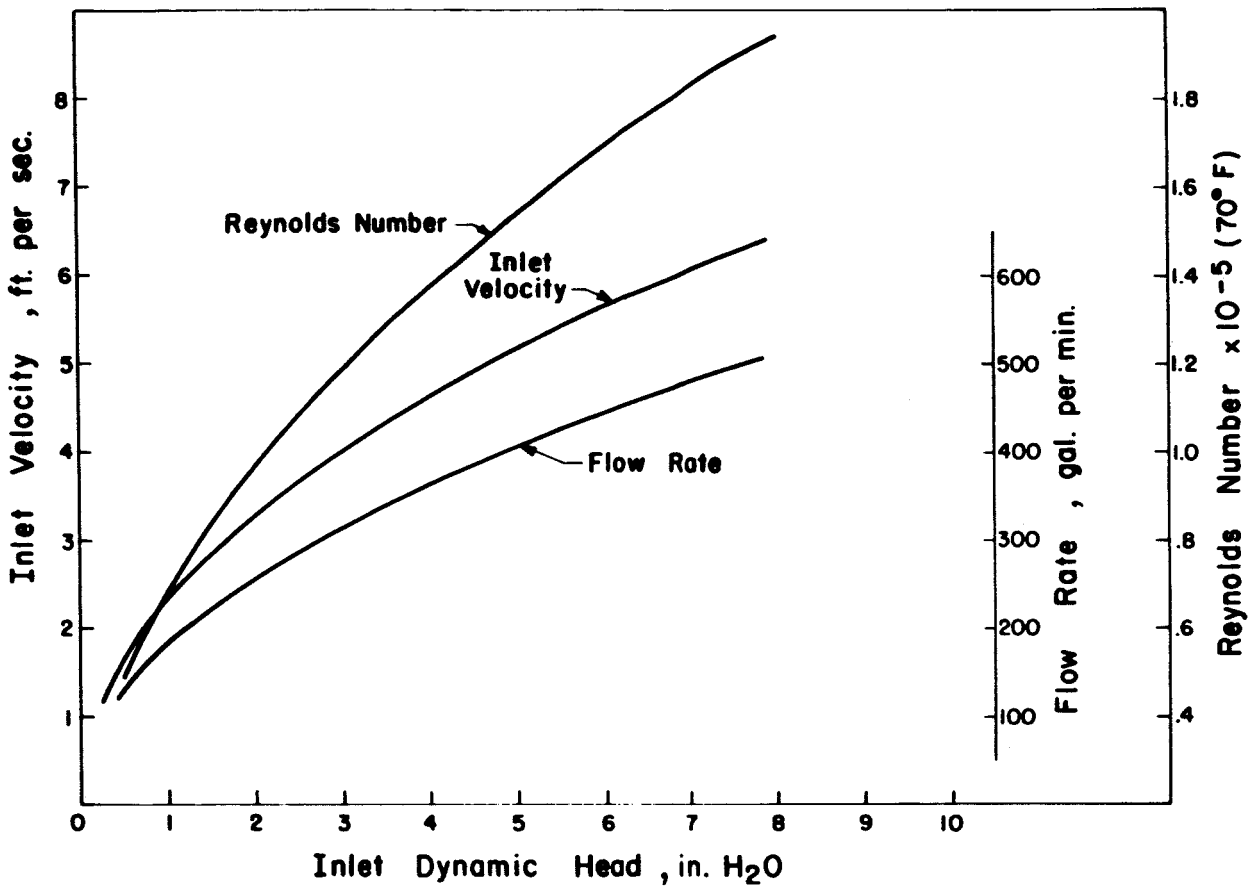

Figure 23. Cascade test sections flow characteristics.

As can be seen in Figure 21 the cascade blades and pressure leads for a test section installed in the flow circuit extended vertically downward across the flow passage and out through a Plexiglas window. Slightly over-sized holes conforming to the blade profile cut in the window received the blades. The clearance between the blades and the window holes presented a difficult sealing problem, since the blades and windows were not expendable and temporary rather than permanent sealing was necessary. Various materials were tried as sealers, such as putty, plastic clay and calking compounds, but they were found to be unsatisfactory. A material finally used, and which proved reasonably satisfactory, was pattern maker's strip-fillet material made of beeswax. This material was warmed slightly and was pressed into the clearance space between the blades and window from both inside and outside the test section and around the window itself.

Each blade was installed with an attached threaded mounting stub which extended from inside the flow channel out through the side wall opposite the window. Blade photographs are shown in Figure 24. The blade mounting holes in the side wall were counter-bored to receive an alignment collar on the mounting stubs. Proper orientation of the blades in a test section was accomplished by setting the blade trailing edges at small punch marks which had been made in the flow channel wall prior to assembly of the test section.

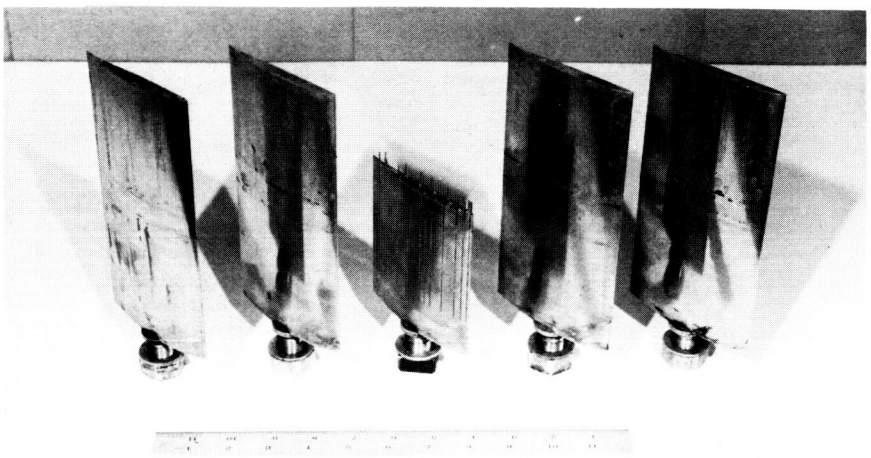

a. The test blades in cascade arrangement.

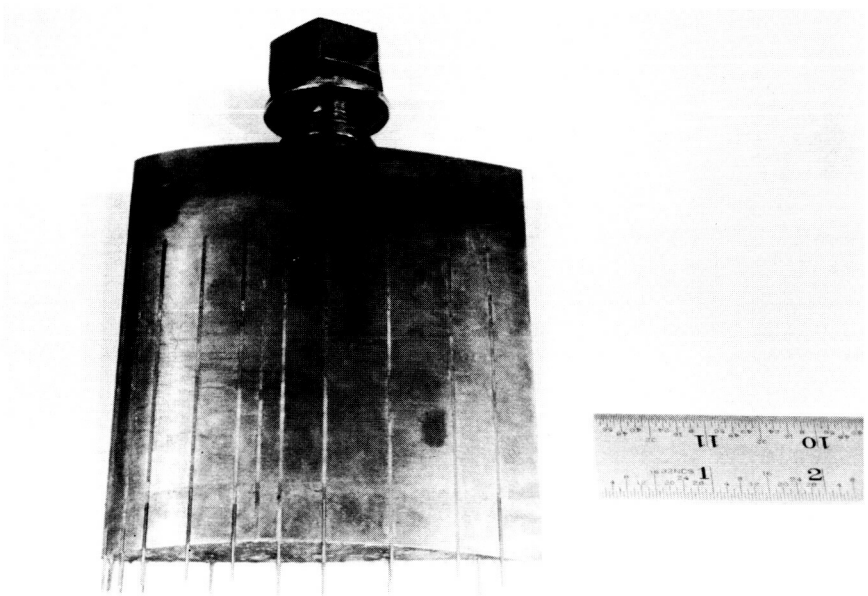

b. The instrumented blade.

Figure 24. Test blades.

Measurement of Cascade Parameters

To obtain measurements of pressure distribution on the instrumented blade, short lengths of small diameter plastic tubing were connected outside the test section window to the exposed ends of the embedded tubes. The plastic tubes in turn attached to stainless steel connector tubes on one side of a connector bar. Short lengths of larger diameter copper tube emerged from the other side of the connector bar serving as connectors for 1/4-inch diameter plastic tubing leading to a valve-selector manifold and manometers as shown in Figure 21.

Piezometric head was measured directly using the water flowing as the indicator fluid. This required the tops of the manometers to be elevated slightly above the level of the water in the head tank. Two inclined manometers with 20-inch scales and least count of 0.02 inches were used. The head to either manometer came from one of the valve selector manifolds and was transmitted directly to the inclined tube, bypassing the manometer well.

Measurement of head values referenced to cascade inlet static head was unsuccessfully tried using a micromanometer with mercury as the indicator fluid; also a system, which was an inversion of normal micromanometer application, using n-Heptane (sp. gr. 0.68) above water as the indicating fluid was tried. Either of these systems would have been desirable on the basis of the increased number of reading divisions (20 times as many) over the inclined manometer system. However, neither of these systems was successful because of the extremely slow response resulting from the relatively long length of small diameter tubes embedded in the instrumented blade. Response time for measurements on the inclined manometers was on the order of 20 or 30 minutes.

The claw-total pressure probe used for total head measurement and flow direction indication is shown in Figure 21. The probe is shown mounted in a probe positioner which located the probe in vertical (spanwise) traverses across the flow channel. A brass slide-bar mechanism shown attached to the base of the probe positioner located the probe horizontally across the flow channel at a measuring station located one-half to three-fourths of a chord length downstream of the blade row. The slide bar was purposely made longer than its bearing piece (which attached to the side wall of the test section) so that exposure of the traversing slot in the side wall would not occur during horizontal positioning of the probe. The two side tubes of the probe were "nulled" to determine flow direction. An inverted U-tube manometer with n-Heptane over water as the indicating fluid was used to determine the null point. It is noted that n-Heptane serves well as an indicator fluid with water flow; it has a relatively low viscosity for good response characteristics and low specific gravity (readings are magnified). It also maintains a well-defined meniscus, being practically immiscible and insoluble in water. The probe total head readings were indicated on the same manometer system used in the blade pressure distribution measurements.

The two inclined manometers used for head measurement were calibrated

against a hook gage which could be read to 10^{-4} feet of water. The calibrations were made by recording various static-head levels in the head tank on the hook gage and on the inclined manometers. Since the scales on the manometers were adjustable, an arbitrary reference head value was selected. Both manometers were adjusted to read the same at the reference point prior to calibration. Hence, for convenience in reading the resultant calibration curves the true values from the hook gage were converted to inches of water and adjusted to the same reference as the manometers. Total head for the system during the test runs was also determined on the hook gage; static head at the inlet to the cascades was measured on one of the inclined manometers using static taps located in the side walls of the test section ahead of the blade row.

Calibration of the claw probe involved determination of a probe reference angle made by positioning the probe, probe positioner with attached slide bar at a calibration station ahead of the blade row. The slide bar was clamped to the test section with its centerline parallel to its line of traverse downstream of the blade row. The probe was inserted into the flow at the calibration station through a hole in the side wall. Hence, flow angles measured in traverses made downstream of the blade row were related to the upstream reference angle to find the cascade turning angles. Also, with the probe stationed ahead of the blades total head for the inlet flow was determined at various flow rates. With corresponding inlet static head and system total head values known, calibration of actual versus ideal inlet dynamic head was made. Hence, during test runs (with the claw probe in traversing position downstream of the blades) the inlet total head could be determined from system total head, inlet static head, and the calibration of actual versus ideal inlet dynamic head.

Testing Procedure

The pressure leads were bled prior to test runs by opening all manifold valves and bleed valves located at the top of the manifolds.

Start-up procedure involved starting the pump, followed by opening of the pump control valve. With the entire flow spilling into the collecting collar and returning to the sump, the test section control valve was opened slowly until the desired flow through the test section was obtained (with some spilling into the collecting collar retained).

Test Results

The experimental results for the three test cascades are summarized in Figures 25 through 30. The profile head coefficient distributions shown in Figures 25, 26 and 27 agree at least qualitatively with equivalent air test data. The tests in air were conducted with elaborate boundary layer control in the test section (5), whereas in the water cascade tests boundary layer control was not used. Also the air data were obtained at blade-chord Reynolds numbers above 200,000. Reynolds numbers for the water cascade tests were appreciably lower, ranging from 89,000 to 135,000. From the comparison of test results in Figures 25 through 27 for different blade-chord Reynolds

number an effect of Reynolds number on head coefficient distribution is evident.

The head coefficient values obtained are in general lower than those for air, indicating higher blade surfaces velocities. This would be expected as a result of the blockage effect of the side- and end-wall boundary layers. From the comparison in Figures 25, 26 and 27 it appears that blockage has greater effect on the pressure surface than on the suction surface, with the effect becoming more extreme as the blade setting angle is increased. Agreement between water and air test results is especially poor near the leading edge and over the aft portion of the blade for a setting angle of 48.2 degrees (Figure 27).

The actual fluid turning angles and head-loss coefficient distributions obtained from claw total-head probe traverses made downstream of the cascade are shown in Figures 28, 29, and 30. In these figures, the horizontal traverse station axis refers to stations located along a line in the traverse plane parallel to the axis of the cascade. The short arrow in the figures locates the projection of the trailing edge of the central blade of the cascade in the traverse plane. The head-loss coefficient is based on the system total head, H, as determined by the water level in the constant head tank rather than on total head at the inlet to the cascade.

The presence of the blade wake is clearly evident in the plots of headloss with the maximum loss in the wake being three to four times as large as that in the wake-free portions of the discharge flow. Also, some skewing of the wake is apparent from shift of the wake location between the mid-span and quarter-span traverses in Figure 29, giving indication of failure to attain a two-dimensional flow.

Contraction of the main stream in the flow through a cascade due to thickening of the boundary layers along test section walls causes acceleration of the flow in opposition to the normal diffusing effect. This results in a lessening of the adverse pressure gradient and, hence, an increase in effective Reynolds number near the trailing edge of the blades as well as deviations in the cascade turning and loss characteristics from those that would be measured in a two-dimensional flow. These effects, which are dependent only on the geometry of the cascade test section, are the principal reasons for apparent differences in results obtained during testing of identical blade configurations in different cascade tunnels.

Stuart (33), by expressing the increase in boundary layer displacement thickness in terms of chord, and by regarding the pressure rise as occurring over the cascade itself, obtained a corrected pressure coefficient based on the cascade outlet conditions. The corrected head coefficient based on Stuart's result is

$$1 + \frac{1}{\xi^2}\left[1 - (1 - \xi)\left(\frac{x}{100}\right)^3\right]^2 [HC - 1]$$

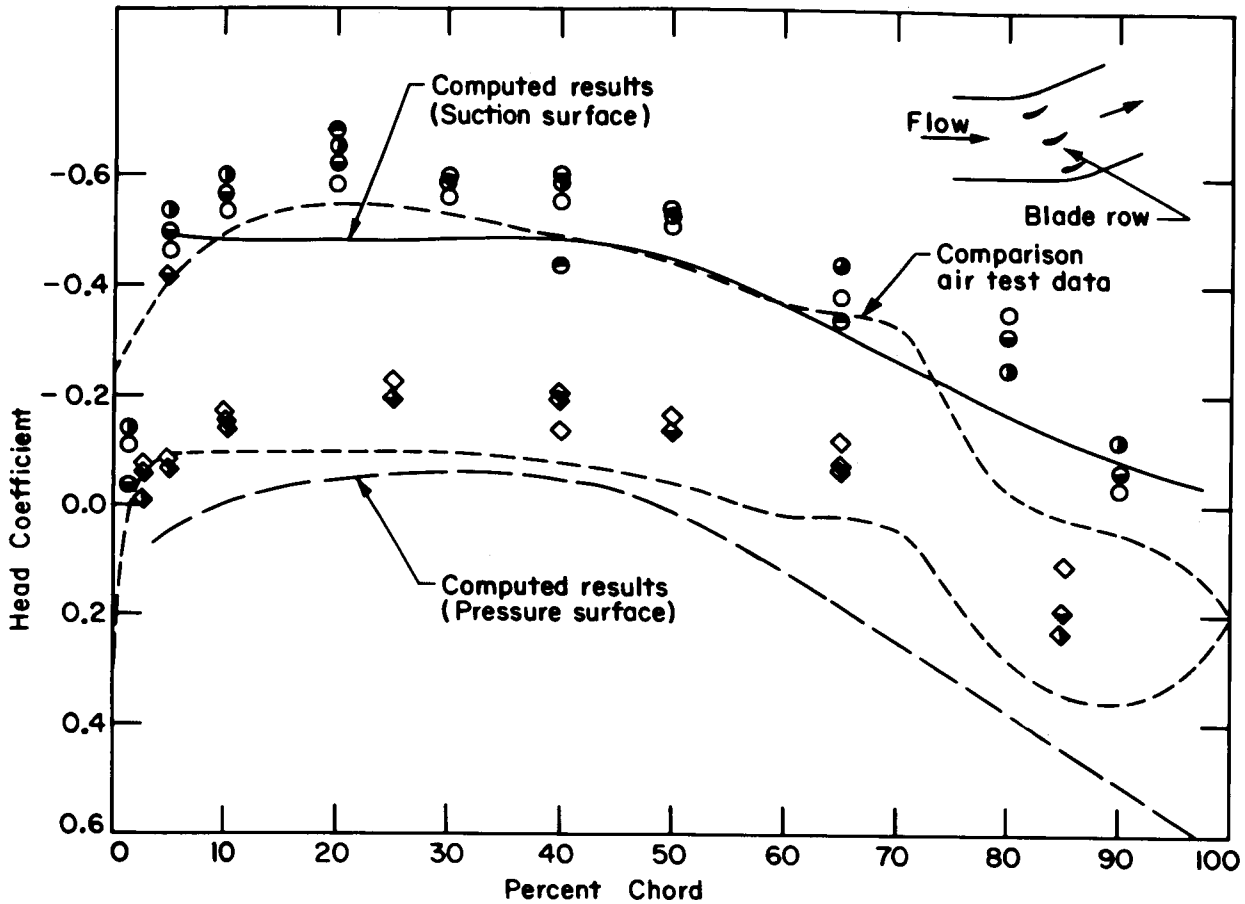

Figure 25. Experimental profile head coefficient distribution for γ = 18.4 degrees. β_i' = 30 degrees, σ = 1.5. NACA 65(A_{10})-810 profile.

Blade chord Reynolds number:
- ○ ◇ 89,000
- ◐ ◆ 108,000
- ◐ ◆ 123,500
- ◑ ◆ 134,000

(The equivalent air test head coefficient distribution shown is taken from Reference 9; computed head coefficient distribution is from Figure 13. Head coefficient is

$$\frac{h - h_i}{h_{t,\,i} - h_i})$$

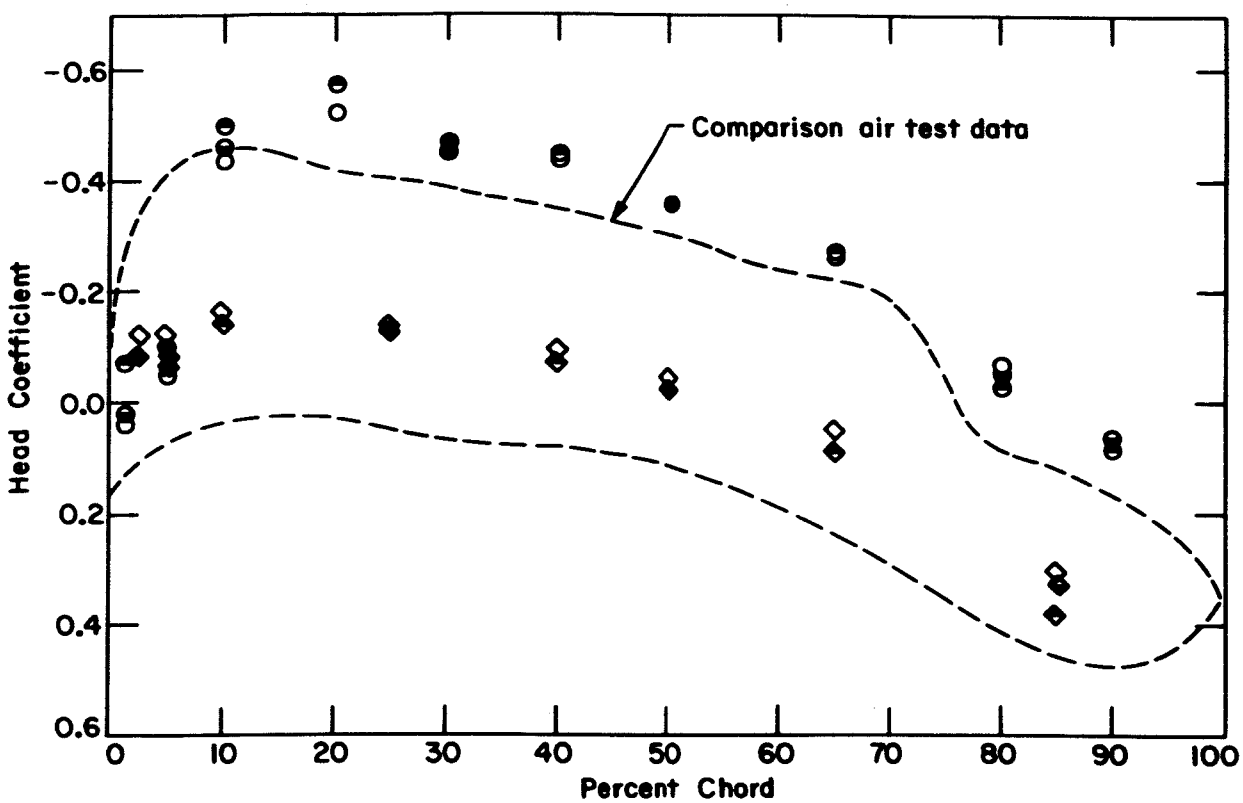

Figure 26. Experimental profile head coefficient distribution for γ = 33.2 degrees. β_i' = 45 degrees, σ = 1.5. NACA 65(A_{10})-810 blade profile.

Blade chord Reynolds number: ○ ◇ 109,500
◒ ◈ 112,000
◒ ◈ 129,000

(Equivalent air test head coefficient distribution shown is taken from Reference 9. Head coefficient is

$$\frac{h - h_i}{h_{t,i} - h_i})$$

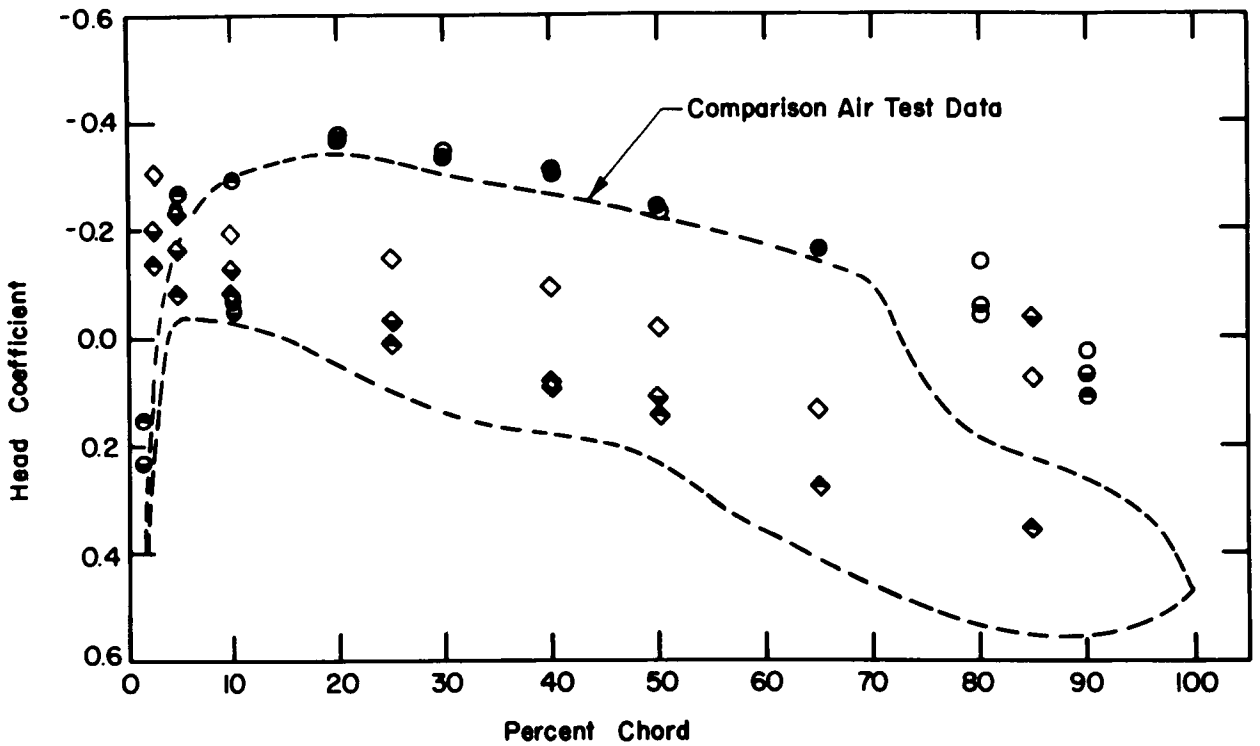

Figure 27. Experimental profile head coefficient distribution for γ = 48.2 degrees. β_i' = 60 degrees, σ = 1.5. NACA 65(A_{10})-810 blade profile.

Blade chord Reynolds number: ○ ◇ 93,500
◒ ◆ 116,000
◒ ◆ 132,500

(Equivalent air test head coefficient distribution shown is taken from Reference 9. Head coefficient is

$$\frac{h - h_i}{h_{t,i} - h_i})$$

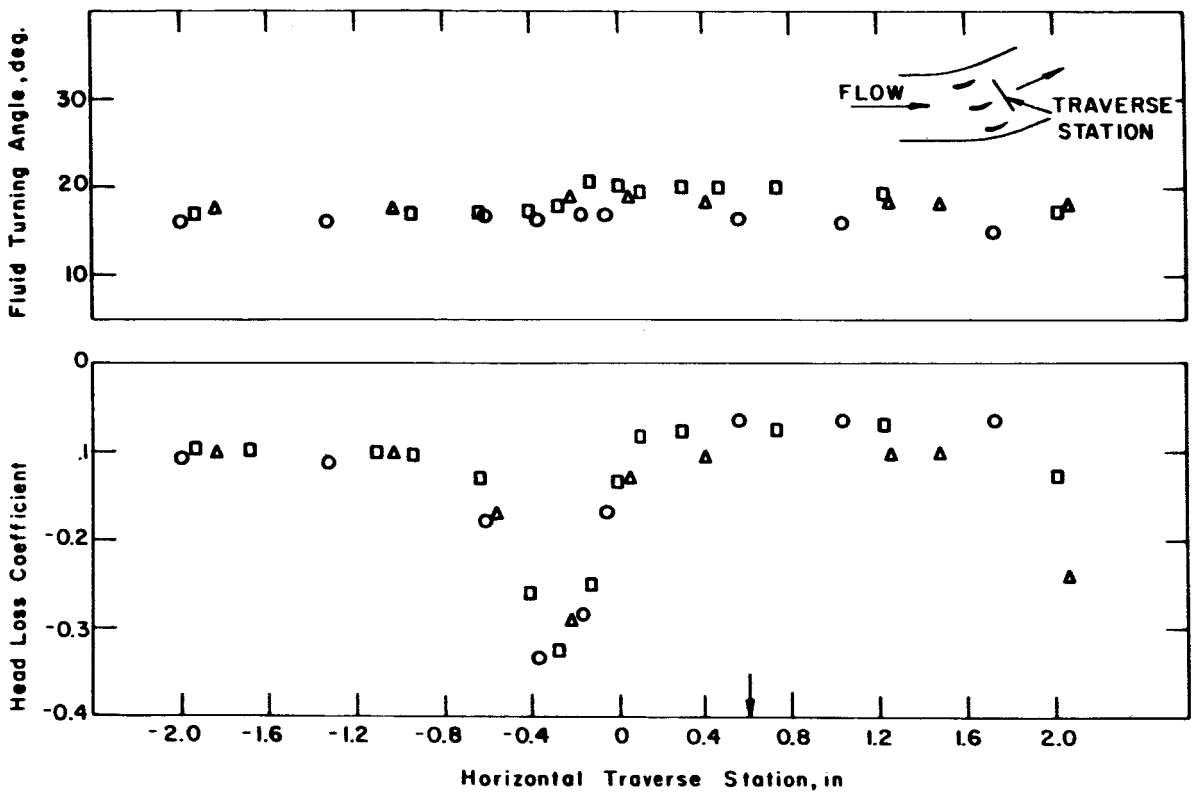

Figure 28. Survey of cascade discharge flow.

γ = 18.4 deg., β_i' = 30 deg., σ = 1.5. NACA 65(A_{10})-810 blade profile.

O 2/3 blade-span station. Blade chord Reynolds number 89,000.

Δ 1/3 blade-span station.

□ Mid-span station. Blade chord Reynolds number 123,500.

(Spanwise stations measured from test section side. Head-loss coefficient is $\frac{h_{t,o} - H}{H - h_i}$. Design turning angle 18.4 deg.)

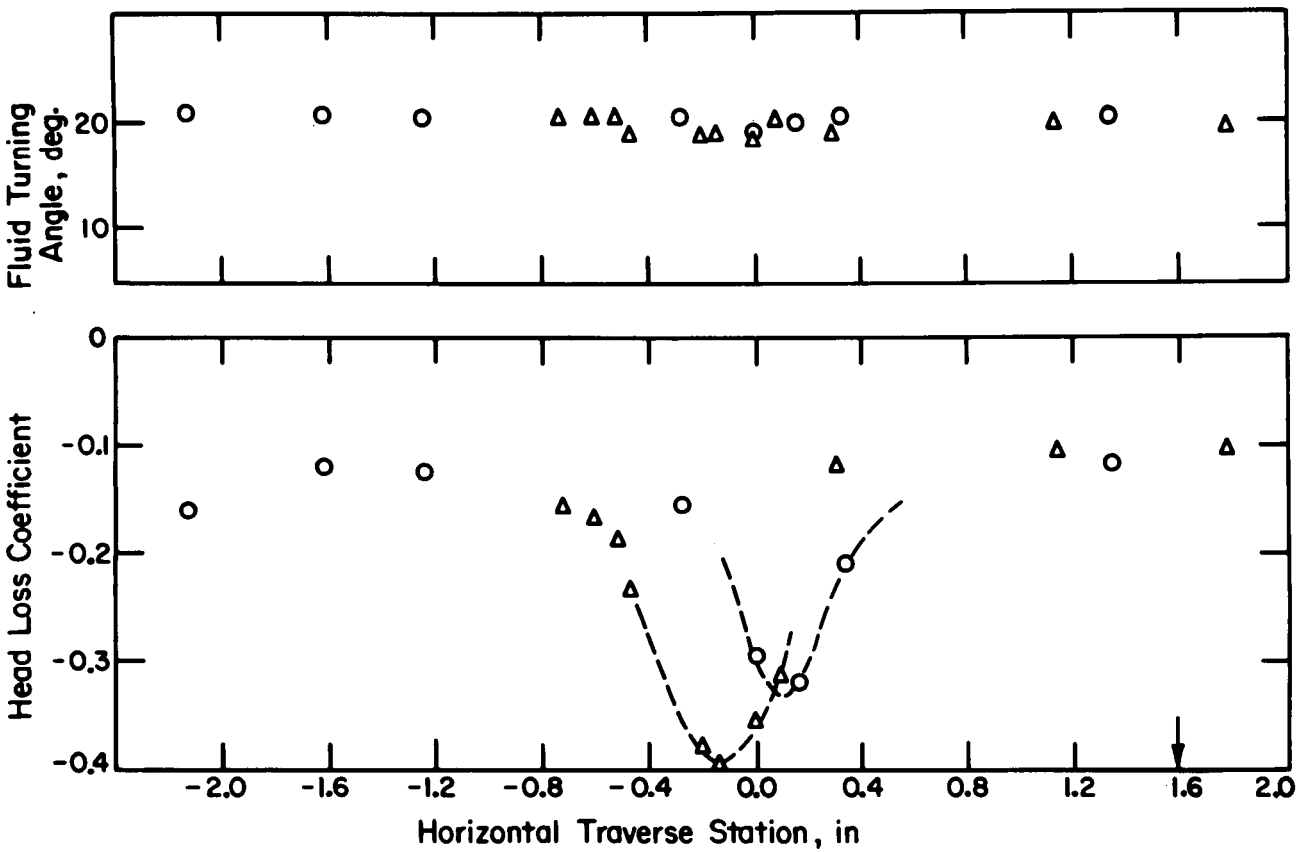

Figure 29. Survey of cascade discharge flow.

γ = 33.2 deg., β_i' = 45 deg., σ = 1.5. NACA 65(A_{10})-810 blade profile.

O Mid-span station. Blade chord Reynolds number 111,000.

Δ 1/4 blade-span station. Blade chord Reynolds number 112,000.

(Spanwise stations measured from test section side wall. Head-loss coefficient is $\frac{h_{t,o} - H}{H - h_i}$. Design turning angle 17.8 deg.)

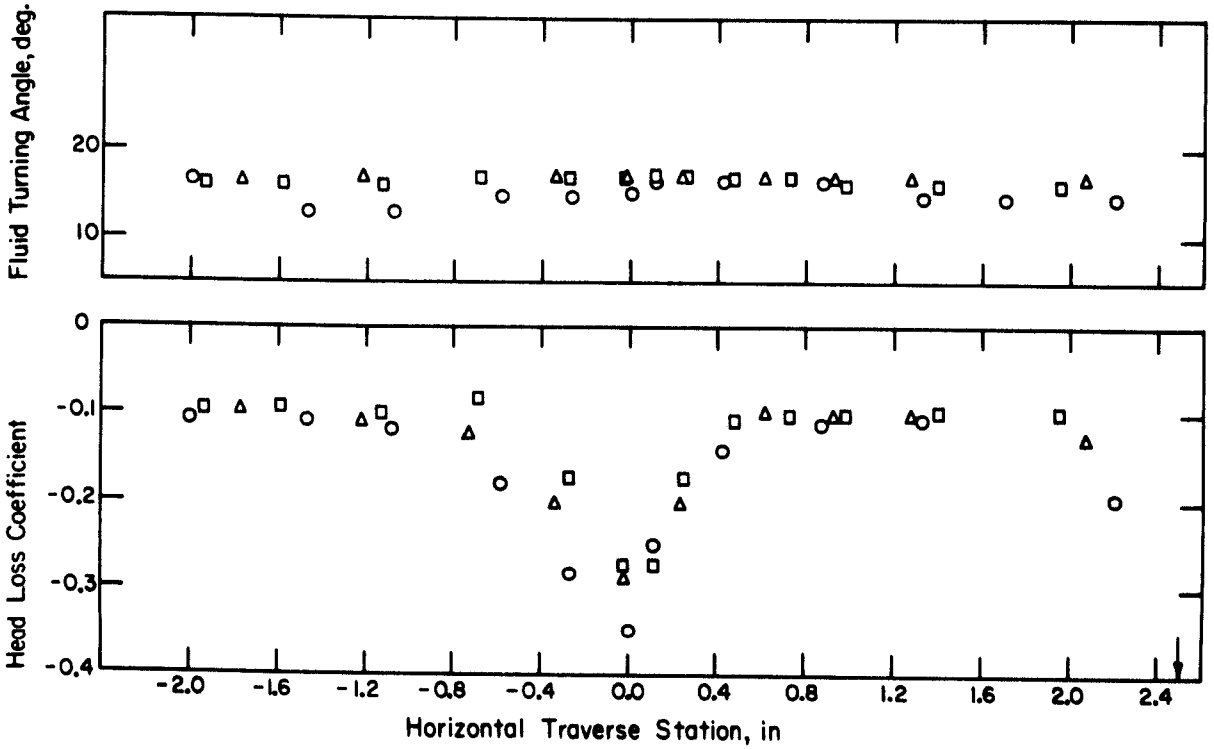

Figure 30. Survey of cascade discharge flow.

γ = 48.2 deg., β_i' = 60 deg., σ = 1.5. NACA 65(A_{10})-810 blade profile.

○ Mid-span station. Blade chord Reynolds number 93, 500.

△ Mid-span station. Blade chord Reynolds number 116, 000.

□ Mid-span station. Blade chord Reynolds number 132, 500.

(Head-loss coefficient is $\frac{h_{t,o} - H}{H - h_i}$. Design turning angle 15.0 deg.)

where HC is the head coefficient as defined for Figures 25 through 27 and the contraction ratio accounting for the flow contraction due to the boundary layer. Stuart presents values of ξ over a range of Reynolds number, inlet flow angle, and turning angle (33); an estimate of ξ for the case represented in Figure 25 with Reynolds number of 108,000 is 0.94.

Values of corrected head coefficient and the test data from Figure 25 for blade-chord Reynolds number of 108,000 which served as the basis for the corrected values are shown in Figure 31. Also shown from Figure 25 are the equivalent air test results (blade chord Reynolds number above 200,000). It is clear in Figure 31 that the corrections failed to bring the water test data into agreement with the two-dimensional air test data; in fact, the correction is in the wrong direction over most of the profile, indicating a greater Reynolds number effect on head coefficient distribution than before. Because the results of the correction procedure were inconclusive further attempts to apply two-dimensional flow corrections to the remaining test data were not made.

CONCLUSIONS

Based on the preceding analysis and results a number of conclusions may be stated:

1. A solution method employing finite difference techniques has been developed for determining the blade-to-blade flow of an incompressible nonviscous fluid through a rotating turbomachine blade row. Axisymmetric stream surfaces with a variable stream-tube thickness function distribution were assumed.
2. A general computer program was developed from which solutions could be obtained in dense computing meshes without excessive computing times. Solutions for selected cascade configurations were determined to illustrate the ability of the program to deal with various blade profiles, blade setting angles, fluid angles, and stream tube configurations.
3. Difficulty was encountered in a number of the solutions in obtaining uniform discharge flows and realistic turning angles as well as agreement between pressure values on the suction and pressure sides of the blades near the leading and trailing edges. Such pressure differences have been reported by Mellor (18) in calculation of two-dimensional blade cascade characteristics using the method of singularities and were eliminated by adjustment of the mean camber line (use of a camber line shape in the calculating system deviating from the true value for the blade profile under study).
4. The results of the analytical and the experimental investigations indicate that for practical design, experimental cascade data will continue to be a necessary supplement to calculation systems.

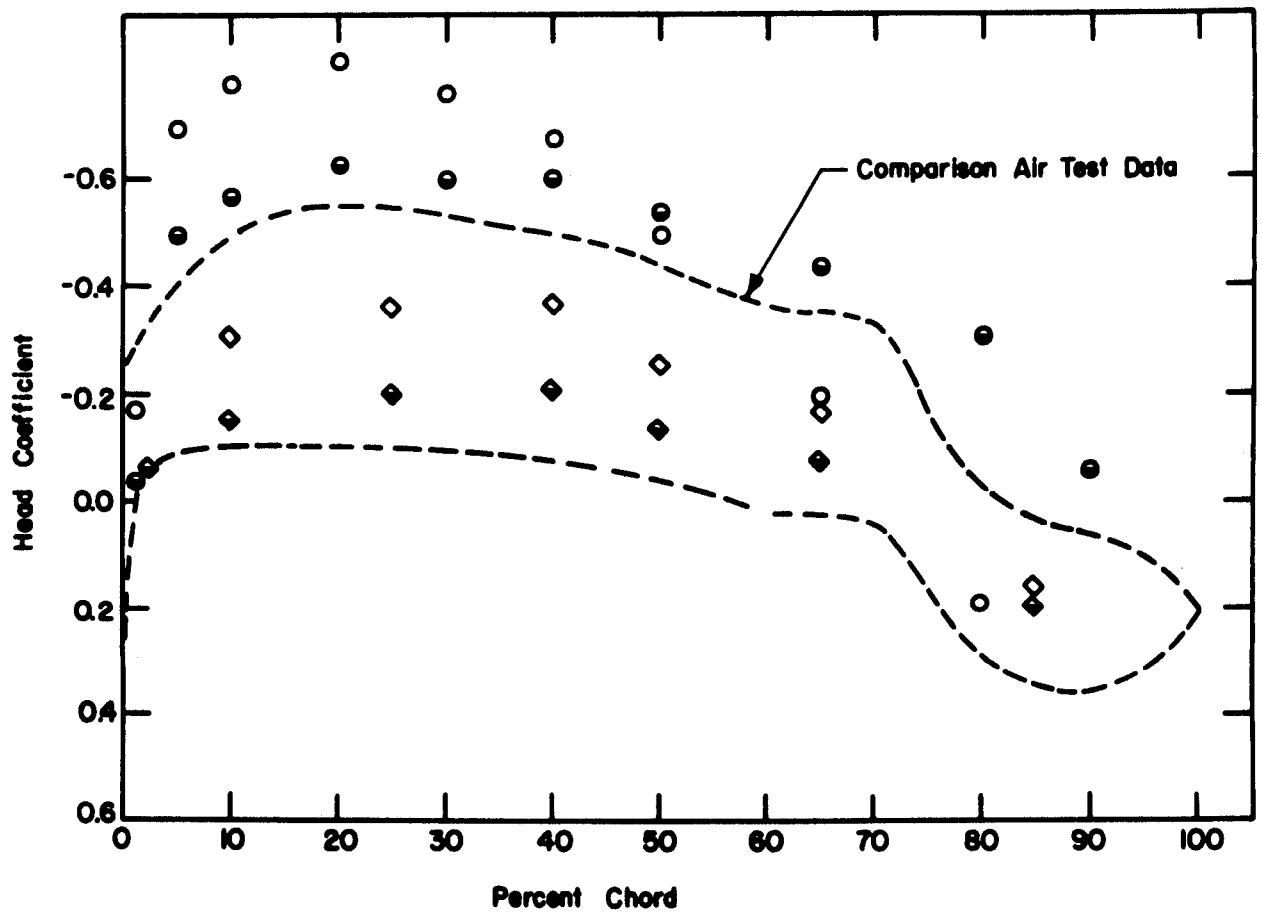

Figure 31. Comparison between corrected head coefficient values and actual test data from Figure 25. Blade chord Reynolds number 108,000.

test data

corrected data

APPENDIX A

Symbols

A	a coefficient
a_0, a_1, a_2	curve-fit parameters (see Equation 59a)
B	a coefficient
b_0, b_1, b_2	curve-fit parameters (see Equation 59b)
C	a coefficient
$c_1, \ldots, c_6$	curve-fit parameters (see Equations 48c, 50c)
c	blade chord, L; a constant
E	shift operator (see Equation 35a)
f	a function
g	acceleration of gravity, LT^{-2}
H	total head, L
H'	relative total head (see Equation 6)
h	piezometric head, L
i	a positive integer; inlet station; incidence angle, angle between inlet flow velocity and tangent to blade mean camber line at leading edge
j	a positive integer
$K_1, \ldots, K_5$	curve-fit parameters (see Equations 39, 41)
k_2, k_3	scale factors (see Equations 26)
l	Lagrange coefficient
M	blade mean camber line
m	orthogonal curvilinear coordinate; length parameter (see Equation 17)
N	a parameter (see Equation 27)
n	orthogonal curvilinear coordinate; number of blades; a positive integer
o	outlet station
p	pressure, FL^{-2}; pressure boundary
q	increment ratio (see Equation 64)
r	radius, L; radius ratio (see Equation 17)

S	stream surface
s	suction; suction boundary; blade spacing in circumferential direction, L
t	blade profile thickness, L
U	wheel speed, LT^{-1}
V	absolute flow velocity, LT^{-1}
W	flow velocity relative to blade row, LT^{-1}; dimensionless flow velocity relative to blade row
X	percent of chord coordinate
x	computing mesh coordinate (see Equation 25a)
x''	first x-station downstream of trailing edge of blades
x'''	outlet x-station
Y	percent of chord coordinate
y	computing mesh coordinate (see Equation 25a)
z	scaled stream function (see Equation 25b)
α	local profile angle measured from chord line
β	flow angle as measured from axial direction
γ	blade setting angle, angle between chord line and axial direction
δ	an increment
Δ	an increment; difference operator
θ	meridional angle
σ	cascade solidity ratio, $\frac{c}{s}$
τ	stream surface thickness function
ϕ	an angle in meridional plane (see Figure 4)
ψ	stream function; dimensionless stream function (see Equation 17); an angle in meridional plane (see Figure 4)
ω	angular speed, T^{-1}; relaxation factor

Subscripts:

i	inlet
M	mean camber line
m	m-component
n	n-component
o	outlet

p	pressure
r	r-component
s	suction
t	total; tip
u	θ-component
z	z-component
0, 1, 2	generic points

Superscripts:

—	input value (see Equations 55 - 63)
*	dimensional value; percent of chord coordinate
'	new value; relative to blade; blade forward edge
^	intermediate value (see Equation 53)

APPENDIX B

HEAD COEFFICIENT RELATION

Substitution of Equation 6 into Equation 7a shows that for between two stations located along a streamline in a steady flow relative to a rotating blade row

$$\Delta \left(h + \frac{W^2}{2g} - \frac{U^2}{2g}\right) = 0$$

Each term of the equation has dimensions of length. The equation can be made dimensionless by dividing through by a squared reference velocity, $\omega^2 r_t^2$, and by multiplying through by 2g:

$$\Delta \left(\frac{2gh}{\omega^2 r_t^2} + W^2 - r^2\right) = 0$$

In this equation, r is radius ratio and W is a dimensionless flow velocity with components W_m, W_u as defined previously in conjunction with Equation 17.

Next, division by the square of the dimensionless velocity at the inlet station to the blade row for the given stream surface gives

$$\Delta \left(\frac{2gh}{W_i^2 \omega^2 r_t^2} + \frac{W^2}{W_i^2} - \frac{r^2}{W_i^2}\right) = 0$$

The first term in this equation defines the head coefficient.

The change which occurs in head coefficient from the inlet station to the blade row to a station further downstream along a relative streamline may be written as

$$\frac{2g\Delta h}{W_i^2\omega^2 r_t^2} = 1 - \left(\frac{W}{W_i}\right)^2 + \frac{r^2 - r_i^2}{W_i^2} \qquad \text{(B1)}$$

in which Δh is the change in piezometric head from its value at the inlet station to the downstream station, and the values of W and r are taken at the downstream station.

According to the velocity triangle in Figure 3

$$W = \frac{W_m}{\cos\beta'}$$

Therefore, the velocity ratio and dimensionless inlet velocity required in Equation B1 can be expressed in terms of flow coefficient, W_m, as

$$\frac{W}{W_i} = \frac{W_m}{W_{m,i}} \frac{\cos\beta_i'}{\cos\beta'} \qquad \text{(B2)}$$

$$W_i = \frac{W_{m,i}}{\cos\beta_i'} \qquad \text{(B3)}$$

It is important to note that if the blade row is stationary ($\omega = 0$) the last term in Equation B1 goes to zero. This is to say that there is only a uniform change in head coefficient throughout the flow in a stationary blade row as the result of change in inlet flow coefficient. Also, for a stationary blade row the stream surface radius and its variation affect head coefficient only indirectly through the velocity ratio, $\frac{W}{W_i}$, as determined from the resultant flow pattern (see Equation 17).

The angles β' at stations along the streamlines corresponding to the blade profile boundaries are directly from the developed profile. The angle β' expressed in terms of profile setting angle, γ, and local profile angle, α, measured from the chord line is (see Figure 33)

$$\beta' = \gamma + \alpha \qquad \text{(B4)}$$

Thus α as a function of percent of chord stations needs to be determined only once and supplied in Equation B4 to determine β' at the various required x-stations in place of finding β' directly for each desired setting angle of the same developed profile.

STREAMLINE INTERPOLATION

To obtain the streamlines, Lagrange polynomials (10) are used to interpolate for the ordinates y in each x-panel for a set of constant z. The interpolation polynomial passes through three generic points $(y_o - 1, z_1)$, (y_o, z_o), $(y_o + 1, z_2)$, $(z_o, z_1, z_2$ are unequally-spaced data close to the interpolate z) and is written

$$y(z) = l_0 y_0 + l_1 (y_0 - 1) + l_2 (y_0 + 1)$$

$$= (l_0 + l_1 + l_2)\, y_0 - l_1 + l_2$$

where

$$l_0 = \frac{(z - z_1)(z - z_2)}{(z_0 - z_1)(z_0 - z_2)}$$

$$l_1 = \frac{(z - z_2)(z - z_0)}{(z_1 - z_2)(z_1 - z_0)}$$

$$l_2 = \frac{(z - z_0)(z - z_1)}{(z_2 - z_0)(z_2 - z_1)}$$

Obviously, if $y(z) = 1$, then

$$l_0 + l_1 + l_2 = 1$$

Therefore, the polynomial can be expressed as

$$y(z) = y_0 - \frac{(z - z_2)(z - z_0)}{(z_1 - z_2)(z_1 - z_0)} + \frac{(z - z_0)(z - z_1)}{(z_2 - z_0)(z_2 - z_1)} \qquad \text{(B5)}$$

APPENDIX C

THE 65(A_{10})-SERIES AIRFOIL IN CASCADE ARRANGEMENT

The NACA 65(A_{10})-series airfoil section is presented in Reference 9 in terms of thickness distribution (with maximum thickness of 10 percent of chord) and a basic mean camber line which can be modified according to the desired "isolated airfoil" lift coefficient. At selected percent of chord stations, X, the ordinate of the mean camber line, Y_M, in percent of chord, the slope of the mean camber line, $\frac{dY_M}{dX}$, and the profile thickness, t, in percent of chord are known. The profile is constructed by fairing a curve through the given points and by constructing a leading-edge radius.

The layout of the profile according to the above method for different camber, blade setting angles and solidities is time consuming and difficult to do with sufficient accuracy for purposes of the blade-to-blade flow solution. Alternatively, the location of the known points on the profile in a particular cascade arrangement can be determined as points (x_s^*, y_s^*), (x_p^*, y_p^*) in a rotated Cartesian coordinate system according to

$$x^*_{s,p} = (X + t \cos \gamma_{s,p}) \cos \gamma - (Y_M + t \sin \gamma_{s,p}) \sin \gamma$$

$$y^*_{s,p} = (X + t \cos \gamma_{s,p}) \sin \gamma + (Y_M + t \sin \gamma_{s,p}) \cos \gamma$$

as may be verified by referring to Figure 32. The angle γ is the profile setting angle measured from the x* (or machine) axis. Also, angles γ_s and γ_p are defined as

$$\gamma_s = \tan^{-1}\left(\frac{dY_M}{dX}\right) + \frac{\pi}{2}$$

and

$$\gamma_p = \gamma_s - \pi$$

The s-boundary of the profile extends from the leading edge point to the trailing edge over the suction (convex) portion of the profile. The p-boundary forms the remainder of the profile. Thus the equations above may be solved (for assigned camber and profile setting angle) and the resultant (x*, y*)

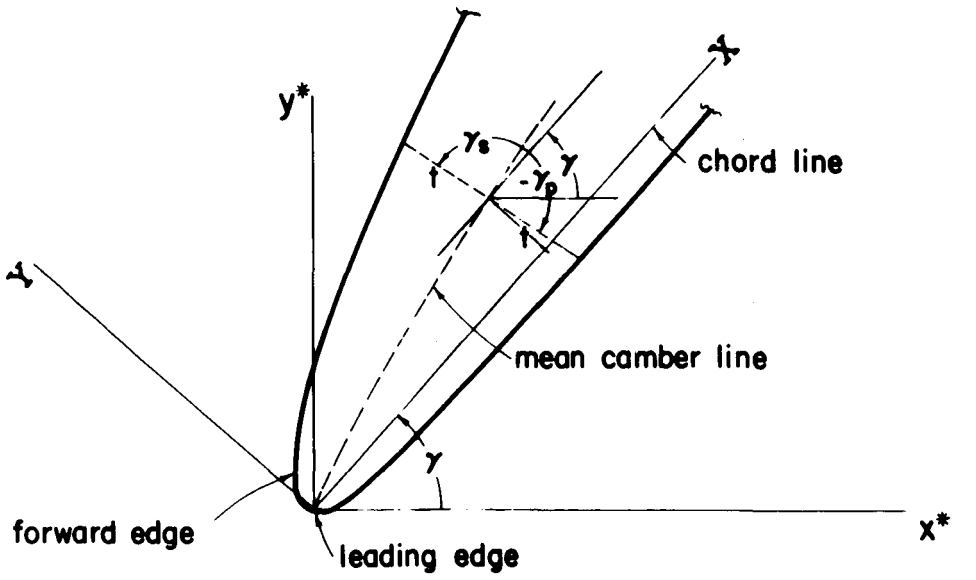

Figure 32. An NACA 65(A_{10})-series blade profile in partial view showing profile construction details.

points for the boundaries plotted in place of graphically constructing the profiles directly from their definition.

A final transformation from x*, y* coordinates to computing grid coordinates involving a translation and change of scale is made according to the equations (see Figure 33)

$$x^* = (x^*)' + \frac{100}{\sigma s}(x - x') \quad , \quad x = x', x' + 1, \ldots, x'' - 1$$

$$Y_s + \Delta_s = Y_s' + \frac{\sigma s}{100}[Y_s^* - (Y^*)']$$

$$Y_p + \Delta_p = Y_s' + s\left[1 + \frac{\sigma}{100}(Y^* - (Y^*)'\right]$$

where s (in units of the computing coordinates x, y) is the assigned blade spacing, $\sigma = \frac{c}{s}$ is the assigned solidity, and $(x^*)'$, $(y^*)'$ are determined from the constructed profile. The ordinate y_s' is the ordinate for the assigned mesh point at the forward-edge point of the profile.

Thus to determine the profile in computing coordinates the profile is first constructed to large scale in the x*, y* coordinates. Next, the points (x^*, y_s^*), (x^*, y_p^*) for the required x values are determined and trans-

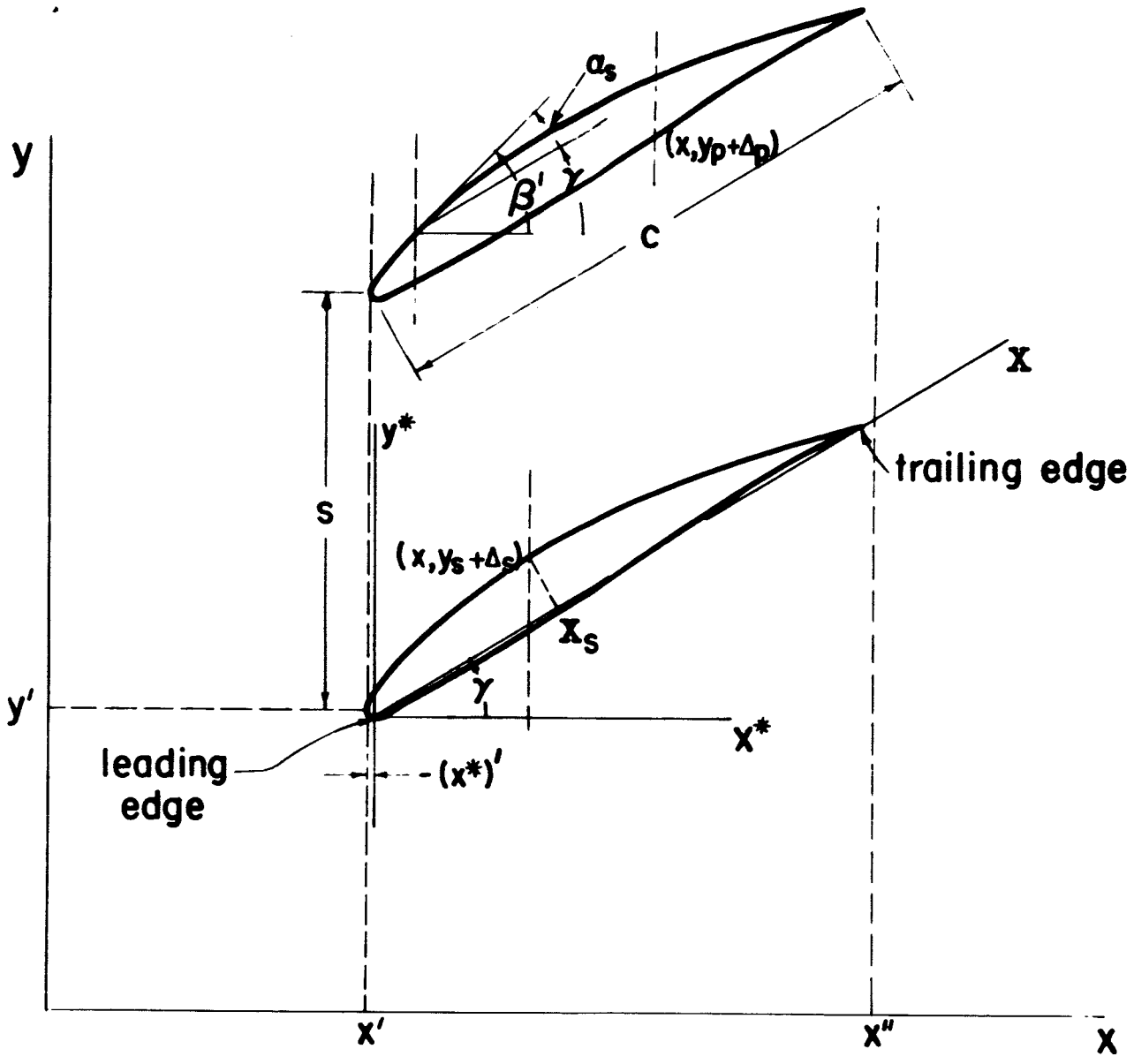

Figure 33. The NACA 65(A_{10})-810 blade profile in plane cascade arrangement with the various coordinate systems shown.

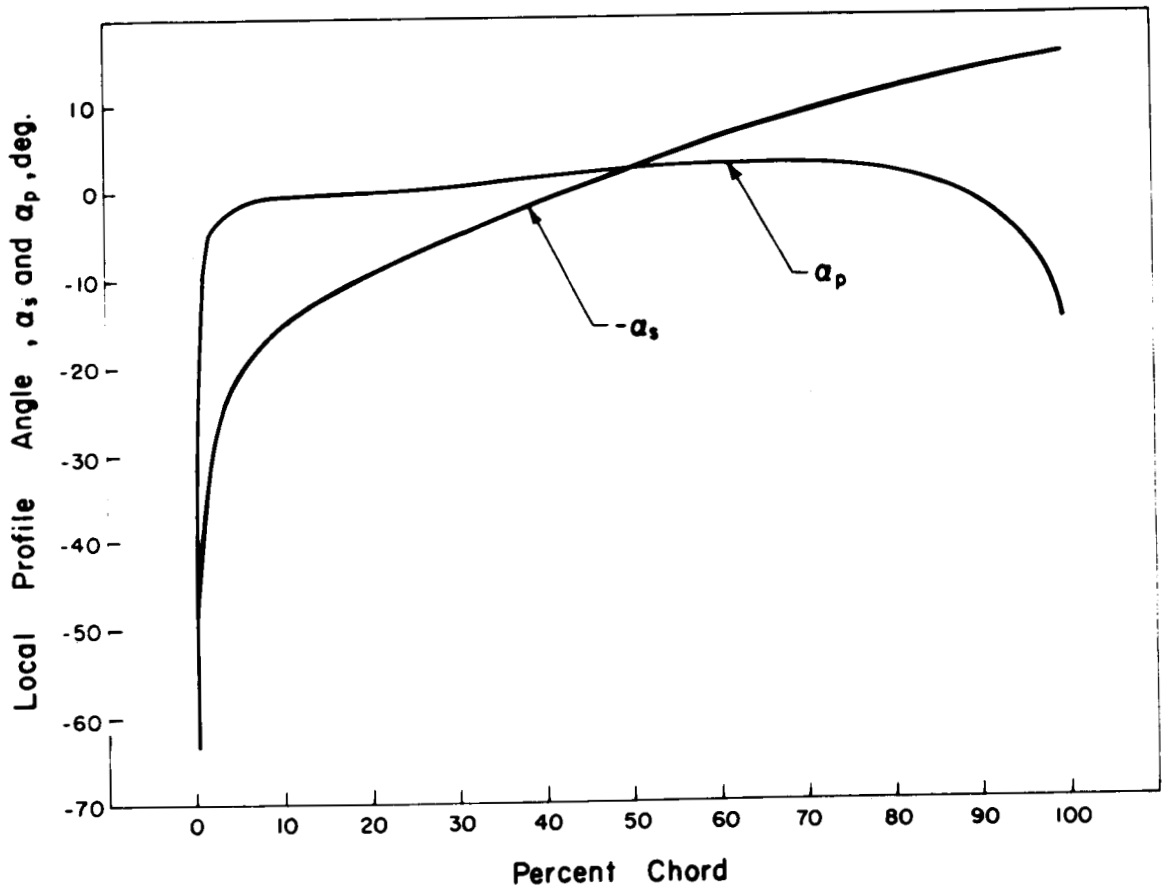

Figure 34. Local profile angle variation for NACA 65(A_{10})-810 blade profile.

formed according to the above equations for $y_s + \Delta_s$ and $y_p + \Delta_p$.

A plot of local profile angle, α_s, α_p, as a function of chord for the $65(A_{10})$-810 profile as determined from a layout of the profile is given in Figure 34. To find α_s, α_p values corresponding to the assigned x values, the percent of chord locations X_s and X_p corresponding to the profile boundary points $(x, y_s + \Delta_s)$ and $(x, y_p + \Delta_p)$ must be determined from the constructed profile (see Figure 33). This enables one to read off the values of α_s and α_p in Figure 34.

APPENDIX D

AN UNCAMBERED PARABOLIC ARC PROFILE IN CASCADE ARRANGEMENT

The equations for the suction and pressure boundaries of the profile shown in Figure 35 are, respectively

$$Y_s = \frac{t}{c}\left(2 - \frac{X}{50}\right) X$$

$$Y_p = - Y_s$$

where X, Y_s and Y_p are in percent of chord, and $\frac{t}{c}$ is the maximum thickness-to-chord ratio. With the equations for the profile boundary known the cascade geometry can be determined without resorting to graphical procedures.

Similar to the case for the $65(A_{10})$ profile, the abscissas x^* in percent of chord for points on the profile boundaries can be evaluated by the transformation (see Figure 35)

$$x^* = X_{s,p} \cos\gamma - Y_{s,p} \sin\gamma$$

$$= X_{s,p} \cos\gamma \pm \frac{t}{c}\left(\frac{X_{s,p}}{50} - 2\right) X_{s,p} \sin\gamma$$

A change of scale to introduce abscissa values measured in the computing mesh coordinates (x, y) is given by

$$\frac{100}{\sigma s}(x - x') = x^*$$

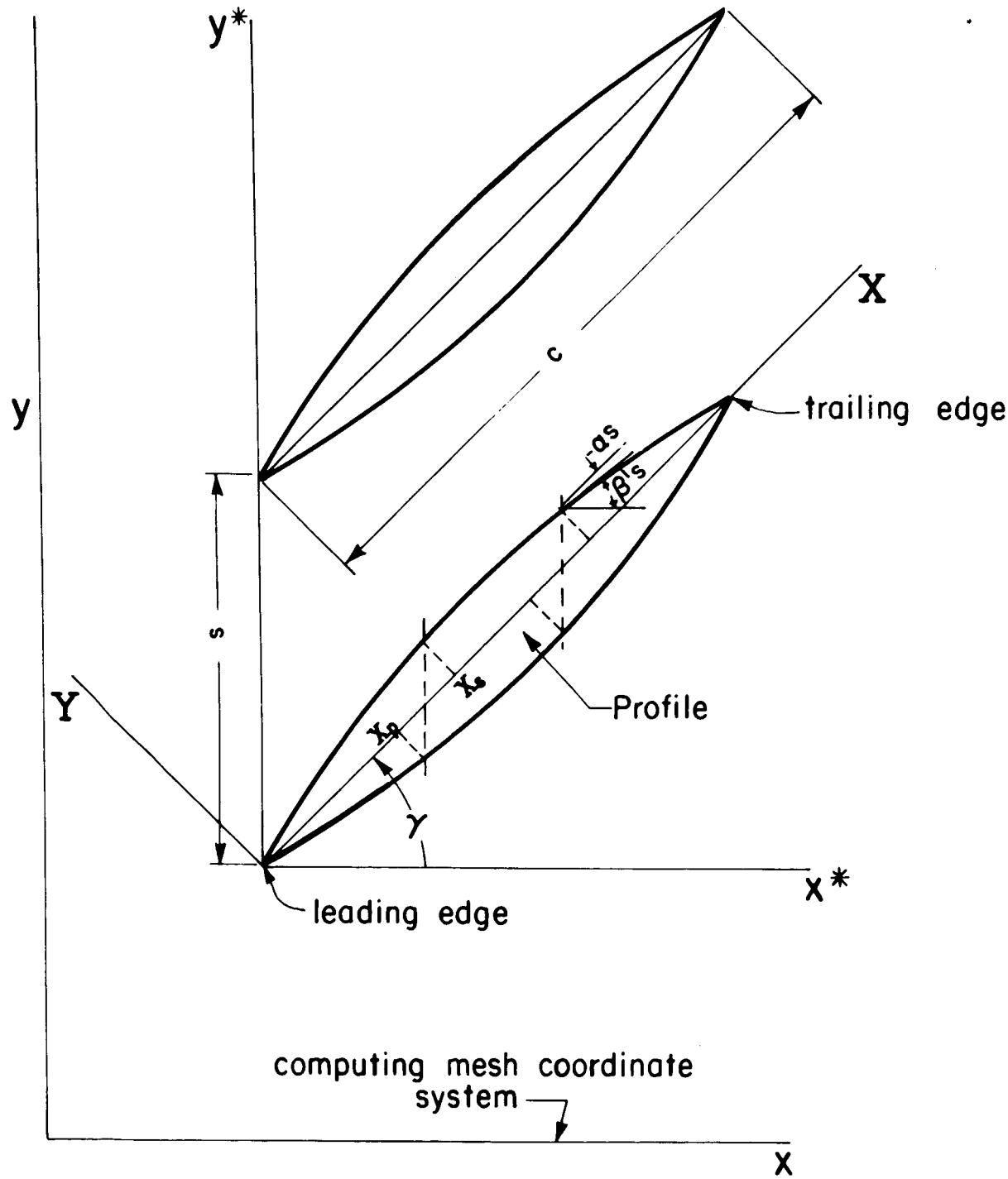

Figure 35. An uncambered parabolic arc profile in cascade arrangement with the various coordinate systems shown.

The problem is to determine X_s, X_p for assigned $(x - x')$ after which the corresponding Y_s, Y_p and $Y_s + \Delta_s$, $Y_p + \Delta_p$ can be determined. The last two equations combined yield a quadratic equation in X_s and X_p:

$$AX^2_{s,p} + BX_{s,p} + C = 0$$

where

$$A = \pm \frac{t}{c} \frac{\sin \gamma}{50}$$

$$B = \cos \gamma \mp 2 \frac{t}{c} \sin \gamma$$

$$C = - \frac{100}{\sigma s} (x - x')$$

The solution with proper choice of sign indicated for the radical term is

$$X_{s,p} = \frac{-B + \sqrt{B^2 - 4AC}}{2A} \quad , \quad A \neq 0$$

Hence, with X_s, X_p known for assigned $(x - x')$ the ordinates for the s- and p-boundaries can be obtained. First, rotation of axis from (X, Y) gives

$$Y^*_{s,p} = X_{s,p} \sin \gamma + Y_{s,p} \cos \gamma$$

which after substitution for Y_s and Y_p in terms of X_s and X_p becomes

$$Y^*_{s,p} = (\sin \gamma \pm 2 \frac{t}{c}) X_{s,p} \mp \frac{t}{c} \frac{\cos \gamma}{50} X^2_{s,p}$$

A change of scale and translation of axis to the computing mesh coordinates gives the final desired ordinates of the profile:

$$Y_s + \Delta_s = Y'_s + \frac{\sigma s}{100} (\sin \gamma + 2 \frac{t}{c}) X_s - \sigma s \frac{t}{c} \frac{\cos \gamma}{5000} X^2_s$$

$$Y_p + \Delta_p = Y'_s + \frac{\sigma s}{100} (\sin \gamma + 2 \frac{t}{c}) X_p + \sigma s \frac{t}{c} \frac{\cos \gamma}{5000} X^2_p$$

In these expressions, mesh point ordinate Y'_s, and profile spacing, s, in units of computing mesh coordinates along with solidity, σ, setting angle, γ, and thickness ratio, $\frac{t}{c}$, are assigned. X_s and X_p are determined for the assigned values of $(x - x')$.

Lastly, to determine the local profile angles α_s, α_p it follows from the defining equation for Y_s that

$$\frac{dY_s}{dX} = 2\,\frac{t}{c}\,(1 - \frac{X}{50})$$

Therefore

$$\alpha_s = \tan^{-1} \left.\frac{dY_s}{dX}\right|_{X_s} = \tan^{-1}\,[2\,\frac{t}{c}\,(1 - \frac{X_s}{50})]$$

where, as previously, X_s is determined for assigned $(x - x')$. Likewise,

$$\alpha_p = \tan^{-1}[2\,\frac{t}{c}\,(\frac{X_p}{50} - 1)]$$

APPENDIX E

COMPUTER PROGRAM FLOW DIAGRAMS

The computer flow diagrams, a main program and a first and second subroutine, are given in the following:

Computer program flow diagram. Main program.

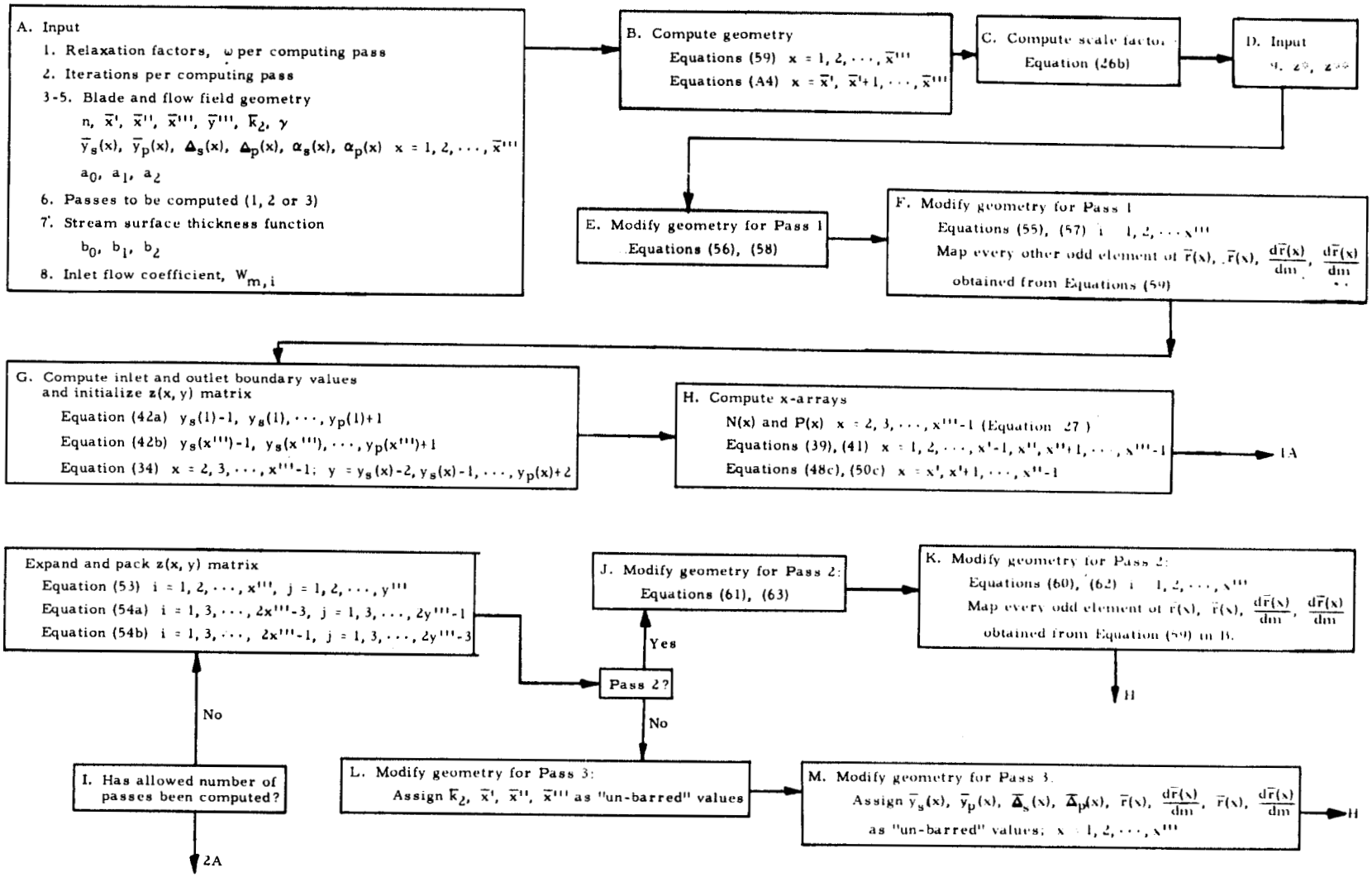

Computer program flow diagram. First sub-routine.

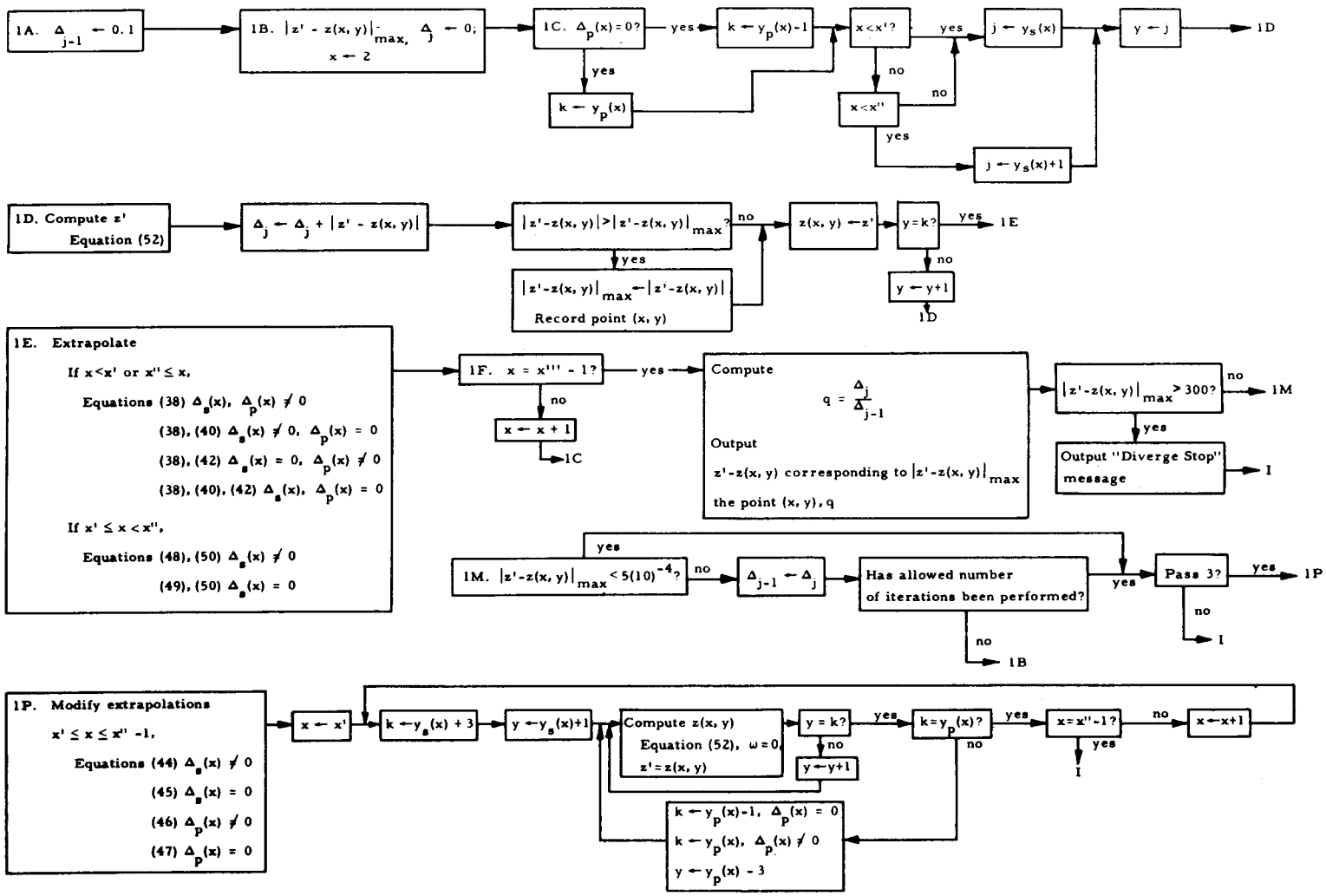

Computer program flow diagram. Second sub-routine.

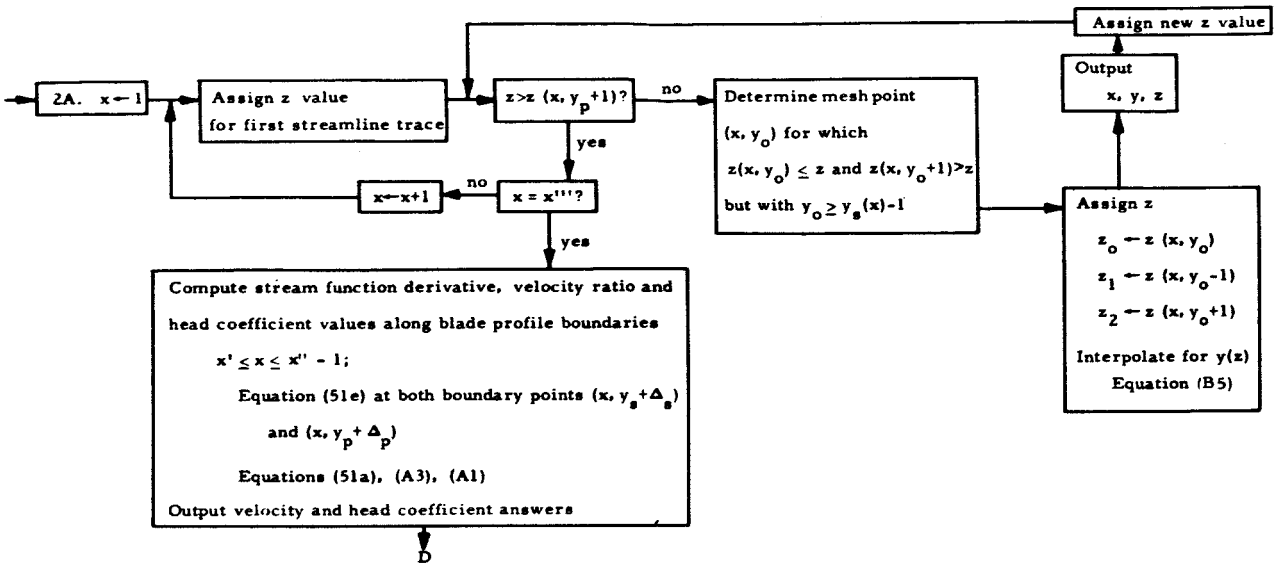

REFERENCES

1. Bauersfeld, [W.] Die Konstruktion der Francis-Schaufel nach der Lorenzschen Turbinentheorie und ihre Eigenschaften. Zeitschrift des Vereines Deutscher Ingenieure. 56:2045-2051. 1912.

2. Bowen, J. T., Sabersky, R. H. and Rannie, W. D. Investigations of axial-flow compressors. Trans. Amer. Soc. Mech. Engr. 73: 1-15. 1951.

3. Brand, L. Vector analysis. New York, N. Y. John Wiley and Sons, Inc. 1957.

4. Csanady, G. T. Theory of turbomachines. New York, N. Y. McGraw-Hill. 1964.

5. Erwin, J. R. and Emery, J. C. Effect of tunnel configuration and testing technique on cascade performance. U. S. Nat. Adv. Comm. Aero. Rep. 1016. 1951.

6. Hamrick, J. T., Ginsburg, A. and Osborn, W. M. Method of analysis for compressible flow through mixed-flow centrifugal impellers of arbitrary design. U. S. Nat. Adv. Comm. Aero. Rep. 1082. 1952.

7. Hartmann, M. J. and Ball, C. L. New problems encountered with pumps and turbines. U. S. Nat. Aero. Space Admin. (Publication) SP-19: 21-33. 1962.

8. Hatch, J. E., Giamati, C. C. and Jackson, R. J. Application of radial-equilibrium condition to axial-flow turbomachine design including consideration of change of entropy with radius downstream of blade row. U. S. Nat. Adv. Comm. Aero. Res. Memo. E54A20. 1954.

9. Herrig, L. J., Emery, J. C. and Erwin, J. R. Systematic two-dimensional cascade tests of NACA 65-series compressor blades at low speeds. U. S. Nat. Adv. Comm. Aero. Tech. Note 3916. 1957.

10. Hildebrand, F. B. Introduction to numerical analysis. New York, N. Y. McGraw-Hill Book Co., Inc. 1956.

11. Holmquist, C. O. and Rannie, W. D. An approximate method of calculating three-dimensional compressible flow in axial turbomachines. Jour. Aero. Sci. 23: 543-556. 1956.

12. Johnsen, I. A. and Bullock, R. O., eds. Aerodynamic design of axial-flow compressors. Vol. I. U. S. Nat. Adv. Comm. Aero. Res. Memo. E56B03. 1956.

13. Keller, C. The theory and performance of axial-flow fans. New York, N. Y. McGraw-Hill Book Co., Inc. 1937.

14. Kramer, J. J. Analysis of incompressible, nonviscous blade-to-blade flow in rotating blade rows. Trans. Amer. Soc. Mech. Engr. 80: 263-275. 1958.

15. Kulsrud, H. E. A practical technique for the determination of the optimum relaxation factor of the successive over-relaxation method. Communications Assoc. Comput. Mach. 4: 184-187. 1961.

16. Lorenz, H. Theorie und Berechnung der Vollturbinen und Kreiselpumpen. Zeitschrift des Vereines Deutscher Ingenieure. 49: 1670-1675. 1905.

17. Marble, F. E. and Michelson, I. Analytical investigation of some three-dimensional flow problems in turbomachines. U. S. Nat. Adv. Comm. Aero. Tech. Note 2614. 1952.

18. Mellor, G. L. An analysis of axial compressor cascade aerodynamics. Parts 1 and 2. Trans Amer. Soc. Mech. Engr. Ser. D, 81: 362-386. 1959.

19. Milne-Thomson, L. M. Theoretical hydrodynamics. 3rd ed. New York, N. Y. Macmillan Co. 1955.

20. Reissner, H. J. and Meyerhoff, L. Analysis of an axial compressor stage with infinitesimal and finite blade spacing. U. S. Nat. Adv. Comm. Aero. Tech. Note 2493. 1951.

21. Robbins, W. H. and Dugan, J. F., Jr. Prediction of off-design performance of multistage compressors. U. S. Nat. Adv. Comm. Aero. Res. Memo. E56B03a: 245-275. 1956.

22. Rouse, H. Elementary mechanics of fluids. New York, N. Y. John Wiley and Sons, Inc. 1946.

23. Rouse, H. and Hassan, M. M. Cavitation-free inlets and contractions. Mech. Engrg. 71: 213-216. 1949.

24. Ruden, P. Investigation of single stage axial fans. U. S. Nat. Adv. Comm. Aero. Tech. Memo. 1062. 1944.

25. Salvadori, M. G. The mathematical solution of engineering problems. New York, N. Y. McGraw-Hill Book Co., Inc. 1948.

26. Schlichting, H. Boundary layer theory. 4th ed. New York, N. Y. McGraw-Hill Book Co., Inc. 1960.

27. Serovy, G. K. and Anderson, E. W. Method for predicting off-design performance of axial-flow compressor blade rows. U. S. Nat. Aero. and Space Admin. Tech. Note D-110. 1959.

28. Smith, L. H., Jr., Traugott, S. C. and Wislicenus, G. S. A practical solution of a three-dimensional flow problem of axial-flow turbomachinery. Trans. Amer. Soc. Mech. Engr. 75: 789-803. 1953.

29. Southwell, R. V. Relaxation methods in theoretical physics. Oxford, England. Clarendon Press. 1946.

30. Spannhake, W. Centrifugal pumps, turbines and propellers. Cambridge, Mass. The Technology Press of the Massachusetts Institute of Technology. 1934.

31. Stanitz, J. D. and Ellis, G. O. Two-dimensional flow on general surfaces of revolution in turbomachines. U. S. Nat. Adv. Comm. Aero. Tech. Note 2654. 1952.

32. Stodola, A. Steam and gas turbines. New York, N. Y. McGraw-Hill Book Co., Inc. 1927.

33. Stuart, D. J. K. Analysis of Reynolds number effects in fluid flow through two-dimensional cascades. Great Britain Aero. Res. Council Rep. and Memo. 2920. 1955.

34. Swan, W. C. A practical method of predicting transonic-compressor performance. Trans. Amer. Soc. Mech. Engr. Ser. A, 83: 322-330. 1961.

35. Vavra, M. H. Aero-thermodynamics and flow in turbomachines. New York, N. Y. John Wiley and Sons, Inc. 1960.

36. von Karman, T. Aerodynamics. Ithaca, N. Y. Cornell University Press. 1954.

37. Wislicenus, G. F. Fluid mechanics of turbomachinery. New York, N. Y. McGraw-Hill Book Co., Inc. 1947.

38. Wu, C. H. A general theory of three-dimensional flow in subsonic and supersonic turbomachines of axial-, radial-, and mixed-flow types. U. S. Nat. Adv. Comm. Aero. Tech. Note 2604. 1952.

39. _____ and Wolfenstein, L. Application of radial equilibrium condition to axial-flow compressor and turbine design. U. S. Nat. Adv. Comm. Aero. Tech. Rep. 955. 1950.

40. Young, D. Iterative methods for solving partial difference equations of elliptic type. Trans. Amer. Math. Soc. 76:92-111. 1954.